Eindhoven University of Technology

MASTER

Analysis of the heart rate mediated blood pressure control in fetal sheep under normal and hypoxic conditions

Zwanenburg, A.A.

Award date:
2011

Link to publication

Analysis of the heart rate mediated blood pressure control in fetal sheep under normal and hypoxic conditions

Alex Zwanenburg

Index

1 Abstract

Objective: To monitor longitudinal changes of baroreflex activity in a fetal sheep model by analysis of the transfer function between low-frequency R-R and systolic blood pressure (SBP) fluctuations after umbilical cord occlusion (UCO) induced asphyxia.

Methods: Fourteen preterm fetal lambs (UCO, n=5 and controls, n=9) were instrumented at 102 days gestation (term 146 days) during caesarian section with a femoral arterial catheter, amniotic pressure catheter, 3-lead ECG and vascular occluder around the umbilical cord (UCO group). After surgery, ewes and fetuses were allowed to recover for 4 days. At 4 days intra-uterine asphyxia was achieved by rapidly filling the vascular occluder for 25-min.

Algorithms were designed for the analysis of ECG blood pressure data. Baroreflex related fluctuations were calculated by transfer function analysis between SBP and R-R fluctuations, using fast Fourier transform, estimated in the low frequency (LF, 0.04-0.15 Hz) band. LF transfer gain (baroreflex sensitivity, BRS, ms/mmHg) and delay (s) were assumed to reflect the baroreflex mediated cardiovascular fluctuations.

Results: Algorithms for R-peak and SBP detection showed a sensitivity of 99.0% and precision of 99.9% and a sensitivity of 98.9% and precision of 99.8%, respectively. Before occlusion, no differences in R-R interval, SBP, and transfer gain and delay were observed between UCO and controls. Median BRS and delay were 7.8 (IQR, 5.6-11.4) ms/mmHg and 4 (IQR, 3-6) s, and 6.2 (IQR, 5.6–8.4) ms/mmHg and 6 (IQR, 3-7) s, respectively. Three days after UCO, BRS gradually decreased in the UCO group, resulting in significantly lower values by the end of the week (UCO median 4.8 (IQR 3.1-6.7) ms/mmHg versus controls 7.7 (IQR 6.7-10.6) ms/mmHg). In UCO group, delay increased to a median value of 7 (IQR, 4-8) s and differed from the controls.

Conclusions: Algorithms developed for R-peak and SBP detection were sensitive and precise. Use of the algorithms enabled the performance of transfer function analysis to derive baroreceptor sensitivity. Intra-uterine asphyxia results in long-lasting effects of baroreflex mediated fluctuations, limiting the possibility to buffer changes in SBP by adapting fetal heart rate.

2 Introduction

Perinatal asphyxia (literally: pulse-less) is a major cause of neurological deficits in later life. Pathological studies suggest that many of these events occur before birth. However, the relationship between specific prenatal events and neurological outcome is not clear (Mallard et al., 1994). Therefore it is relevant to understand the effect of asphyxia on various physiological mechanisms, including the cardiovascular system, and to study means to prevent the pathophysiological effects of asphyxia.

To ensure adequate blood pressure and hence tissue perfusion, blood pressure is controlled by a variety of reflex mechanisms including the baro- and chemoreflex. In this thesis, we focused on baroreflex-mediated heart rate response, a prevalent mechanism for blood pressure control during homeostasis. This mechanism, which develops during early fetal life, regulates short-term fluctuations in blood pressure. The effect of asphyxia on the immature baroreflex is not well understood. A poor baroreflex function may contribute to blood pressure instabilities, leading to impaired cerebral perfusion or hemorrhage (Pryds et al., 1996).

To study the immature baroreflex following asphyxia, a fetal sheep model is frequently used as biological model. Sheep fetuses have a qualitatively similar cardiovascular response to complete occlusion of the umbilical cord to that of the near-term fetus. At Maastricht University, chronically instrumented fetal sheep at 0.7 gestational age (equivalent to 28-30 weeks of gestation in human) (McIntosh et al., 1979) were subjected to systemic asphyxia by umbilical cord occlusion. The fetal cortical electroencephalogram (EEG), blood pressure (BP), electrocardiogram (ECG) and fetal blood gases were measured the first week after the insult. In this thesis, the signal analysis of the physiological signals obtained from this animal experiment is described.

The first part of this thesis contains a publication showing the results of baroreflex mediated heart rate response after asphyxia. In the subsequent section, relevant anatomy and physiology of the cardiovascular system are highlighted. The next section includes a detailed description of the algorithms used to study the heart rate mediated baroreflex. This section is followed by observations and recommendations to improve the algorithms used in this study. In the appendix, the signal analysis of electrocortical activity following induced asphyxia is demonstrated.

3 Heart rate mediated blood pressure control in fetal sheep under normal and hypoxic conditions

Ward Jennekens[1,2], Reint Jellema[3,4], Alex Zwanenburg[2], Daan Ophelders[3], Rik Vullings[5], Arne van Hunnik[6], Carola van Pul[1], Laura Bennet[7], Boris W. Kramer[3,4,8], Peter Andriessen[9]

[1] Dept. of Clinical Physics, Máxima Medical Centre, Veldhoven, The Netherlands

[2] Dept. of Applied Physics, Eindhoven University of Technology, Eindhoven, The Netherlands

[3] Dept. of Pediatrics, Maastricht University Medical Center, Maastricht, The Netherlands

[4] School of Mental Health and Neuroscience, Maastricht University, Maastricht, The Netherlands

[5] Dept. of Electrical Engineering, Eindhoven University of Technology, Eindhoven, The Netherlands

[6] Dept. of Physiology, Maastricht University, Maastricht, The Netherlands

[7] Dept. of Physiology, Faculty of Medical and Health Sciences, The University of Auckland, Auckland, New Zealand

[8] School of Oncology and Developmental Biology, Maastricht University, Maastricht, The Netherlands

[9] Neonatal Intensive Care Unit, Máxima Medical Centre, Veldhoven, The Netherlands

Corresponding author: P. Andriessen, Máxima Medical Centre, Neonatal Intensive Care Unit, PO Box 7777, 5500 MB Veldhoven, The Netherlands, e-mail: p.andriessen@mmc.nl

3.1 Introduction

Preterm infants, i.e. infants born before 32 weeks of gestation (GA), have a higher incidence of neurological morbidity and mortality compared to term infants (Volpe, 1997). Neurological sequelae in preterm infants may be the consequence of asphyxia during fetal life (Nelson et al., 1991) . Hemodynamic factors during asphyxia and the post-asphyxia reperfusion phase contribute considerably to these neurological disorders (Volpe, 1997; Liem et al., 2010). To ensure adequate blood flow to organs throughout the body, including the brain, blood pressure is controlled by baro- and chemoreflex mechanisms. These are negative feedback systems incorporating receptors to sense changes in arterial pressure or oxygen (Timmers et al., 2003). The most important arterial baro- and chemoreceptors are located in the carotid sinus (at the bifurcation of external and internal carotids) and in the aortic arch. Under normoxaemia, the baroreflex stabilizes perfusion pressure in the face of disturbances of circulatory homeostasis by adapting heart rate, myocardial contraction and vascular resistance. A poorly developed baroreflex function could contribute to blood pressure instabilities, which may lead to impaired cerebral perfusion or hemorrhage (Pryds et al., 1996). A better understanding of the dynamics underlying the control mechanisms regulating blood pressure may be useful to improve diagnosis of these disorders.

Assessment of the baroreflex function, in specific of heart rate mediated blood pressure control, can be obtained through quantification of baroreceptor sensitivity. Baroreceptor sensitivity may simply be defined as the change in heart rate (or R-R interval) in response to changes in arterial blood pressure, and may be estimated from (time-domain or spectral) analysis of spontaneous fluctuations in R-R intervals and blood pressure (de Boer et al., 1985; Honzíková et al., 1992; Head et al., 2001; Ursino et

al., 2003; Laude et al., 2004; Rovere et al., 2008). Low-frequency (LF) fluctuations in arterial blood pressure with a wave length of approximate 10 s (also called Mayer waves) have historically been attributed to baroreflex activity (Penáz et al., 1978). The oscillations are assumed to be caused by a (delayed) feedback control and probably mediated through the sympathetic and parasympathetic innervations of the baroreflex (Akselrod et al., 1985). Currently, our understanding of the cardiovascular response of the human preterm fetus or infant is limited (Jennekens et al., 2011a) and knowledge of fetal baroreflex is mostly based on animal models (Segar et al., 1992; Booth et al., 2009; Gunn et al., 2009). The most commonly used model for studying the development of the cardiovascular system is the sheep model. The neural development of sheep at 0.85 of gestation approximates that of the term human (McIntosh et al., 1979). Sheep have been shown to develop a functional baroreceptor reflex around 0.6 GA (Segar et al., 1992). There is conflicting evidence on the exact manifestation of baroreceptor reflex maturation. While some studies show an increasing baroreflex sensitivity with gestational age, for animal models (Shinebourne et al., 1972) as well as humans neonates (Gournay et al., 2002; Andriessen et al., 2005) , other studies show no significant maturational change (Maloney et al., 1977; Frasch et al., 2007). There are also studies indicating that baroreceptor sensitivity decreases during development as well as after birth in sheep (Blanco et al., 1988; Segar et al., 1992; Segar, 1997). A recent study shows that in preterm sheep of 0.7 GA the baroreceptor reflex is heart rate mediated and there is no significant control by the renal sympathetic nerve, which regulates vascular resistance (Booth et al., 2009). In the term sheep vascular resistance control is present (Segar et al., 1992) , indicating a different maturational tempo for each component of the baroreceptor reflex feedback system. These findings might explain the apparent discrepancies between the other studies.

The cardiovascular system of the term or near-term fetus responds to asphyxia by changing heart rate and redistributing cardiac output to preserve the limited energy resources and maintain adequate supply to the brain. This response is mediated by combined input from chemoreceptor and baroreceptor activity. Chemoreceptors detect variations in oxygen concentration in the arterial blood, whilst also monitoring carbon dioxide and pH. They are located in the aortic body and carotid body, on the arch of the aorta and on the common carotid artery, respectively. Hypoxia stimulates these chemoreceptors, leading to rapid fetal heart rate deceleration proportional to the severity of the hypoxia (Bennet et al., 2009). Blood pressure is maintained by peripheral vasoconstriction (Bennet et al., 2009), redistributing blood flow to favour the brain, heart and adrenals (Peeters et al., 1979). Current knowledge about how the preterm fetus, possibly hampered by an immature blood pressure regulation, responds to hypoxia is limited. Experiments by Bennet et al have shown that the immature sheep fetus can survive prolonged periods of asphyxia, but resulting hypotension and hypoperfusion may contribute to cerebral injury as seen in human preterm fetuses (Bennet et al., 1999; George et al., 2004; Bennet et al., 2009). These studies mostly focus on acute effects of asphyxia, monitoring fetal sheep for periods up to 72 hours (Bennet et al., 1999; George et al., 2004). Changes in the baroreflex feedback system have not been examined for longer than several days after the initial period of asphyxia.

The aim of this study is (1) to quantify baroreflex mediated heart rate response (baroreflex sensitivity, BRS) by transfer function analysis between low-frequency R-R and systolic blood pressure (SBP) fluctuations in an instrumented fetal sheep model and (2) to evaluate longitudinal changes of baroreflex mediated heart rate response during the first 7 days after umbilical cord occlusion (UCO) induced asphyxia.

3.2 Methods

3.2.1 Animals

Texel ewes were date-mated and the fetuses were randomized for umbilical cord occlusion (UCO) or control. The study group consisted of 14 fetal sheep (9 controls and 5 UCO). Fetal instrumentation was performed at 0.7 GA (102 days, term = 146 days). The study was conducted at Maastricht University Medical Center, Maastricht, the Netherlands, and was approved by the local Animal Ethics Research

Committee.

3.2.2 Experimental preparations

The pregnant ewes were deprived of food, but not water, 24 hours before surgery. They were sedated using 1-2% isoflurane, guided by depth of sedation. After a lower midline incision, the fetus was carefully extracted through a small incision of the uterus. The fetus was instrumented with a 3.5 French Argyle umbilical vessel catheter (Tyco Health Care Group, Mansfield MA U.S.A.) in the femoral artery. The arterial catheter was utilized for continuous monitoring of fetal arterial pressure. A vascular occluder (OC16HD, in vivo Metric, Healdsburg CA U.S.A) was placed around the umbilical cord. Three custom-made silver electrodes with fixed leads (Cooner, Chatsworth CA, U.S.A.) were inserted in the subdermis and fixed with sutures. These electrodes were used for electrocardiography and formed an Einthoven triangle. The fetus was then repositioned in the uterus. A catheter was inserted into the amniotic sac to monitor the amniotic fluid pressure. Before closure the amniotic cavity was filled with warm sterile saline (NaCl 0.9%). All fetal catheters and electrode leads were exteriorised through the flank of the ewe. The lower midline incision was securely sutured. After surgery, the ewe was allowed to recover and housed in a confined space to allow continuous perfusion of catheters with heparinised saline. Post-surgery ewes received five days of intravenous amoxicillin (1000 mg) / clavulanic-acid (200 mg). During the complete course of the experiment (11 days) the animals had ad libitum access to water and food.

3.2.3 Experimental design

Experiments were conducted at 102 (operation) to 113 (sacrifice) days of gestation. After a recovery period of four days (GA, 106 days) the umbilical cord of the fetuses in the UCO group was occluded by rapidly inflating the occluder with sterile saline of a defined volume known to completely inflate the occluder. Verification of the occlusion was obtained by observation of a sudden drop in heart rate (see Figure 1). The occlusion was discontinued after 25 minutes or (earlier) when mean arterial blood pressure dropped below 8 mmHg or asystole occurred. At the end of the occlusion, the lambs always suffered from severe bradycardia (heart rate < 90 bpm, normal approximately 180 bpm) or even complete cardiac arrest. Most fetuses recovered uneventfully the first days after surgery. Infection, low fetal weight, mortality and instrumentation problems resulted in later drop-out. If there was no increase in heart rate within 20 seconds after the end of occlusion, resuscitation was started using an injection of adrenalin (0.1 mg/kg). Arterial blood gas analysis (pO_2, pCO_2, pH) was performed before, during and after umbilical cord occlusion to monitor the metabolic state during hypoxic-ischemia and recovery. Fetuses were studied for 7 days post-occlusion. At the end of the experiment (11 days post-surgery), both ewe and fetus were euthanised by administration of pentobarbital (200 mg/kg).

3.2.4 Data acquisition

Blood pressure, amniotic pressure and ECG data were acquired and digitized by a MPAQ unit (Maastricht-Programmable AcQuisition system, Maastricht Instruments BV, Maastricht, the Netherlands). Analog filtering was applied to the ECG data, with a 1 Hz high-pass filter and a 200 Hz low-pass filter. Blood pressure and amniotic pressure data were not filtered. All data were sampled at 1000 Hz. Finally, data was stored on a hard drive for off-line analysis.

3.2.5 Data analysis

Data was processed off-line using MATLAB R2009a (The MathWorks, Inc., Natick, Massachusetts, U.S.A.). Recordings were divided into 30-minute segments for analysis. ECG data was filtered using a 50 Hz infinite impulse response notch filter and 20 Hz high-pass and 80 Hz low-pass 4th-order Butterworth filters, empirically found to be optimal for the R-peak detection algorithm used. Fetal blood pressure signals were filtered using a 50 Hz infinite impulse response notch filter and 2 Hz high-

pass and 16 Hz low-pass 4th-order Butterworth filters to facilitate detection by the diastole and systole detection algorithm. Fetal blood pressure was corrected for offset by subtraction of the low-pass filtered amniotic fluid pressure.

In each 30-minute segment, R-peaks of the QRS-complex were detected by adaptive filtering of the second derivative of the ECG signal. As R-peaks are characterized by relatively fast changes compared to other features in the ECG, the second derivative of the ECG constitutes a suitable way to perform R-peak detection. In each 30-minute segment, the algorithm is trained using the first 20 seconds of data in order to estimate the magnitude of the R-peaks and to calculate the range of R-R intervals. Subsequently, the algorithm uses the range of R-R intervals to predict the location of the next R-peak. To verify the R-peak detection, the magnitude of the predicted R-peak is compared with the magnitude estimated by the training set. Both magnitude estimation and range of R-R intervals are updated to include the most recent values. After conducting R-peak detection on the 30-minute segment, an R-R interval time series was created.

The first derivative of the blood pressure signal was used to locate the position of the diastolic and systolic peak. The location of the peaks was used to find the corresponding diastolic and systolic blood pressure (SBP) values in the original signal. Afterwards, a time series of systolic and diastolic blood pressure values was created.

The unevenly time-spaced R-R interval and SBP series were convolved with a boxcar function and subsequently resampled at 4Hz using nearest-neighbor interpolation to obtain equidistant sample points. For variability analysis, the offset of the R-R interval and SBP series were removed by a 0.03 Hz high-pass Butterworth filter.

3.2.6 Spectral analysis and transfer-function analysis

Spectral analysis offers the opportunity to decompose spontaneously occurring fluctuations in blood pressure and R-R interval time series into a power spectrum, and to relate the character of the fluctuations to physiological processes. Transfer function analysis (cross-spectral analysis) between arterial blood pressure and R-R interval series in the low-frequency band (0.04-0.15 Hz) is a useful estimate of baroreflex sensitivity (de Boer et al., 1985; Robbe et al., 1987; Camm et al., 1996). This methodology was adapted for preterm infants and we refer to previous papers for further details (Andriessen et al., 2003; Andriessen et al., 2005). As the values of blood pressure and R-R intervals obtained from the fetal sheep are comparable with values found in preterm infants, the same spectral analysis methodology was followed.

In short, each 30 minute segment was divided into nine non-overlapping 192-second segments. The average auto- and cross spectra of R-R interval and SBP were calculated for each 192-second segment. Each 192-second segment was divided into five half-overlapping 64-second segments. A Parzen-window was applied to each of the half-overlapping segments to reduce spectral leakage. The 64-second segments were then discrete Fourier transformed and for each 64-seconds segment the power spectra were calculated. These power spectra were corrected by application of a Parzen-window, and five 64-second segments were averaged to obtain the mean auto- and cross-power spectral density functions. Total spectral power (0.04-2 Hz) and LF (0.04-0.15 Hz) spectral power were calculated from the auto spectra of R-R interval and SBP series.

From the cross spectra of R-R interval and SBP series, the coherence, transfer gain and transfer phase were calculated for the LF band. As the reliability of transfer function depends on coherence between the signals, transfer function parameters were only assessed if coherence > 0.50. Baroreflex sensitivity was calculated as the LF transfer gain and assessed at the frequency bin with the highest coherence within the LF band. The lower edge of this bin was used as representation of the LF peak. Baroreflex delay was calculated by dividing the transfer phase at the corresponding frequency bin by 2π -times this frequency. Time domain cross correlation of the R-R interval and SBP series was used to correct for $2n\pi$ phase shifts.

3.2.7 Time domain estimates of variability

Heart rate variability (HRV) was assessed for each 192-second segment by calculating the mean R-R interval and standard deviation (SD-RR) (Camm et al., 1996). Likewise, blood pressure variability (BPV) was assessed by calculating the mean SBP and standard deviation (SD-SBP).

To verify results obtained by spectral analysis, baroreceptor sensitivity was also analysed in the time domain. To obtain a measure for baroreceptor sensitivity in the time domain, the SD-RR was divided by SD-SBP (Andriessen et al., 2003).

3.2.8 Data processing

Hence, each parameter of a 192-second segment was denoted by a single value. Subsequently, for further analysis of the population data, the median per 30-minute segment was calculated from the single values of the underlying 192-second segments. The median value was used because normality was not a priori assumed and to reduce the influence of statistical outliers. For the analysis of maturational effects and long-term monitoring, the median values were grouped for 6 hours and 24 hours, respectively. Baseline values for long-term monitoring were assessed in the 24 hours before UCO. Values for the third and seventh day were assessed between 60 - 84 hours and 150 - 174 hours after UCO, respectively.

3.2.9 Statistics

Blood gas data were expressed as mean ± SEM. Group comparisons for blood gas analysis were performed using the two-sided unpaired student t-test for unequal sample numbers and unequal variance. The data included for long-term monitoring were expressed as median and interquartile range (IQR) and group comparisons were analysed using the Mann-Whitney U test. The maturational effects on time domain and frequency domain spectral measures were evaluated using multilevel analysis: linear regression was estimated using the random effects model, which extends the generalized linear model to allow for analysis of repeated measurements between and within subjects. Regression analysis results are shown with the a- and b-coefficient (a, intercept; b, slope of regression line). A p-value < 0.05 was considered significant.

3.3 Results

3.3.1 Baseline values of cardiovascular and transfer function parameters

Baseline values for both the UCO and the control group were derived in the 24 hours before the UCO. These values are presented in Table 1. Time domain estimates of variability were comparable in both groups. Transfer function analysis showed no differences in the LF frequency peak between both groups. A slight but significant difference in coherence values was noted between both groups. Transfer function gain was comparable in both groups: 6.2 (5.6 – 8.4) ms/mmHg for controls versus 7.8 (5.6 – 11.4) ms/mmHg in the UCO group. Transfer function delay showed comparable baseline values.

3.3.2 Acute cardiovascular response and blood gas analysis to umbilical cord occlusion

A representative example of the cardiovascular changes and blood gas analysis in response to UCO is presented in Figure 1. Directly after umbilical cord occlusion, the R-R interval rapidly increased to approximately 600 ms, followed by a steady increase to 1100 ms at the end of the UCO. After the occlusion the R-R interval remained reduced compared to baseline.

The SBP shows a broad initial peak, where the SBP exceeds baseline levels for approximately 5 minutes

yielding a maximum of approximately 65 mmHg. This is followed by a gradual decrease in SBP to a nadir of 10 mmHg by the end of the UCO. Post-occlusion the blood pressure values were higher than baseline values.

SD-RR increases directly after the start of the UCO, before decreasing to baseline levels at approximately 5 minutes, followed by a transient increase in the late occlusion phase. During the immediate post-occlusion phase, the SD-RR is decreased compared to baseline levels.
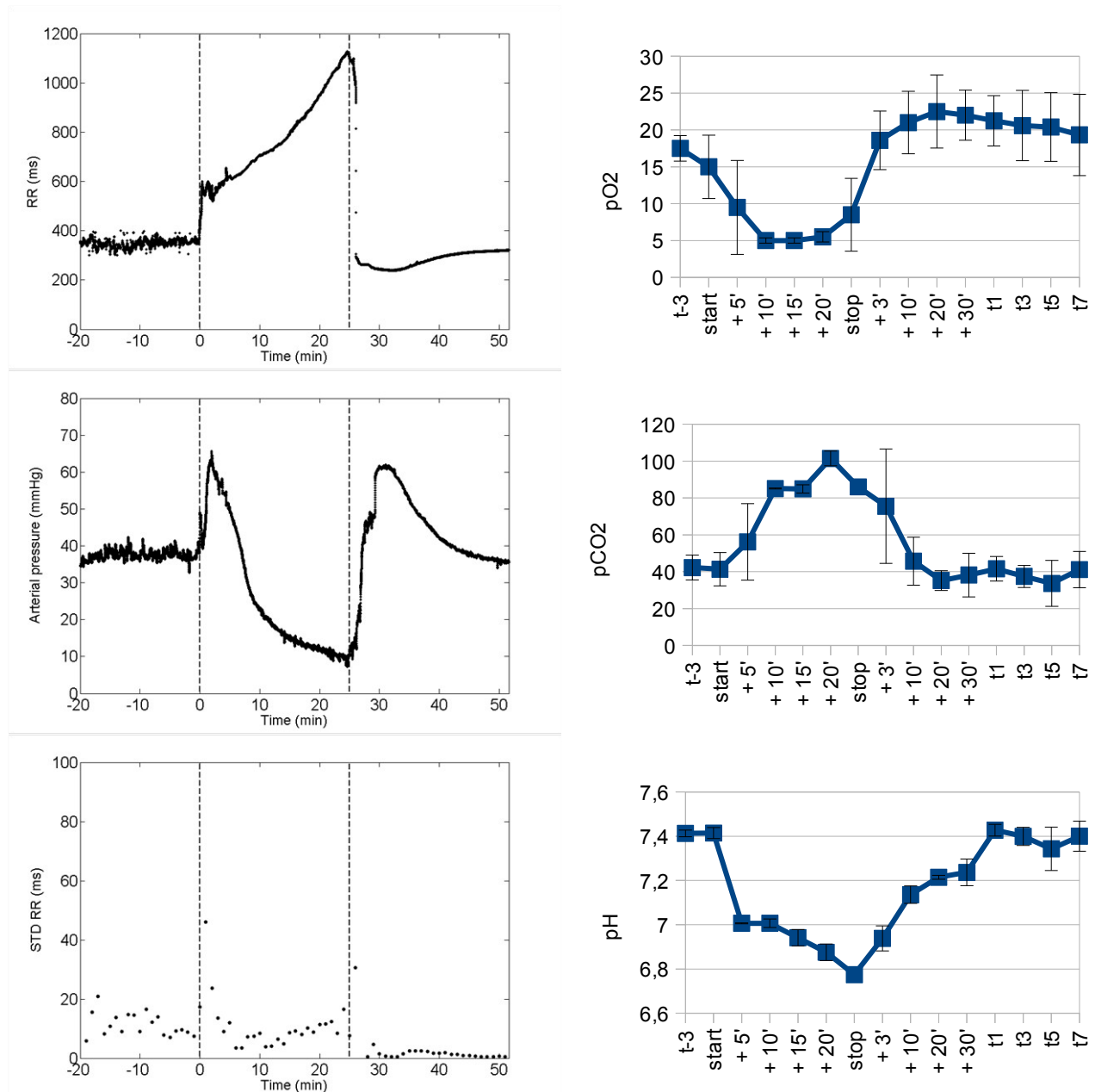
Figure 1: Response to UCO in fetal sheep. Left panels show the time sequence of changes in R-R interval mean arterial blood pressure (mmHg) and HRV (ms). Data are presented as mean ± SEM per 1-minute interval and displayed from 20 minutes before umbilical cord occlusion (indicated by the vertical red bars) until 25 minutes after occlusion.

Right panels show the changes in blood gas analysis during UCO: blood pO₂ (mmHg), pCO₂ (mmHg) and pH during complete umbilical cord occlusion for 25 minutes and subsequent reperfusion. Data presented as mean ± SEM during complete umbilical cord occlusion for 25 minutes, subsequent reperfusion and follow-ups at day 1, 3, 5 and 7 post-occlusion.

Umbilical cord occlusion was associated the development of a severe acidosis. In addition there was a significant fall in pO_2 during occlusion. During recovery pH, pO_2 and pCO_2 returned to baseline values.

3.3.3 Long-term monitoring of cardiovascular and transfer function parameters

Values for the cardiovascular and transfer function parameters for both the UCO and the control group were calculated for the third and seventh day after the UCO. These values are presented in Table 1. Blood gas analysis during the experiment is also shown in Table 1.

At the third day after UCO, R-R interval, SD-RR and SBP for the UCO group were significantly different from the controls. No significant difference in SD-SBP was observed. Spectral power analysis showed no differences in LF and total power for the R-R interval and SBP series. Transfer function analysis showed no differences in coherence, frequency, gain and delay.

At the seventh day after UCO, R-R interval, SBP and SD-SBP showed no differences. In contrast SD-RR was significantly reduced. Spectral power analysis showed significant differences in LF and total power

	Control (n=9)			UCO (n=5)		
	Baseline	t = 3 days	t = 7 days	Baseline	t = 3 days	t = 7 days
Blood gas analysis						
pH	7.41 ± 0.04	7.39 ± 0.04	7.38 ± 0.05	7.41 ± 0.03	7.40 ± 0.04	7.40 ± 0.07
Arterial pCO_2 (mmHg)	42 ± 6	42 ± 4	31 ± 10	41 ± 9	37 ± 6	41 ± 10
Arterial pO_2 (mmHg)	17 ± 2	18 ± 2	17 ± 3	15 ± 4	21 ± 5	19 ± 6
R-R interval series						
R-R interval (ms)	328 (315-341)	332 (310-343)	345 (327-363)	332 (322-341)	351 (326-363)†	347 (332-357)
SD-RR (ms)	21 (15-25)	20 (15-26)	21 (18-27)	21 (17-24)	15 (6-20)†	11 (9-16)*
Total power (ms^2)	684 (200-1672)	533 (151-1196)	1005 (554-1717)	956 (171-1505)	630 (1-1886)	48 (6-263)*
LF power (ms^2)	512 (165-1019)	374 (124-848)	795 (534-1242)	430 (135-1330)	588 (0-1627)	47 (4-229)*
SBP series						
SBP (mmHg)	46 (43-48)	43 (41-45)	49 (45-50)	47 (39-55)	48 (43-50)†	52 (45-57)
SD-SBP (mmHg)	1.8 (1.7-2.1)	1.9 (1.7-2.0)	2.2 (2.0-2.3)	1.8 (1.7-1.9)	2.0 (1.5-2.2)	1.9 (1.7-2.4)
Total power ($mmHg^2$)	0.06 (0.05-0.10)	0.06 (0.05-0.10)	0.12 (0.08-0.15)	0.06 (0.04-0.07)	0.04 (0.01-0.12)	0.05 (0.02-0.08)†
LF power ($mmHg^2$)	0.06 (0.04-0.10)	0.05 (0.04-0.09)	0.09 (0.07-0.13)	0.06 (0.03-0.07)	0.04 (0.01-0.11)	0.05 (0.02-0.08)†
Transfer function						
Frequency (Hz)	0.09 (0.09-0.10)	0.09 (0.09-0.10)	0.09 (0.09-0.11)	0.09 (0.09-0.11)	0.09 (0.09-0.11)	0.09 (0.08-0.09)
Coherence	0.62 (0.61-0.65)	0.66 (0.64-0.67)	0.65 (0.63-0.68)	0.64 (0.63-0.67)†	0.66 (0.64-0.69)	0.63 (0.61-0.65)
Gain (ms/mmHg)	6.2 (5.6-8.4)	7.9 (5.1-9.0)	7.7 (6.7-10.6)	7.8 (5.6-11.4)	8.6 (2.0-9.5)	4.8 (3.1-6.7)*
Delay (s)	5.5 (3.3-6.8)	4.2 (2.2-5.7)	4.3 (3.2-5.9)	4.0 (3.3-5.6)	3.6 (3.0-5.4)	6.6 (3.7-7.6) †

Table 1: Blood gas analyses, cardiovascular parameters and transfer function parameters in the baseline period and 3 and 7 days post-UCO. Baseline values were determined during the 24 hours before occlusion. Values are expressed as mean ± SEM or median (IQR).
* $p < 0.01$, † $p < 0.05$ (comparison between UCO and control at corresponding day)

for the R-R interval and SBP series between UCO and controls. In the UCO group, LF and total power for the R-R interval showed a 15 to 20-times reduction, compared to controls. For the SBP series, LF and total power were reduced by a factor of 2. Transfer function analysis showed no difference in LF frequency and coherence. Transfer function gain was lower in the UCO group (4.8 with IQR: 3.1 – 6.7, versus 7.7 with IQR: 6.7 – 10.6 ms/mmHg) and transfer function delay was higher.

Long-term development of the R-R interval, SD-RR, SBP and SD-SBP and the transfer function parameters are shown in Figure 2 and Figure 3 respectively.

3.3.4 Maturation of cardiovascular and transfer function parameters

The maturational effects on time domain and frequency domain spectral measures were evaluated using multilevel regression analysis for both the control and UCO group, in the time period between UCO and the seventh day post-UCO. Regression analysis results are shown in Table 2.

The control group showed a significant increase in R-R interval, SD-RR, SBP and SD-SBP. The transfer function gain increased (0.4 ± 0.1) ms/mmHg per day, while the transfer function delay did not show a significant change.

The UCO group a showed significant increase in SD-SBP, approximately 2.5-fold the magnitude of the SD-SBP increase in the control group. In contrast, R-R interval, SD-RR and SBP did not show significant change. The transfer function gain decreased by (-0.7 ± 0.1) ms/mmHg per day, and the transfer function delay increased by (0.5 ± 0.1) s per day.

	Control b (change/day)	UCO b (change/day)
R-R interval series		
R-R interval (ms)	2.8 ± 0.6*	ns
SD-RR (ms)	0.8 ± 0.2*	ns
Total power (ms^2)	-	-
LF power (ms^2)	-	-
SBP series		
SBP (mmHg)	0.4 ± 0.1*	ns
SD-SBP (mmHg)	0.04 ± 0.02†	0.10 ± 0.02*
Total power (mmHg^2)	-	-
LF power (mmHg^2)	-	-
Transfer function		
Frequency (Hz)	ns	-0.002 ± 0.001*
Coherence	ns	-0.006 ± 0.002*
Gain (ms/mmHg)	0.4 ± 0.1*	-0.7 ± 0.1*
Delay (s)	ns	0.5 ± 0.1*

*Table 2: Results of multi-level regression analysis using a generalized linear model. Regression analysis is performed according to: $f(t) = a + bx$, with a the offset, b the slope and t the time in days with corresponding to the time of occlusion for the UCO group. Values are expressed as estimate ± standard error. * $p < 0.01$, † $p < 0.05$ and ns = not significant.*
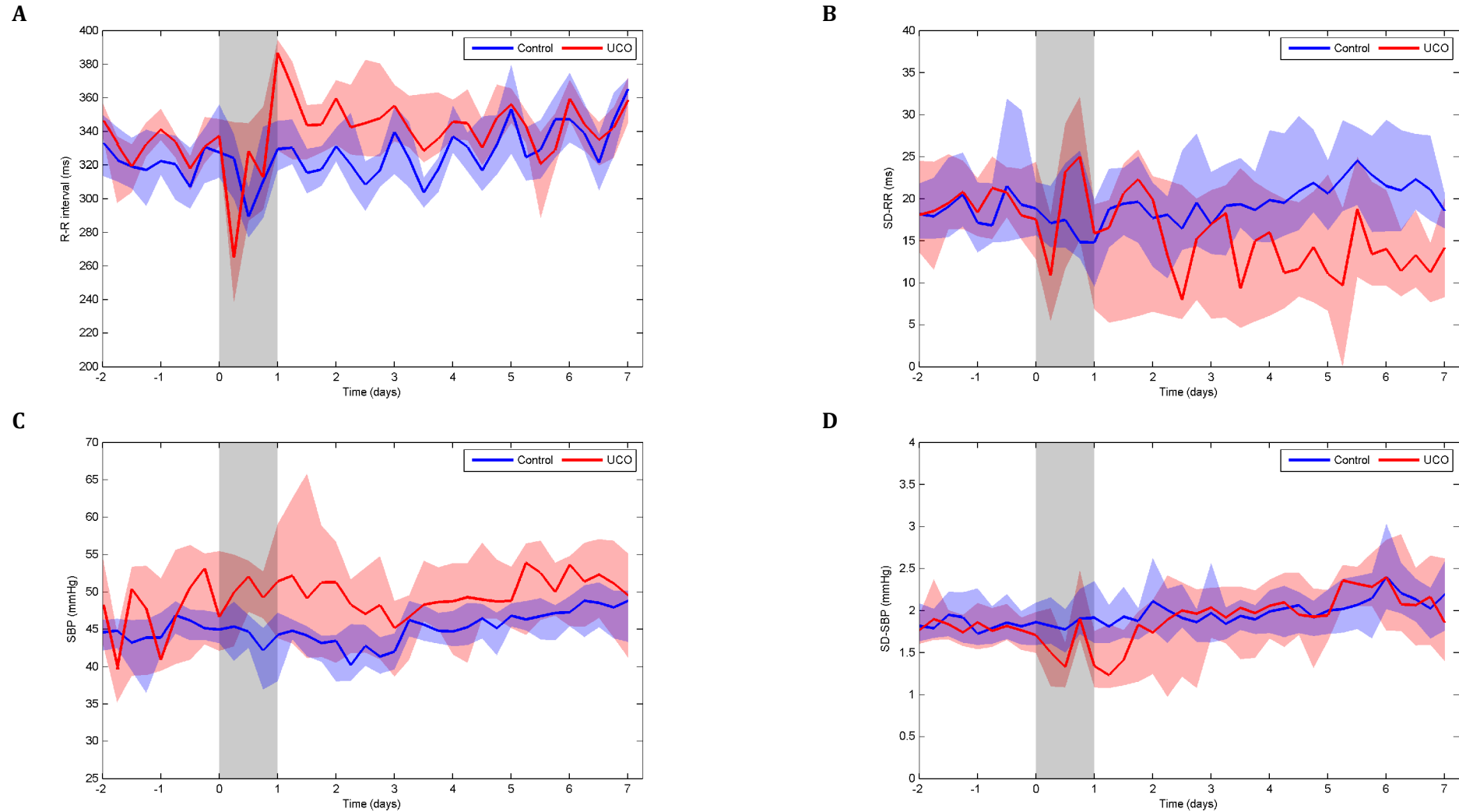
Figure 2: Plots of the longitudinal development of the R-R interval length (**A**), heart rate variability (HRV) (**B**), systolic blood pressure (SBP) (**C**) and blood pressure variability (BPV) (**D**). The x-axis represents time in days. Time t=0 corresponds with the time of the occlusion. The vertical grey bar indicates the 24-hour interval containing the UCO, which is discarded in the transfer function analysis. The blue and red lines indicate the control and UCO group, respectively. Data are shown as median (solid line) and interquartile range (shaded area) for each 6 hour period.
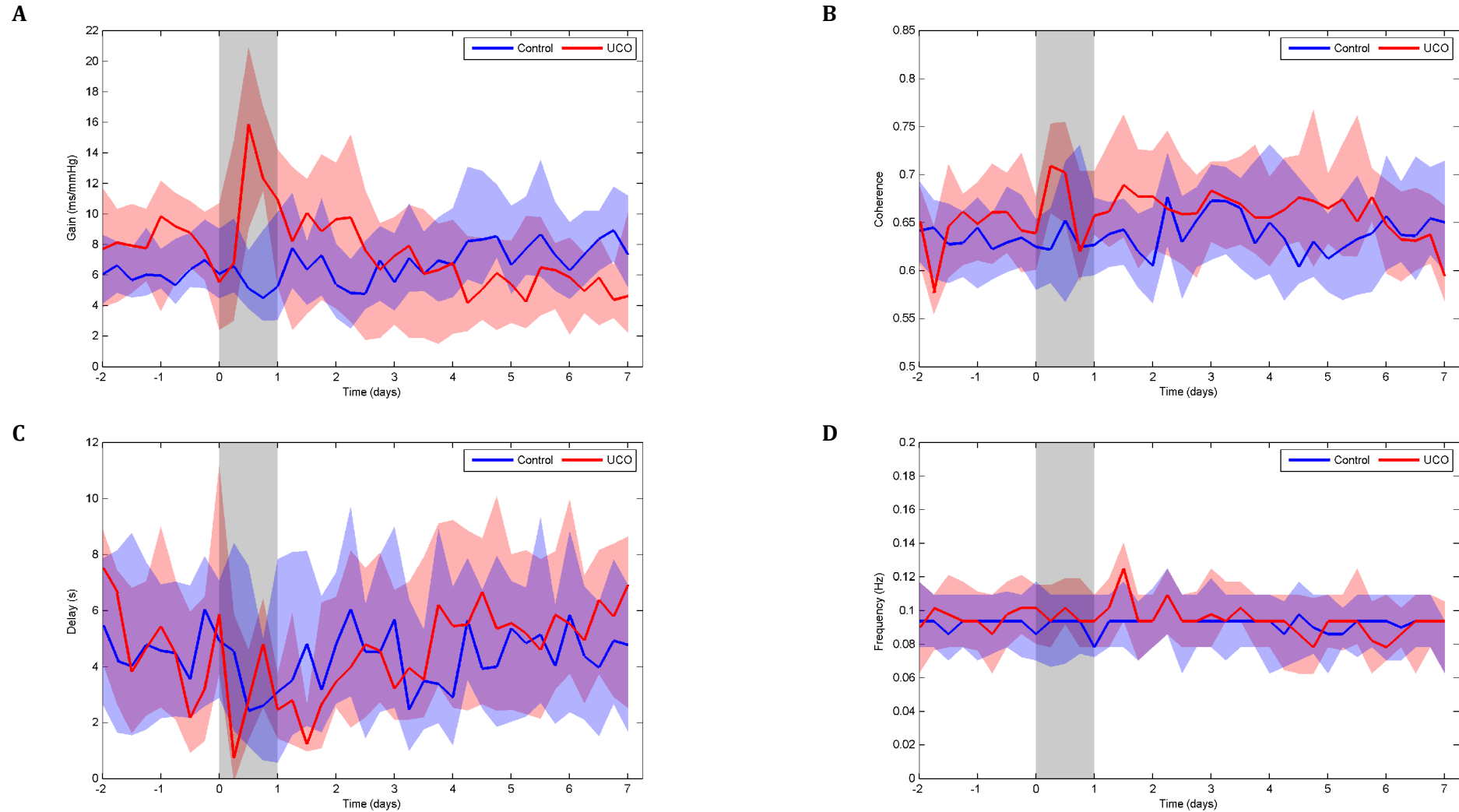
*Figure 3: Plots of the longitudinal development of the transfer gain (**A**), coherence (**B**), delay (**C**) and low-frequency (LF) band (**D**). The x-axis represents time in days. Time t=0 corresponds with the time of the occlusion. The vertical grey bar indicates the 24-hour interval containing the UCO, which is discarded in the transfer function analysis. The blue and red lines indicate the control and UCO group, respectively. Data are shown as median (solid line) and interquartile range (shaded area) for each 6 hour period.*

3.4 Discussion

The present study demonstrates that intra-uterine induced asphyxia in preterm fetal sheep results in long-term effects of baroreflex mediated fluctuations. In the first 7 days after prolonged umbilical cord occlusion, heart rate variability decreases dramatically and baroreflex sensitivity (BRS) decreases gradually to show lower values than controls by the end of the first week. These results suggest that intra-uterine asphyxia limits the baroreflex activity to buffer changes in SBP by adapting fetal R-R interval. As a consequence of this cardiovascular instability the preterm brain may be prone to blood pressure fluctuations, leading to disruption of the immature vascular architecture and neonatal encephalopathy (Perlman, 2009).

3.4.1 Acute cardiovascular response to fetal hypoxia

Our study is performed in an instrumented preterm fetal sheep model of 0.7 GA, equivalent to the neural development of 26 to 28 weeks human gestation (McIntosh et al., 1979). Prolonged umbilical cord occlusion resulted in fetal hypoxia and metabolic acidosis, showing the cardiovascular responses as seen in comparable studies (Bennet et al., 2009; Gunn et al., 2009). Immediately after occlusion a sustained bradycardia occurs throughout the occlusion. The reduction in ventricular output resulted in an initially gradual increase in blood pressure. During prolonged occlusion blood pressure fell to critical low values of approximately 10 mmHg. Following the end of occlusion, blood pressure and heart rate recovered rapidly with a brief period of hypertension and tachycardia. These observations are consistent with other fetal, neonatal and adult data on immediate hemodynamic changes after asphyxia (Rosenberg, 1988; Mallard et al., 1994; Hossmann, 1997; Pourcyrous et al., 1997; Bennet et al., 1999).

The involvement of a chemoreflex-mediated response to acute hypoxia has been studied in near-term fetal sheep (Bartelds et al., 1993; Giussani et al., 1993; Green et al., 1998). These studies show evidence that the carotid chemoreceptors provide the afferent limb of the reflex. The bradycardia is mediated through a muscarinic (parasympathetic) efferent pathway, as it can be blocked by atropine or vagotomy. The peripheral vasoconstriction is mediated through an α-adrenergic mechanism, mediated both neurally by a carotid chemoreflex and via hormonal release of the adrenal medulla. The fact that increase in arterial blood pressure during hypoxia is slow and gradual, whereas the bradycardia is rapid in onset and last only a few minutes, suggests that it is a chemoreflex rather than a baroreflex response.

3.4.2 Baroreflex function

In the present study we focuses on the baroreflex-mediated interactions between LF fluctuations of SBP and R-R intervals during the normoxaemic recovery state, hence after the immediate cardiovascular effects of acute hypoxia and asphyxia. We were interested in the long-term effect (0-7 days after the insult) of induced fetal asphyxia on baroreflex function, i.e. BRS and delay of the reflex arc. Note that under normoxaemic condition, baroreflex rather than chemoreflex is involved in the interactions between arterial blood pressure and fetal heart rate (Jensen et al., 1995).

The evaluation of baroreflex function is useful for the assessment of autonomic cardiovascular control (Rovere et al., 2008). Evaluation of baroreflex function by spectral methods is based on the concept that each spontaneous oscillation in blood pressure elicits an oscillation at the same frequency in R-R interval by the effect of arterial baroreflex activity. Two main oscillations are usually considered in human adults: one associated with baroreflex activity and fluctuations centred around 0.1 Hz (low-frequency, LF band; 0.04-0.15 Hz), and the other associated with respiratory activity (high-frequency, HF band; 0.15-0.40 Hz)(Camm et al., 1996). According to the transfer function method, BRS is calculated as the value of the transfer function modulus and phase (i.e. gain and delay) between SBP and R-R interval in the LF frequency, considering the coherence is ≥ 0.5 (Robbe et al., 1987). The coherence threshold is arbitrarily chosen to assume reliable transfer function estimates. Coherence

serves as the frequency domain analogue of r^2, the coefficient of determination. Like r^2, its value lies between 0 and 1, with values near 1 indicating a strong linear relation between the two series. Thus, the coherence level indicates the strength of the linear association and provides an estimate of variability in phase between two variables (e.g. blood pressure and R-R interval series). The level of 0.50 indicates a relation between two signals based on 50% shared variance.

The transfer function methodology has been used in several studies of human preterm infants (Andriessen et al., 2003; Andriessen et al., 2005). As the values of SBP and R-R intervals obtained from the fetal sheep were comparable with values found in preterm infants, the same spectral analysis methodology was followed. Transfer function analysis in this study showed high coherence values in the LF band (approximately 0.60), suggesting reliable estimates of transfer function gain and phase.

3.4.3 Long-term effects of asphyxia

During longitudinal monitoring of the UCO group, the LF transfer function gain gradually decreased over time, leading to a significantly lower gain at 7 days post-UCO compared to the control group. Consistent with this finding is the time-domain observation of a decreased SD-RR, while SD-SBP remains unchanged. In contrast, the LF transfer function delay between blood pressure variations and subsequent heart rate variations increased compared to the control group. The gradual decrease of spontaneous baroreflex sensitivity and the increase in delay between variations in heart rate and systolic blood pressure indicate that asphyxia results in a deregulation of the baroreceptor reflex arc.

Baroreflex-mediated heart rate control comprises a balance between two counter-acting branches of the autonomic nervous system: heart rate may be increased by sympathetic activity and decreased by parasympathetic activity (Jennekens et al., 2011a). Because of differences in neuronal architecture between these branches (long versus short neurons; type of neurotransmitter), rapid onset and offset of parasympathetic cardiac responses allow for beat-to-beat regulation of heart rate, whereas the slow temporal response to sympathetic stimulation precludes such dynamic regulation (Jennekens et al., 2011a). Therefore, each branch has a specific transfer delay associated with heart rate regulation. Furthermore, the transfer gain of sympathetic and parasympathetic heart rate regulation may differ (Ursino et al., 2003). The net effect of this regulation is reflected in spontaneous LF fluctuations of the R-R interval, driven by blood pressure perturbations. A decreased LF transfer function gain and increased LF transfer function delay as observed in our study may result from changes in the dynamics of the individual sympathetic and parasympathetic pathways, and/or from changes in the balance between these pathways.

As the parasympathetic effect on heart rate changes is fast compared to sympathetic effect, an increased delay may indicate a greater relative contribution of sympathetic regulation. This is supported by our finding that the total power of the R-R interval in the frequency range between 0.04 and 0.50 Hz, i.e. including both LF and HF band, mainly consists of power in the LF band at the seventh day post-UCO, whereas the HF band contribution, i.e. a measure for parasympathetic activity, is minimized. These results suggest that intra-uterine asphyxia limits the baroreflex activity to buffer changes in SBP by adapting fetal R-R interval.

The afferent signals from the baroreceptor output are projected on the nucleus of the solitary tract, which is located in the medulla region, to be processed and transferred to the blood pressure regulation effectors. George et al. studied sheep fetuses subjected to intra-uterine umbilical cord occlusion at 0.6 GA (George et al., 2004). They observed severe neuronal loss in the sub-cortical regions of the brain, specifically the medulla oblongata, for UCO duration of 30 minutes. Such an occlusion is comparable to the near-terminal occlusion applied in our study (Wassink et al., 2007). Although histological data was not available in our study, we assume that asphyxia induced comparable neuronal losses in the medulla oblongata. This neuronal loss may impact the processing of afferent nerve signals and therefore the baroreflex function, thereby decreasing regulation efficacy. Our analysis showed that this deregulation gradually increases over the course of several days. This finding also highlights the importance of study length. At 3 days after UCO, the end-point for some other studies (Bennet et al., 1999; George et al., 2004), baroreflex transfer function parameters of our UCO

group were not significantly different from the control group, potentially obscuring long-term asphyxia-induced functional loss. In contrast to the frequency-domain transfer function parameters, time-domain heart rate variability (SD-RR) was already significantly decreased at 3 days post-UCO, and gradually decreased further during the remainder of the study. This observation is in agreement with Ikeda et al., who showed that decreased long-term fetal heart rate variability at 24-72 hours of recovery after UCO showed to be an indicator of the severity of histological damage in the near-term fetal brain (Ikeda et al., 1998).

3.4.4 Maturational effects of baroreflex activity

Results of our study indicate that the baroreflex function matures during fetal life, as shown by the increase in LF transfer function gain for the control group between 0.75 and 0.77 GA. These results confirm findings by Shinebourne et al., who noted that the baroreflex function was active from approximately 85 days of gestation (0.6 GA), and the magnitude of fetal heart rate response to blood pressure changes increased towards term (Shinebourne et al., 1972). For human neonates, increasing baroreflex sensitivity has also been observed (Gournay et al., 2002; Andriessen et al., 2005). However, our results are in contrast to other studies, finding a decrease in baroreflex sensitivity during development (Blanco et al., 1988; Segar et al., 1992; Segar, 1997). Furthermore, there are a few studies that show no significant maturation of the baroreflex sensitivity (Maloney et al., 1977; Frasch et al., 2007).

There are two possible explanations for these contrasting findings. First, it is known that the different pathways of the baroreflex feedback system mature at different rates. For example, in preterm sheep of 0.7 GA there is no significant control by the renal sympathetic nerve, which regulates vascular resistance (Booth et al., 2009), whereas in the term sheep vascular resistance control is present (Segar et al., 1992). In our study, fetal sheep were instrumented at 0.7 GA, and maturational changes were studied between 0.75 and 0.77 GA. The studies by Maloney et al. (1977), Blanco et al. (1988), Segar et al. (1992) and Frasch et al. (2007) have little to no overlap in GA, or their results lack the temporal resolution required to compare results to our findings directly.

Second, the discrepancies may be due to methodological differences. Quantification of spontaneous baroreflex sensitivity by spectral methods and quantification by injection of drugs or aortic compression do not necessarily produce comparable results (Watkins et al., 1996; Maestri et al., 1998; Persson et al., 2001). Spontaneous variations in blood pressure are normally in the order of several mmHg, whereas experiments using invasive quantification methods generally study heart rate responses to larger blood pressure changes, e.g. 35-106 mmHg in 0.60-0.77 GA fetal sheep by Blanco et al. (1988). The heart rate response to blood pressure changes is non-linear, and can be characterized by a sigmoidal input-output relation with maximum responses around the (normal) operating point and decreased regulation capacity at the extremes (Ursino et al., 2003). Baroreceptor sensitivity is traditionally defined as the maximum slope of the sigmoidal function. Depending on the measurement conditions, i.e. deviation from operating point, the slope of the sigmoidal function differs in magnitude. Hence, baroreceptor sensitivity values obtained from invasive measurements may not be comparable to results from spontaneous baroreflex measurements. Furthermore, invasive methods may influence the characteristics of the closed-loop baroreflex feedback system.

3.4.5 Pathophysiological implications

There is evidence that reduced baroreflex sensitivity is a risk factor for several cardiovascular conditions, such as myocardial infarction (Rovere et al., 1998), chronic heart failure (Mortara et al., 1997; Pinna et al., 2005) and hemorrhage (Sykora et al., 2008) in human adult subjects. Reduction in fetal heart rate variability is associated with fetal hypoxia and academia in human preterm (Matsuda et al., 2003) and term fetus (Williams et al., 2003). However, despite the highly adverse outcomes of moderate to severe encephalopathy around birth the predictive value for cerebral palsy of abnormal fetal heart rate patterns is consistently weak (Nelson et al., 1996). Our study demonstrates a clear association between reduced baroreflex sensitivity and fetal asphyxia, indicating the additional

prognostic value of blood pressure measurements. For obvious reasons, direct measurement of fetal blood pressure in humans is not possible. Therefore, derived measures of fetal blood pressure may facilitate the quantification of fetal baroreceptor sensitivity.

3.4.6 Limitations

First, a limitation of this study is the relatively small number of fetal sheep subjected to asphyxia. Most fetuses recovered uneventfully the first days after surgery; however infection, low fetal weight, mortality and instrumentation problems resulted in later drop-out. Despite this limitation, acute cardiovascular responses were comparable to other studies (Bennet et al., 1999; George et al., 2004; Wassink et al., 2007). In addition, the statistical analysis revealed no significant baseline differences between UCO and control group, while significant changes in transfer function parameters were observed compared to the control group following the intervention. Therefore, we consider our results valid and representative for asphyxia in a fetal sheep model.

Second, our results indicate loss of neuronal function after induced asphyxia. However, because imaging and histological data were unavailable, the extent of neuronal damage is unknown.

Third, we focused on heart-rate mediated blood pressure regulation. Other components of the baroreflex feedback system, i.e. vasoregulation and myocardial contractility, were not taken into account. Other studies directly measured sympathetic nerve activity to estimate these regulation components (Booth et al., 2009). As these techniques are invasive, they are therefore not easily applicable in humans. Because of the availability of monitoring signals in the NICU, we focused on heart-rate mediated blood pressure regulation. Note that transfer function analysis in preterm infants (Andriessen et al., 2005) shows comparable results to our study. However, it remains a challenge to translate the application to human fetal monitoring of baroreflex function, as fetal blood pressure data are generally unavailable.

3.5 Conclusion

In conclusion, this is the first study to quantify baroreflex mediated heart rate response in a preterm fetal sheep model by transfer function analysis of R-R interval and SBP fluctuations, and to show long-term effects on baroreflex function after intra-uterine umbilical cord occlusion induced asphyxia. Our results show that intra-uterine asphyxia limits baroreflex efficacy to buffer changes in SBP by adapting fetal R-R interval after the first 7 days following umbilical cord occlusion. As a consequence, the preterm brain may be prone to blood pressure fluctuations, possibly leading to disruption of the immature vascular architecture and neonatal encephalopathy.

4   Basic concepts

In this section some basic concepts are clarified. The method used to determine the blood pressure regulation through the baroreceptor reflex – which is described later in this section – relies on two input parameters, the heart rate and blood pressure. The cardiac function is central to both of these, and the section starts with a description of the anatomy of the heart in general, before proceeding to the anatomical features found especially during fetal life. Heart rate is determined by analysis of the recordings of the electrical field that originates from the controlled contraction and relaxation of the heart during a cardiac cycle. Hence, we will explore the conductive system that allows the heart to contract in such a coordinated fashion, before proceeding to the actual generation of such a recording, referred to as the electrocardiogram or ECG, including some major features present therein.

Naturally, cardiac contractions influence blood pressure. The main function of the heart is to provide enough pressure so that even the most remote and minute blood vessels, especially tissue and organs will receive oxygen-rich blood. Blood pressure is therefore described, followed by a description of one of the important regulatory mechanisms for blood pressure – and the subject of this study – the baroreceptor reflex - or baroreflex - is mentioned, which is the subject of the next section. This is subsequently followed by a general overview of the spectral analysis of heart rate and blood pressure variability. The variations in heart rate and blood pressure occur in distinctive frequency bands, tied to different physiological mechanisms and this plays an important role in the method used to analyse baroreceptor sensitivity.

4.1   Heart anatomy

Information for this section was derived from several sources (Barnett, 2005; Hill et al., 2005; Iaizzo, 2005; Laske et al., 2005; Martinsen et al., 2005; Weinhaus et al., 2005; Ashworth, 2007).

In this study, we examine the baroreceptor sensitivity in the sheep model. The human heart and the ovine heart are quite similar, both anatomically and functionally. A schematic overview of the heart is shown in Figure 4. The heart consists of four separate chambers, the left and right atria and the left and right ventricles. The left and right parts of the heart are completely separated by a tissue called the
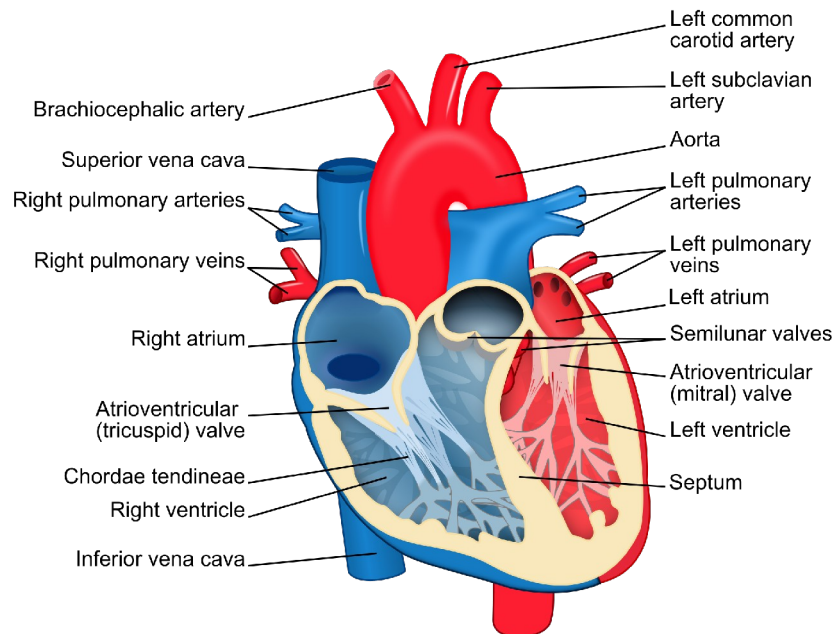

Figure 4: Schematic overview of the adult human heart with major components labelled. Blue marks those areas where oxygen-poor blood flows and red those where oxygen-rich blood flows.

septum, whereas the atrium and ventricle of each part are separated by an atrioventricular valve, allowing blood to flow from the atrium to the ventricle. These valves fill a gap in the central fibrous body, which is a tough layer of connective tissue that plays an important role by providing support for the heart during atrial and ventricular contraction as well electrically insulating the myocardium of the ventricles from the atria.

The right atrium of the heart receives oxygen-poor blood from the systemic circulation through the vena cava. By contracting the right atrium, blood is forced into the right ventricle through the tricuspid valve. A subsequent contraction of the right ventricle forces the blood through the pulmonary valve into the pulmonary arteries, which are part of the pulmonary circulation. Blood passes through the lungs where blood gasses are exchanged with the air present in the lungs. It is collected again in the left atrium. By contracting the left atrium, the now oxygen-rich blood travels through the mitral valve into the left ventricle. From here the blood will enter the systemic circulation yet again. A contraction of the left ventricle will force the blood through the aortic valve into the aorta.

The outer wall of the heart is composed of three layers, which are referred to as the endocardium, the myocardium and the epicardium, where the epicardium forms the external layer. The endocardium is the layer that is in direct contact with the blood and serves as a blood barrier, among other functions. The myocardium consists largely of cardiac muscle cells, which are responsible for the contraction of the different chambers of the heart.

4.1.1 Fetal and neonatal cardiac anatomy

The rudimentary human heart is formed very early in human life. At 22 days after fertilisation, and shortly after the neural tube closes, the heart, which is now a linear tube starts beating for the first time. In the following 6 to 7 days, the tube folds, placing the different sections of the heart in the right position. Technically, at this point in time, the heart is still a tube. The heart begins to divide itself, forming the ventricular septum between the two ventricles to separate these ventricles, forming the valves and a double septum that, after birth, separates the atria. At 9 weeks after fertilisation, this process is mostly complete.
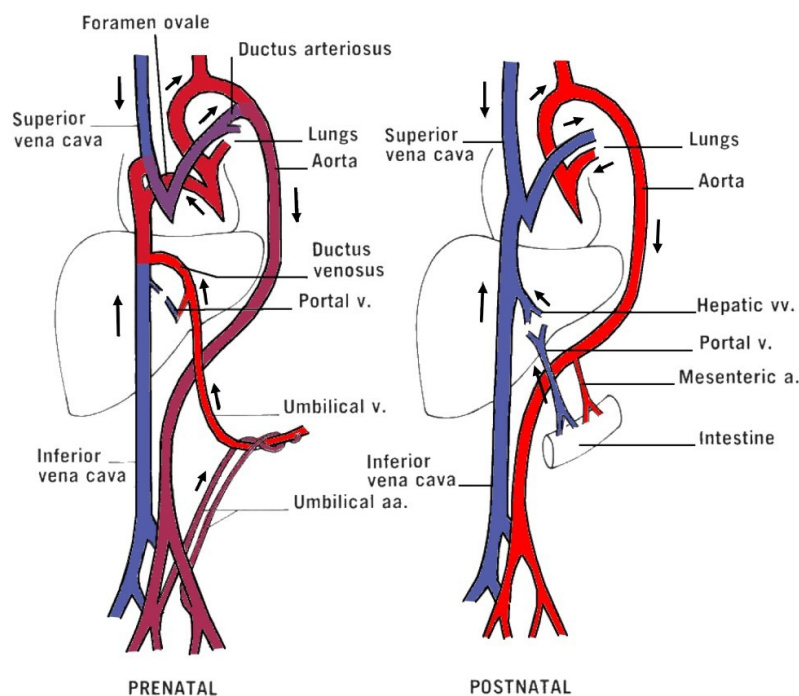

Figure 5: Circulation in the fetus and the neonate. The differences in coloration represent differences in oxygenation of the blood: red contains that most oxygen and dark blue the least-oxygenated blood.

The fetus receives nutrients and oxygen through the umbilical cord, and the circulatory system is different from that of the neonate, as is shown in Figure 5. Because the fetus is entirely reliant on an oxygen supply from the mother, the two atria are not completely separated before birth. The atria are connected by the foramen ovale as to shunt a portion of oxygen rich blood entering the heart from the right atrium directly to the left part of the heart and to avoid the pulmonary circulation. Several other features are present to facilitate the flow of oxygenated blood as well, such as the ductus arteriosus, which diverts a portion of the blood flow to the lungs to the aorta. After birth the foramen ovale and ductus arteriosus close, leading to the circulation found in neonatal and adult subjects.

4.1.2 Conduction system of the heart

For the heart to pump effectively, it is necessary that the contractions of the myocardial cells are performed in a organised fashion. The heart has a conduction system enabling it to do so, schematically shown in Figure 6. Although potentially any of the conductive cells of the heart can trigger a cardiac contraction, the cardiac contraction is usually initiated by a group of pacemaker cells. The discharge rate of these cells is in almost all cases higher than that of the rest of the myocytes. Other modified myocytes spread the electrical excitation generated by the pacemaker cells, even though they might be able to function as pacemakers themselves.

The primary pacemaker of the heart is the sinoatrial (SA) node, which is positioned at the apex of the right atrium. The myocardiac cells that make up this piece of tissue normally generate excitations between the 60 and 100 times per minute in adults. The actual heart rate generated by the SA node is modified by sympathetic and parasympathetic nerves, hormones and the chemical composition of the surrounding environment, such as the oxygen level of the blood and nutrients present therein.

The excitation generated by the sinoatrial node travels through three different tracts to another node, which is called the atrioventricular node. As this excitation travels through these tracts, the depolarisation spreads through surrounding cardiac muscle, causing the contraction of the atria. The central fibrous body prevents the depolarising wave from spreading to the ventricles. The AV node extends downwards into ventricles through the bundle of His. The bundle splits into the right and left bundle branches, which enable propagation of the excitation into the right and left ventricles respectively. Further down, both branches split into a network of Purkinje fibres, which enables the surrounding cardiac muscle to contract rapidly. This system allows the cardiac muscle to contract systematically, and to propel blood into the aorta and the pulmonary arteries from the left and right ventricles respectively.

Myocytes have special features that allows for rapid propagation of the excitation. They are connected
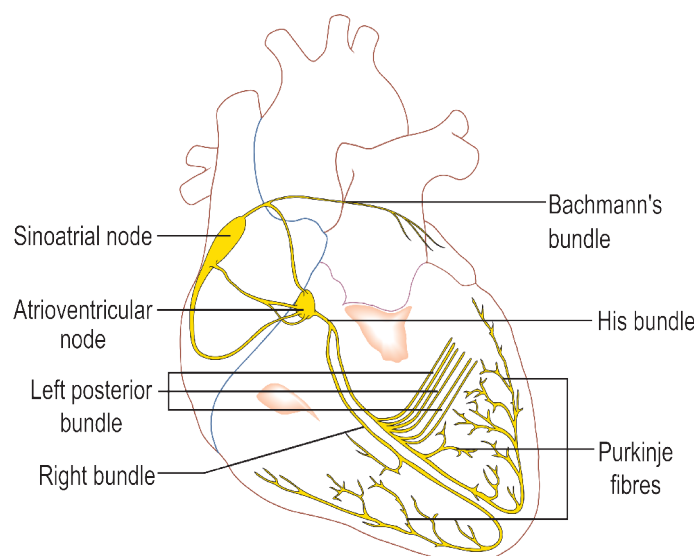

Figure 6: Electrical conduction system of the heart .

end-to-end by structures that are known as intercalated disks. These disks consists of the sarcolemma, or muscle cell membrane, of the muscle cells. They join the cells together by mechanical attachment and protein channels. The electrical connection between the cells is formed by a specific protein, connexin, and is known as a gap junction. These channels allow ion movements between cells.

4.1.3 Cardiac action potentials

The resting membrane potential of cardiac muscle cells is approximately -90 mV. The membrane potential describes the potential difference between the intracellular and extracellular space. The potential is predominantly caused by the differences in the concentrations of potassium, sodium, chloride and calcium ions in the extracellular and intracellular space and by the membrane permeabilities for these respective ions. An action potential is generated when the membrane potential becomes more positive, approximately at -60 mV, setting in motion the Hodgkin cycle. The potential difference causes sodium channels to open, allowing sodium ions to flow into the cell. This is referred to as phase 0. The membrane depolarisation opens the voltage-gated calcium and closes the potassium channels, allowing calcium ions to enter the cell while decreasing the flow of potassium ions exiting the cell. As the sodium channels begin to close, an initial repolarisation occurs, which is called phase 1. Phase 2 is a plateau where the influx of calcium ions is balanced by the small efflux of potassium ions from the cell. The cell repolarises - phase 3 - when the voltage-gated potassium channels open and the calcium channels close, allowing potassium to exit the cell more easily. After repolarisation the cardiac cell enters phase 4, where it is at rest. Sodium ions leave the cell , and potassium ions enter the cell.

The above is generally true for so-called fast-response cardiac cells such as the cells forming the atrial and ventricular muscle and Purkinje fibres. Slow-response cells, such as the sinoatrial and atrioventricular cells, behave differently. During the resting phase, the membrane potential spontaneously increases slowly. The underlying mechanisms are thought to be (1) a progressive decrease in the membrane permeability for potassium ions, (2) a minor increase in the membrane permeability for sodium ions and (3) a general increase in membrane permeability for calcium ions, when compared to fast-response cardiac cells. The action potential for slow-response cells furthermore lacks the steep depolarisation slope and the plateau phase is far less pronounced. The slowly increasing membrane potential is the cause of the spontaneous generation of action potentials in pacemaker cells. The time course of the membrane potential of both fast and slow response cardiac cells is shown in Figure 7.

Myocytes have a refractory period, where the membrane is unresponsive to further external stimuli after initial depolarisation. From the start of phase 0 with the onset of the membrane depolarisation until approximately halfway the repolarisation phase, the cell is in the absolute or effective refractory period and cannot generate a new action potential. The period after this and leading up to the return of the membrane potential to its resting value is the relative refractory period. A new action potential can
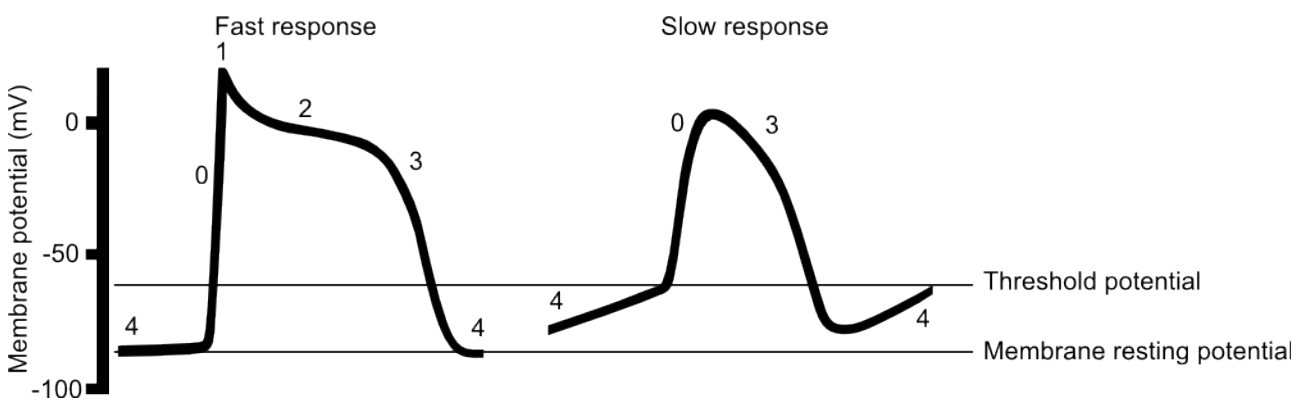

Figure 7: Membrane potential for fast and slow response cardiac cells. The numbers represent different phases of the action potential, namely membrane depolarisation (0), initial repolarisation (1), plateau (2), repolarisation (3) and rest (4). Both the membrane resting potential (± -90 mV) and threshold potential (± -60 mV) have been marked. Based on Laske et al. (2005).

be generated during this period. This implies that the heart rate has a maximum.

4.2 The Electrocardiogram

Information for this section was derived from Dupre et al. (2005) and Sörnmo et al. (2005).

Earlier we described that, in healthy subjects, the generation of an electric pulse by the sinoatrial node sets in motion a process which sees this activation propagated into both atria and afterwards into the ventricles, whilst setting in motion the coordinated depolarisation of the cardiac muscle tissue. It is possible to describe why this activation is actually propagated. The cell membrane potential of a myocyte at rest is known to be at -90mV. By raising this potential above -60mV, the cell membrane quickly depolarises by the opening of voltage-gated ion channels, allowing positively charged ions to enter the cytoplasm. This movement of positively charged ions into the cell automatically lowers the concentration of these ions in the environment near to the cell. Because locally the potential of the extracellular fluid is now lowered with regards to the extracellular fluid in general, this causes a flow of charged particles to this location, lowering the membrane potential difference of nearby cells. This is further aided by the gap junctions, which allow the positive ions inside a myocyte to move to the neighbouring myocyte, thereby causing the membrane potential difference to decrease further, and depolarising these cells as well.

Because the depolarising wave travels through the heart in a very coordinated fashion, it is possible to measure the generated multipole field using electrodes. The incredibly complicated field generated by this wave is often conceptually simplified and replaced by a vector to facilitate an understanding of the mechanisms at work. This vector is known as 'net dipole', 'the electrical axis of the heart' or 'mean electrical vector'.

The electrodes used to measure the net dipole can be placed both on the skin or invasively. Measurements are then performed using an electrode with another electrode or a combination of electrodes as the reference channel. One of the earliest electrocardiograms (ECG) was recorded using electrodes positioned on the right and left arm and the left leg, forming what is now known as Einthoven's triangle, named so after the Dutch scientist who first described it (Einthoven, 1912). This remains one of the conventional electrode placements and can be used to illustrate some important aspects related to the interpretation of the ECG. In Figure 9 we observe that each one of the bipolar leads measures the magnitude of the projection of the net dipole along the vector between two electrodes.

An ECG has several features related to distinct phases in the cardiac cycle, as shown in both Figure 8 and 9. These are the P wave, the QRS complex and the T wave. The P wave denotes the depolarisations of the atria. The QRS complex is caused by the ventricular depolarisation and the T wave is related to the subsequent repolarisation of the ventricles. The R peak is often the most notable feature of the ECG. It is a sharp and narrow peak and is often used to determine heart rate by detecting R peaks and calculating the interval between subsequent peaks.
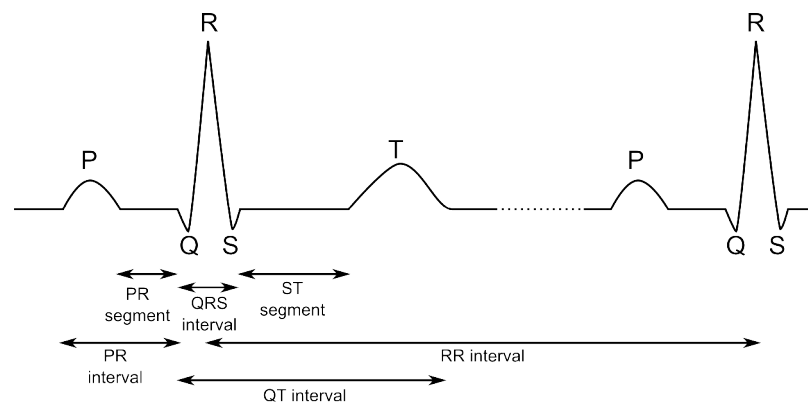
Figure 8: A typical ECG waveform for one and a half heart period.

Progress of depolarisation
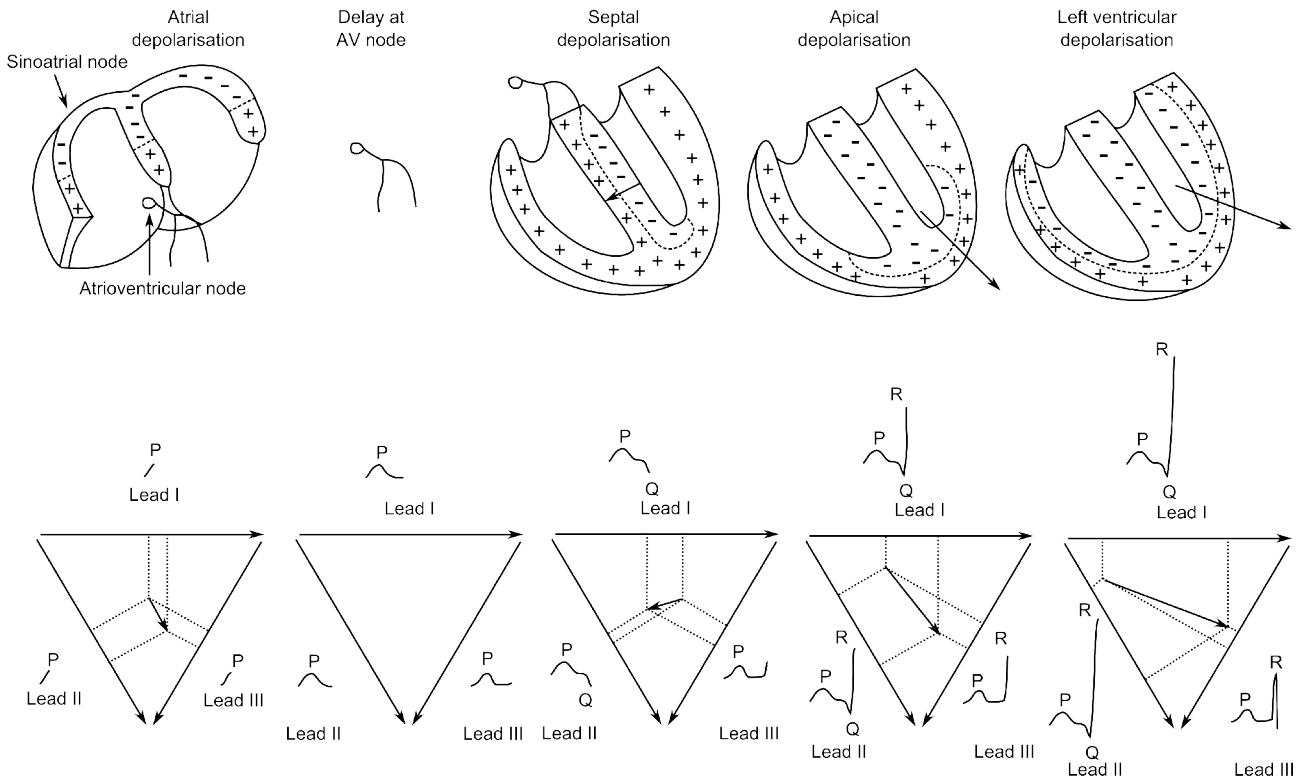
End of depolarisation and repolarisation
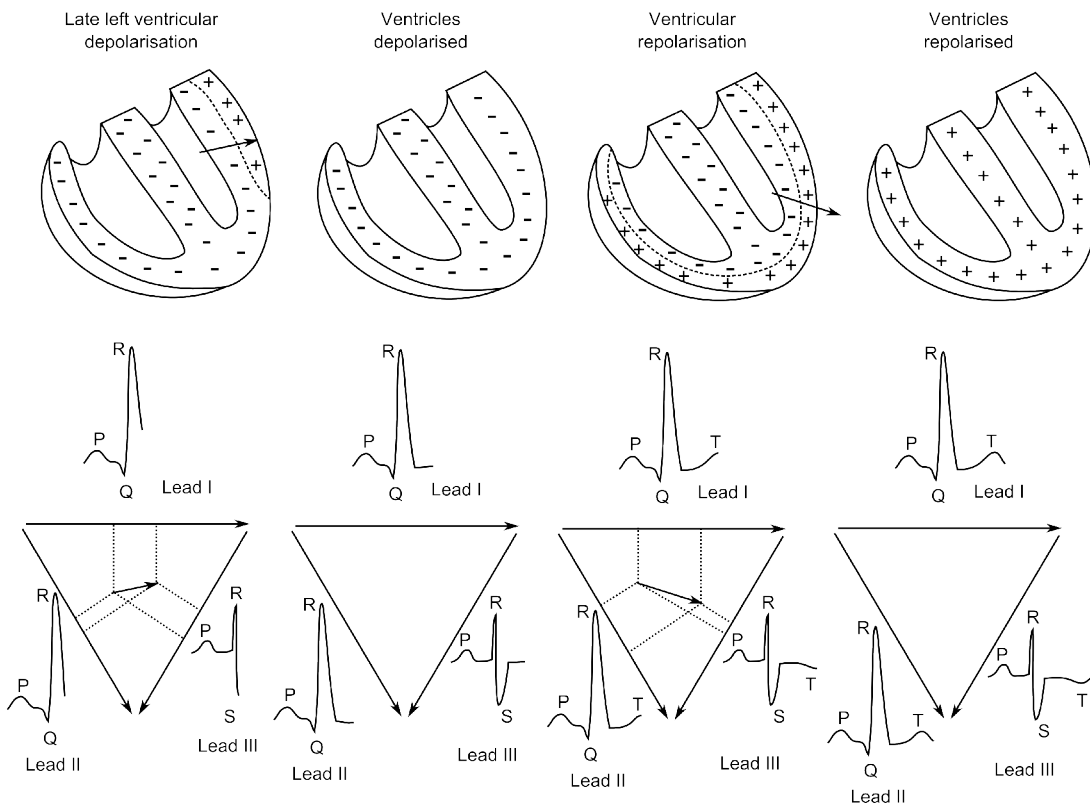
Figure 9: Generation of the ECG in the Einthoven leads during one heart period. Each heart shows the charge seperation in the myocardium, with the charge at the depolarisation front as reference. The resulting net dipole vector is drawn and projected on the limb leads of the Einthoven triangle and the resulting ECG is drawn for each lead. Figure adapted from Dupre et al. (2005).

22
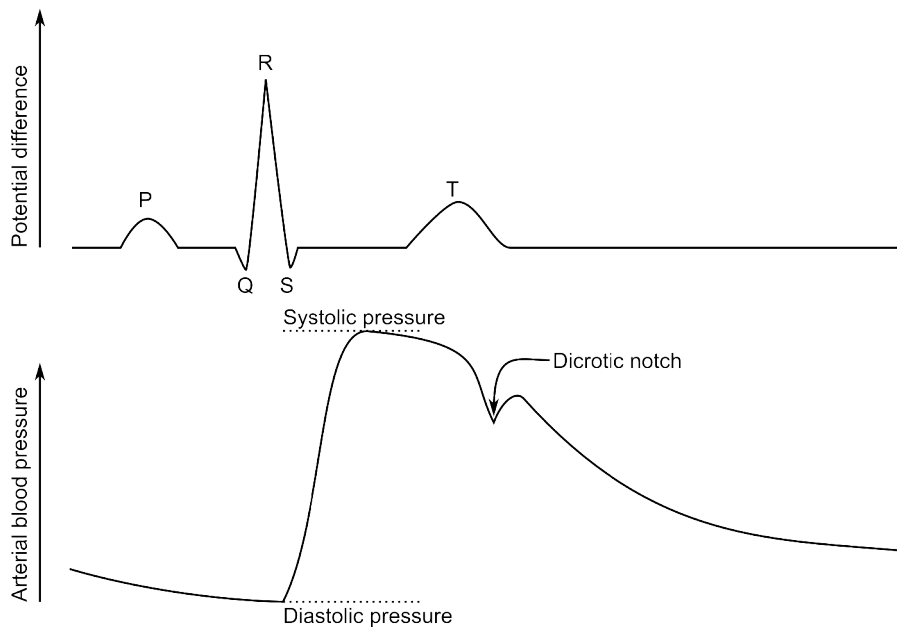
Figure 10: ECG and blood pressure for one heart period. Arterial pressure rises at the opening of the aortic valve. When the aortic valve closes, it causes the dicrotic notch in the arterial blood pressure. Figure adapted from Bojanov (2005).

4.3 Blood pressure

Information contained in this section is derived from Bojanov (2005).

Contractions of the left ventricle produce measurable pressure waves in the arterial part of the systemic circulation. The actual pressure generated depends largely on the cardiac output and the systemic vascular resistance. The systemic vascular resistance itself is generated by the progressive bifurcation of the arteries into smaller vessels and is maintained by the limited compliance of arterial walls to changes in pressure.

A blood pressure wave has some distinctive features, as seen in Figure 10. The maximum pressure, the peak of the pressure wave, is called the systolic pressure, whereas the lowest pressure is referred to as the diastolic pressure. Dependent on the measurement method, one can also find a dicrotic notch after the peak, which is generated by closing of the aortic valve and delayed response by blood inertia.

Maintaining a certain blood pressure is vital to the survival of the organism. Insufficient pressure prevents adequate perfusion of peripheral tissue. This leads to a deficiency of oxygen and nutrients and an accumulation of waste products in those tissues. Continuing deprivation from oxygenated blood causes tissue damage. In contrast, blood pressures that are too high can damage the vascular system, leading to e.g. hemorrhage (Chobanian et al., 2003).

4.4 Baroreflex

Information contained in this section is derived from Fitzgerald et al. (2005).

Regulation of systemic blood pressure is vital for physical well-being. The baroreflex is one of the mechanisms employed to maintain the blood pressure homeostasis. The baroreflex counteracts changes in blood pressure, and is often described as a negative feedback loop.

Distension of blood vessel walls is monitored by stretch-sensitive sensory neurons. Baroreceptors specifically refer to these neurons in areas where there are concentrated, i.e. the aortic arch and the carotid sinuses of the left and right internal carotid arteries. The baroreceptors are especially sensitive to short-term variations in blood pressure – long-term changes in blood pressure seem to be predominantly regulated by different mechanisms (Akselrod et al., 1985; Camm et al., 1996).
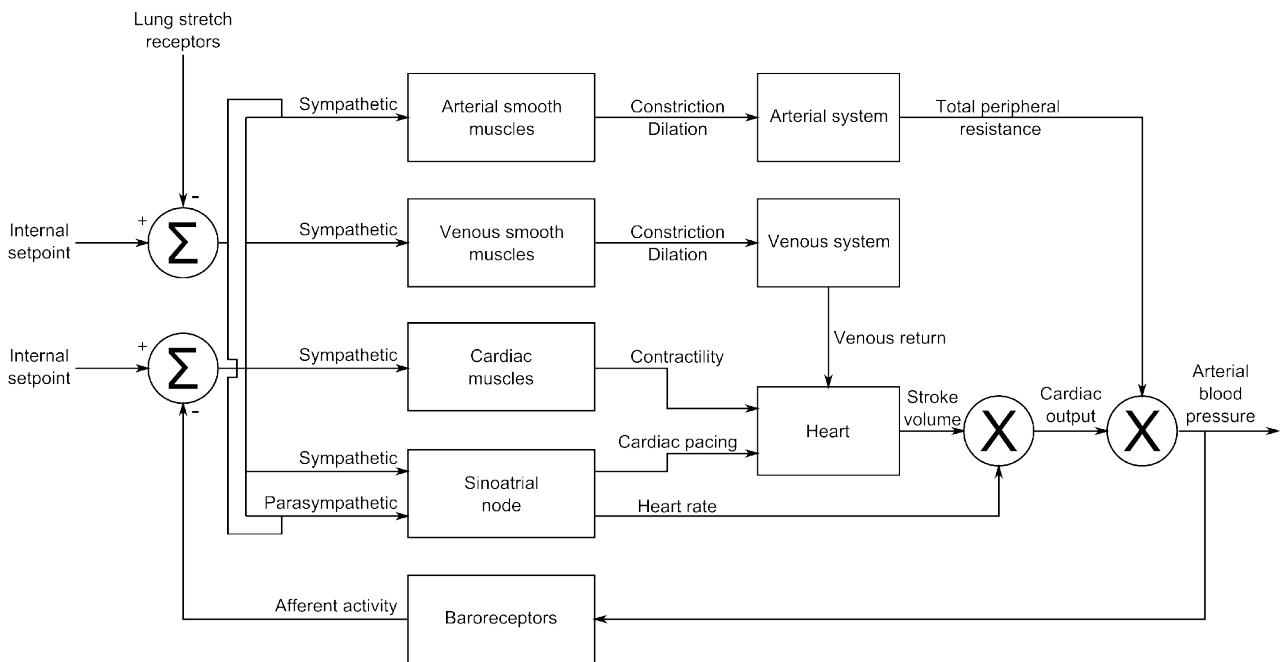
Figure 11: The closed loop control of systemic arterial blood pressure, consisting of a negative feedback by baroreceptors and pressure regulation through the four effectors (arterial and venous smooth muscles, cardiac muscle and the sinoatrial node). The arterial smooth muscles and the sinoatrial node are also influenced by respiration. Adapted from Dat (2010) , who based it on ten Voorde (1992) .

Action potentials triggered in the baroreceptors are relayed to the brainstem, and are transferred to neurons in the nucleus of the solitary tract in the medulla oblongata. Together with action potentials from lung stretch receptors, the action potentials from the baroreceptors form the input of the baroreflex. The output of the negative feedback system is the arterial blood pressure. There are four main effectors, namely the sinoatrial node, which influences cardiac pacing, cardiac muscle contractility, which affects both stroke volume and pressure, the smooth arterial muscles, which directly influences peripheral resistance, and the smooth venous muscles, which influences venous return. An overview of the various pathways and effectors is shown in Figure 11 and Figure 12.

Assessment of the baroreflex function, in specific of heart rate mediated blood pressure control, can be obtained through quantification of baroreceptor sensitivity. Baroreceptor sensitivity may simply be defined as the change in heart rate (or R-R interval) in response to changes in arterial blood pressure, and may be estimated from (time-domain or spectral) analysis of spontaneous fluctuations in R-R
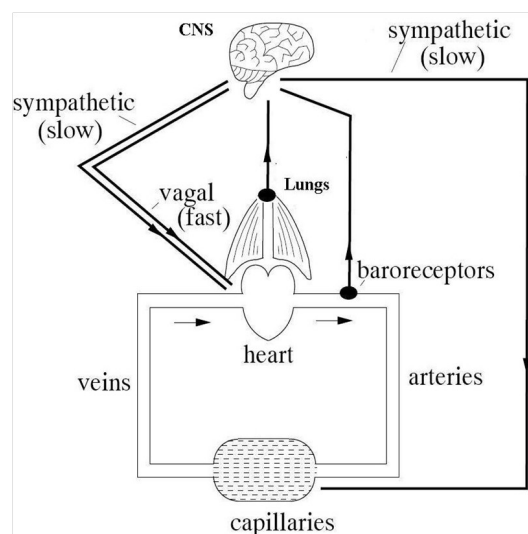
Figure 12: Schematic overview of the baro-receptor reflex. Adapted from Dat (2010).

intervals and blood pressure (de Boer et al., 1985; Robbe et al., 1987; Honzíková et al., 1992; Head et al., 2001; Ursino et al., 2003; Laude et al., 2004; Rovere et al., 2008). This study uses the transfer function method pioneered by Robbe et al. (1987), who used this method to study the linear coupling between the SBP and the heart rate in the LF band to measure the baroreflex sensitivity and who compared the results to that of invasive measurements and found these to be similar.

4.5 Spectral analysis of heart rate and blood pressure variability

The variations in heart rate and systolic blood pressure are known to be linked to different physiological processes. Spectral analysis is one of the methods employed to study these variations. The Task force of the European Society of Cardiology and the North American Society of Pacing and Electrophysiology (Camm et al., 1996) defined the bands of frequency components of heart rate variability for adult human subjects:

- Ultra-low frequencies (ULF) less than 0.003 Hz: variations include those caused by the circadian rhythm.

- Very-low frequencies (VLF) from 0.003 – 0.04 Hz: variations induced by thermoregulation and humoural systems (Taylor et al., 1998).

- Low frequencies (LF) from 0.04 – 0.15 Hz: variations related to baroreceptor activity. This is influenced by both sympathetic and parasympathetic activity (Japundzic-Zigon, 1998).

- High frequencies (HF) from 0.15 – 0.4 Hz: variations related to baroreceptor activity. Unlike LF, these are influenced by parasympathetic activity only.

Variations in systolic blood pressure are not as well-defined, with usually the HF band being dependent on the model studied. One definition is by Parati et al. (1995):

- LF from 0.07 – 0.15 Hz: variations caused by sympathetic influence of the baroreflex on vascular dilation and contraction and heart rate (Japundzic-Zigon, 1998) .

- HF from 0.15 – 0.5 Hz: usually associated with the mechanical effects of respiration (Japundzic-Zigon, 1998) as well as the feedback from HF heart rate band to blood pressure (Akselrod et al., 1985; Saul et al., 1991).

These values are found in adult humans. Both LF and HF bands are quite similar in fetal sheep (Lumbers et al., 1999; Jardine et al., 2002; Li et al., 2004; Gaillot et al., 2005; Batchinsky et al., 2007; Frasch et al., 2007). Although the HF-bands are less pronounced due to a lack actual respiration in fetuses, they do exhibit fetal breathing movements.

5 Methodology

This section explains part of the methodology summarised in the previous section and describes the implications of our involvement in two studies carried out in collaboration with Maastricht University. With regards to the methods, the R-peak and the systole and diastole peak detection algorithms are described extensively, followed by a concise description of spectral analysis and the transfer function method.

5.1 Cooperation with MUMC on the subject of fetal monitoring

Our first involvement was in the study by Matthias Seehase, see 'Early propofol administration to the maternal-fetal-unit improved fetal EEG and reduced cerebral apoptosis in late preterm lambs suffering from severe asphyxia.' in Appendix II for further details. In earlier work carried out within the medical physics group at Máxima Medical Centre, algorithms were developed to analyse electroencephalograms (EEG), which potentially could provide further evidence for the presence of cerebral damage.

Upon analysis of the preliminary data from Maastricht University, one of the first things noticed was the difference in spectral power between the separate leads on the right and left hemisphere. While some difference is obviously to be expected, the spectral power in the right hemisphere was consistently greater than in the left hemisphere for all subjects. Aside from this, the length of data recorded usually was in the order of several minutes, which was sufficient for the study; however longer sections of data are preferable, not in the least because this allows the researcher to study evolving processes that take place on the scale of hours and also because artefact reduction in EEG involves discarding segments of data.

We were involved early on in the study carried out by Reint Jellema, see Publication Reint in Appendix II for further details. Our findings and remarks in the previous study had implications on the ongoing experiment. This did not pertain to the actual design of the study, but rather to data acquisition. Based on the finding of discrepancies between the leads of the right and left hemisphere, a faulty amplifier was found and replaced. Filter settings were adapted to prevent filtering of the low-frequency δ-1 EEG-band (0.5 – 1 Hz). Likewise measurement times were increased from minutes to hours and later on to continuous measurements for the duration of the experiment. This was feasible because the subjects were permanently instrumented.

5.2 Analysis and algorithms

Our initial work on the study of Reint Jellema was on EEG analysis. The same subjects were also instrumented to record lead I and lead II of the Einthoven triangle as well as both arterial and amniotic blood pressure, which allowed us to analyse the baroreceptor sensitivity through the transfer function method. The transfer function method requires us to process both ECG and blood pressure to find the heart rate and systolic blood pressure respectively.

We will describe the various algorithms and methods used for analysis starting with the R-peak detection and systolic pressure detection algorithms. After this, we will look into the spectral analysis of the heart rate and blood pressure variations as this ties into the transfer function method described more in-depth at the end of this section.

Our final remark before exploring the R-peak detection algorithm is on data management. Data was sampled at 1000 Hz for 8 channels – 4 EEG, 2 ECG and 2 blood pressure channels. As the desktop computer provided at the MMC had a 32-bit copy of Windows XP installed, there was a hard limit on the amount of memory that can be allocated to a single file and to useable RAM space as well. Early on it proved quite easy to hit this hard limit on RAM space by running some simple algorithms in MATLAB, which by necessity was a 32-bit version as well. Therefore, the very first thing done was to split the data files into more manageable 30 minute segments, while also separating EEG data from the

cardiovascular data to reduce load times from an external hard-drive as much as possible. Reduction of load times was necessary as it was found that the algorithms would actually spend a large amount of time loading the files from the connected external hard-drive.

5.2.1 R-peak detection

Because of experimental constraints, the R-peak detection algorithm had to have the following characteristics:

- Computationally fast – In total, 2252 hours – 93 days – of data had to be analysed. A computationally fast algorithm should reduce analysis times significantly to several days at most.

- Robust – Detection in the presence of artefacts should be reliable.

- Precise and sensitive – The algorithm should be able to find peaks accurately, without introducing extra peaks or missing peaks.

- Adaptive (slow) – The algorithm can handle slow variations in peak positions.

- Adaptive (event) – The algorithm can handle sudden events that cause R-R intervals to increase suddenly, such as the onset of UCO.

- Off-line analysis – Real-time analysis capabilities are not needed. Data is gathered for analysis during the study and not immediately processed.

- Implementable as a subroutine – Data was stored in separate files. Subsequent analysis without human intervention is needed to speed up processing and implementation as a subroutine enables us to do so.

An algorithm was written with the characteristics mentioned above. It is based on the following empirical observations:

1. R-peaks are events of short duration compared to other features in the ECG.

2. R-peaks are events of high amplitude.

3. R-R intervals show only limited variation.

4. R-peak amplitudes show only limited variation.

The algorithm can be divided into two parts, training and adaptive detection, which will be described later in this section. First, the basic signal transform will be described.

5.2.1.1 Basic signal transform

The algorithm transforms the raw ECG signal to facilitate detection. As observed earlier, the R-peak is both short in duration and of high amplitude in comparison to other ECG features. This has several implications. The first is that if one is to perform a Fourier analysis of the R-peak, Fourier coefficients corresponding to low frequencies will be relatively small. Secondly, the second derivative of the signal shows large fluctuations around the R-peak.

The raw signal is first filtered using a 4th order Butterworth bandpass filter between 20 and 80 Hz and an IIR 50 Hz notch filter. These settings were empirically chosen as they suppressed most features aside from the R-peak.
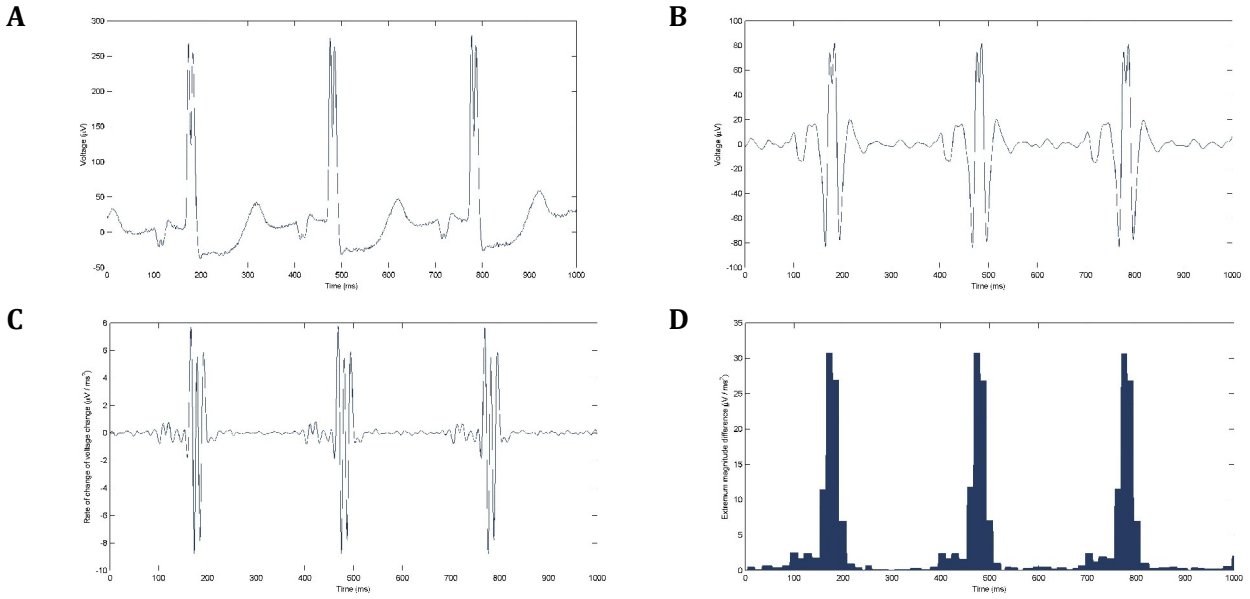
*Figure 13: Transformation of the ECG signal. **A**: Original ECG signal. **B**: ECG after filtering with bandpass and notch filter. **C**: Second derivative of filtered ECG. **D**: The magnitude difference representation derived from the second derivative of the filtered ECG. Note that the vertical axes are scaled differently. This has no consequences for the subsequent analysis.*

The second derivative of the filtered signal is then calculated by discrete convolution of the signal with a (1,-2,1) vector, which are the coefficients for the discrete implementation of the second derivative $f^{(2)}(i) = f(i-1) - 2f(i) + f(i+1)$. The second derivative representation has the advantage that the actual R-peak is represented as either a local maximum or a local minimum, referred to as p_0, flanked by two nearby local minima or local maxima respectively, referred to as p_{-1} and p_1, depending on the direction of the original R-peak. Within the period of one heartbeat, moreover, the magnitude difference $s_{0,ante}$ between the peak p_0 and p_{-1} and the magnitude difference $s_{0,post}$ between p_0 and p_1 exceed the differences $s_{n,ante}$ and $s_{n,post}$ between other extrema $p_{2n,n\neq0}$ and p_{2n-1} and p_{2n+1}. For threshold purposes, the signal is represented by setting the magnitude w between p_{2n-1} and p_{2n+1} as $w_n = s_{n,ante} + s_{n,post}$ for each local maximum or minimum n - depending on the direction of the R-peak in the original signal representation.

The transformation of the original ECG signal to the magnitude difference representation (MDR) is shown in Figure 13.

5.2.1.2 Peak direction

The R-peak has a certain direction in the lead analysed, either positive or negative. The algorithm requires the actual direction for optimal detection performance.

To detect the direction of the R-peak a subset of the ECG dataset is transformed as described earlier, once assuming the R-peak is positive and once assuming it is negative, generating two different representations. The R-peaks in the correct representation will have a higher magnitude. Because at this stage the algorithm does not actually detect R-peaks, it determines the 98th percentile, as the R-peaks in the signal are responsible for <5% of the temporal content – though the actual percentage depends on heart rate. The representation with the highest value for P_{98} is regarded as the optimal representation.

5.2.1.3 Training

The algorithm makes use of observations 3 and 4, which state that R-R intervals and R-peak amplitudes show only limited variation. However, it does not a priori assume values for the R-R interval and the R-peak magnitude – now represented in the magnitude difference representation by the magnitude w_n. However, for the algorithm to be adaptive and accurate, an initial estimate for both values is necessary. These are calculated during the training phase.

The direction of the R-peak has been determined previously. The first 20 seconds of data are analysed by transforming the original signal to the MDR, and determining the 95th percentile. Sections of the data where magnitude $w > p_{95}$ are marked. Each section contains a local maximum, which is considered to represent the interval in which the R-peak is located. The position of the actual R-peak is found in the original signal by analysis of the data in the interval. The R-peak itself is a maximum or minimum, depending on its deflection, and is easily detected because it is necessarily the only maximum or minimum in this interval.

Both the position v of the R-peak and the magnitude w are stored for the first 10 R-peaks. These values constitute the training data.

5.2.1.4 Adaptive detection

While training the algorithm the position v and the magnitude w were determined for 10 R-peaks retrospectively. In the adaptive detection part, this is done prospectively. Because of observation 3, the next R-peak is likely to be located one R-R interval after the previous detected peak. The actual R-R intervals are calculated later on, but as a surrogate the median $v_{median, RR}$ of the peak-to-peak distances $v_{i, RR} = v_i - v_{i-1}$ of the 10 previous peaks is used.

Observation 3 suggests that there is little variation in R-R intervals, not that there is no variation. Designating the next peak by adding the median peak-to-peak distance to the last known peak is an imprecise method, because there is a spread in the length of R-R intervals. The use of a window function is an obvious choice. The algorithm uses the following window function:

$$
g(n) = \begin{cases}
0 & 0 < n < n_{refrac} \\
0.5 - 0.5 * \cos\left(\pi\left(\dfrac{n - n_{refrac}}{n_{est} - n_{refrac}}\right)\right) & n_{refrac} \leqslant n < n_{est} \\
1 & n = n_{est} \\
0.5 + 0.5 * \cos\left(\pi\left(\dfrac{n - n_{est}}{n_{length} - n_{est}}\right)\right) & n_{est} < n \leqslant n_{length}
\end{cases} \quad , \tag{1}
$$

where n is the sample number, counted from the previous peak, n_{refrac} the number of samples in the AV nodal refractory period, for which a low value of 120 ms was used – compared with the values in literature e.g. (DuBrow et al., 1976; Janse et al., 1976; Mehta et al., 1981) – to prevent early beats from remaining undetected due to windowing, n_{est} the median of peak-to-peak distances $v_{median, RR}$ and thus the most likely position of the R-peak, n_{length} the total sample length of the subsection studied, being defined as $n_{length} = 1.3\, v_{median, RR}$.

The window function will be applied to a subsection of data in the MDR, starting at the position of the last detected peak v_i and ending at $v_i + n_{length}$. The window length is thus as long the data subsection. A modified representation of MDR is derived by calculating the pointwise product of the window and the data subsection, that is, if $f(n)$ is the data in the subsection and $g(n)$ is the window function, then $h(n) = (f(1)g(1), f(2)g(2), ..., f(n_{length})g(n_{length}))$ is the series of datapoints in the modified MDR. The process described above is shown in Figure 14.
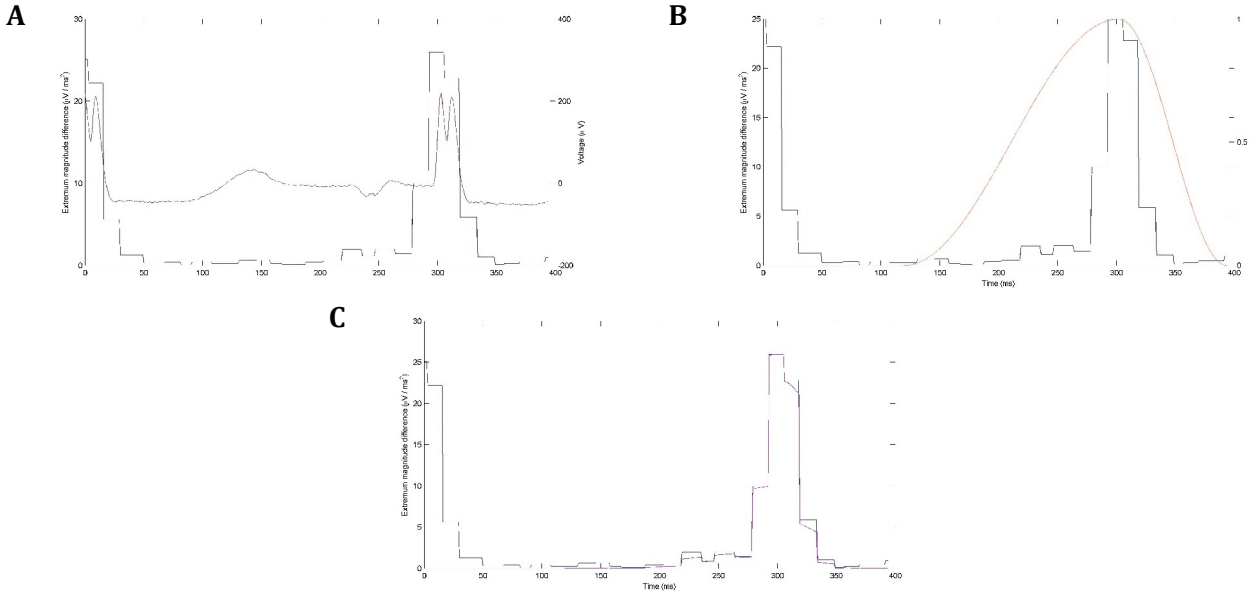
*Figure 14: Visualisation of several steps of the adaptive detection algorithm. **A**: MDR with the original ECG. **B**: MDR with the window function for this section of data. **C**: MDR with the MDR modified by pointwise multiplication of the window function.*

In this modified MDR, the algorithm seeks the maximum value. The position of this maximum corresponds with a magnitude w in the MDR. Magnitude w is compared with the magnitude w_i of the previous 10 detected peaks as follows. First the mean w_{mean} and the standard deviation w_{std} are calculated. A maximum deviation in magnitude is determined as follows:

$$w_{dev} = \begin{cases} 0.3\, w_{mean} & w_{std} < 0.100\, w_{mean} \\ 0.5\, w_{mean} & w_{std} > 0.167\, w_{mean} \\ 3\, w_{std} & 0.100\, w_{mean} < w_{std} < 0.167\, w_{mean} \end{cases} \tag{2}$$

These values were manually optimised for detection. If the condition $|w - w_{mean}| < w_{dev}$ is satisfied, it is accepted and the position v and magnitude w are stored.

When the local maximum is rejected as a peak, which occurs under sudden heart rate decelerations usually, both the subsection and window are extended by $0.3\, v_{median,RR}$ and the estimated peak position n_{est} is shifted by the same number of samples. Then analysis is performed as previously described until a peak is found.

5.2.1.5 Missing beat detection

Occasionally, a beat is missed during detection. This part of the algorithm is triggered when the number of samples between two subsequent samples exceeds the threshold $v_i - v_{i-1} \geqslant 1.9\, v_{median,RR}$. It is now assumed that the algorithm missed a peak around $v_i - v_{median,RR}$. A subsection of the data in the MDR is selected in the interval $\left[v_i - v_{median,RR} - n_{ext}, v_i - v_{median,RR} + n_{ext} \right]$, where n_{ext} is the number of samples corresponding with a time interval of 30 ms, arbitrarily chosen to limit the false detection of beats.

The window function is defined as

$$g(n) = 0.5 - 0.5 \cdot \cos\left(\pi\left(\frac{n}{n_{ext}} \right) \right) \ , \tag{3}$$

30

	Set 1		Set 2		Set 3		Total	
	Incl	Excl	Incl	Excl	Incl	Excl	Incl	Excl
R-peaks (visual)	547	531	493	483	633	613	1673	1627
R-peaks (detected; true)	541	531	493	483	623	613	1657	1627
R-peaks (detected; false)	1	0	0	0	0	0	1	0
R-peaks (undetected; true)	6	0	0	0	10	0	16	0

Table 3: Results of the R-peak detection including and excluding the peaks identified during training. R-peaks (visual) are R-peaks that were identified by visual inspection of the signal. R-peaks (detected; true) are R-peaks that were correctly identified by the algorithm. R-peaks (detected; false) are R-peaks that were identified by the algorithm, but were not identified visually. R-peaks (undetected; true) are R-peaks that were found visually, but that the algorithm did not identify.

with n defined as the number of samples from $v_i - v_{median, RR} - n_{ext}$.

The window is applied to the subsection by using the pointwise product. The algorithm seeks the maximum value in the modified MDR, which corresponds with a magnitude w in the unmodified MDR. Magnitude w is compared with the magnitude w_i of the previous 10 detected peaks as follows. First the mean w_{mean} is calculated based on the values of w_i. If the condition $0.4 w_{mean} < w < 1.5 w_{mean}$ is satisfied, this detection is marked as a peak and its position v and magnitude w is stored.

Missing beat detection is repeated until subtraction of $v_{median, RR}$ from the position of the most recently detected beat would yield a position that is before the original v_{i-1}.

5.2.1.6 Post-processing

After performing peak detection on the entire dataset, the R-R intervals are calculated. To do this, first the position v_i of each R-peak is determined more precisely as $v_{i, prec}$ by parabolic fitting, modified from Toonen (1998), see 'Parabolic fitting' on page 42.

The R-R intervals are then calculated as

$$RR_i = \frac{v_{i, prec} - v_{i-1, prec}}{f_{sample}} \quad , \tag{4}$$

with f_{sample} the sample frequency in Hertz.

5.2.1.7 Algorithm accuracy

To determine the accuracy of the algorithm, three 192 second segments of data from different fetal lambs were selected randomly. R-peaks present are annotated manually and compared with the R-peaks found by the detection algorithm. The results of this analysis are shown in Table 3.

Sensitivity of the algorithm on the total dataset is 99.0% if the peaks identified during training are included and 100.0% if they are excluded. Precision is 99.9% and 100.0% respectively.

5.2.2 Systole and diastole detection

Another algorithm was developed to detect both systolic and diastolic pressures per heart period. It should have the following characteristics:

- Computationally fast – Since the algorithm has to analyse the same 2252 hours of data as the R-peak detection algorithm, analysis time is to be reduced to several days at most.

- Robust – Detection in the presence of artefacts should be reliable.

- Precise and sensitive – The algorithm should be able to detect systolic and diastolic pressures accurately.

- Versatile – can handle abnormal pressure waveforms such as pulsus biferiens.

- Off-line analysis – Real-time analysis capabilities are not needed.

- Implementable as a subroutine – Data was stored in separate files. Subsequent analysis without human intervention is needed to speed up processing and implementation as a subroutine enables us to do so.

An algorithm was written with the characteristics above – only robustness was found to be difficult to enforce in the presence of baseline drifts and pulse pressure attenuation. The algorithm is based on the following observations:

1. Every cardiac contraction produces a pressure wave.

2. The diastolic pressure is the minimum pressure before the onset of the pressure wave.

3. The systolic pressure is the pressure at the peak of the pressure wave.

Because of observation 1 the algorithm uses the R-peaks detected by the R-peak detection algorithm as an input.

5.2.2.1 Basic signal transform

The arterial blood pressure signal was first filtered using an IIR 50Hz notch filter to remove mains noise. The signal was then filtered using a 4th order Butterworth low-pass filter with a cut-off frequency of 16 Hz to suppress noise. The amniotic fluid pressure signal was then filtered using a 4th order Butterworth low-pass filter with a cut-off frequency of 6 Hz. The amniotic fluid pressure is used as an offset for the arterial blood pressure. High frequency contents in the amniotic fluid pressure are mainly noise and this is corrected for by filtering. The low-pass filtered arterial blood pressure is corrected for offset by subtraction of the amniotic fluid pressure.

From this point the algorithm works with two different representations of the arterial blood pressure. The first is the low-pass filtered arterial blood pressure signal and the second will be generated using the low-pass filtered representation (LPFR) as the basis.

According to observations 1, 2 and 3 the algorithm should find the minimum and maximum pressure in every heart period. One way to accomplish this is to find the locations where the first derivative of the signal is 0. Low frequency components below 2 Hz are suppressed by filtering the LPFR with a 4th order Butterworth high-pass filter with a cut-off frequency of 2 Hz since these were found to have little bearing on the actual shape of the pressure waves and for facilitating detection the baseline needs to be removed. The first derivative is calculated using a discrete form of Newtons backward difference $f^{(1)}(i) = f(i) - f(i-1)$.

The transformation from the original blood pressure signals to the first derivative representation (FDR) is shown in Figure 15.
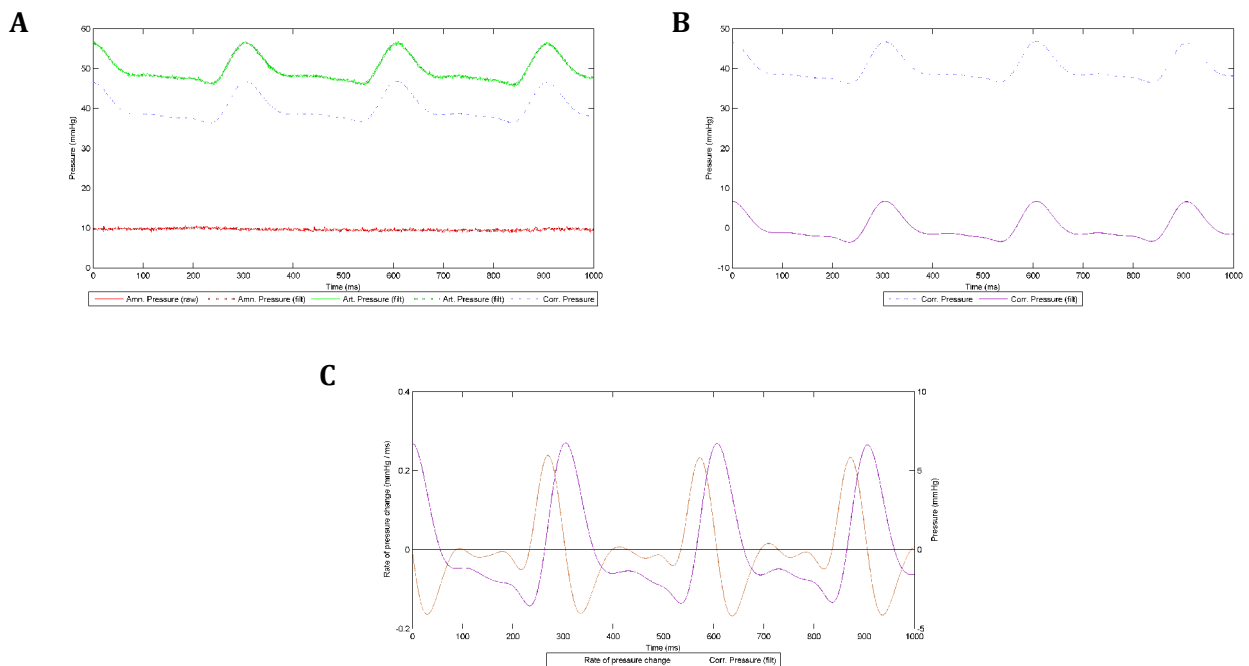
*Figure 15: Visualisation of several steps in the signal transformation process. **A**: Original and filtered amniotic and arterial pressures and the corrected pressure produced by subtraction of the amniotic pressure from the arterial pressure. **B**: Corrected pressure and the result of high-pass filtering. **C**: The high-pass filtered pressure and its first derivative.*

5.2.2.2 Training

The algorithm needs to establish an estimate for the maximum of the slope of a pressure wave for future use. The first 20 seconds of data are analysed to find the first 10 pressure waves. The value of the 95th percentile of the data in the first 20 seconds of the first derivative representation is calculated. Observations 2 and 3 suggest that the pressure slope between the diastole and the systole is positive. The algorithm generates a list of all non-negative sections in the FDR and combines the sections in the list that lie within 20 ms of each other to correct for occasionally occurring temporary decreases in the slope between the diastole and systole. Sections in the list which corresponded with sections of data with values greater than P_{95} are selected and matched to the nearest preceding R-peak. The maximum of the data in the first 10 of these sections is stored, as well as the positions of the start and end sample of the sections, as these represent the diastolic and systolic pressures respectively and will be used in post-processing.

5.2.2.3 Detection

The detection algorithm is beat-triggered. For each detected R-peak the section of the FDR data studied starts at the sample 15 ms before the R-peak and ends at the sample 30 ms before the next R-peak. This interval was chosen as both diastolic and systolic pressures could be reliably determined in this interval. As in the training phase, the algorithm lists subsections of non-negative data, determines the maxima of each of these subsections and sorts the maxima in a descending manner. It then uses various criteria to decide upon which subsection to use. These criteria are shown in a flowchart in 'Systole and diastole detection algorithm' on page 45. The positions of the start and end sample and the value of the maxima are stored.

The same procedure is followed for each detected R-peak until the second last R-peak has been reached.

	Set 1		Set 2		Set 3		Total	
	Incl	Excl	Incl	Excl	Incl	Excl	Incl	Excl
DBP/ SBP (visual)	546	530	491	481	632	612	1669	1623
DBP/ SBP (detected; true)	539	529	491	481	621	611	1651	1621
DBP/ SBP (detected; false)	0	0	1	1	0	0	1	1
DBP/ SBP (undetected; true)	7	1	0	0	11	1	16	2

Table 4: Results of systole and diastole detection both including and excluding those pressure waves corresponding to R-peaks identified during training of the R-peak detection algorithm. DBP/ SBP (visual) are systoles and diastoles that were identified by visual inspection of the signal. DBP/ SBP (detected; true) are systoles and diastoles that were correctly identified by the algorithm. DBP/ SBP (detected; false) are systoles and diastoles that were identified by the algorithm, but were not identified visually. DBP/ SBP (undetected; true) are systoles and diastoles that were found visually, but that the algorithm did not identify.

5.2.2.4 Post-processing

The positions of the start and end samples stored represent position of the diastolic and systolic pressures respectively. To retrieve the actual diastolic and systolic pressures, the positions are used to find the local minimum and maximum respectively within 20 ms of the positions in the LPFR.

5.2.2.5 Algorithm accuracy

To determine the accuracy of the algorithm, three 192 second segments of data from different fetal lambs were selected blindly. The segments are the same as the segments studied to determine the accuracy of R-peak detection. Pressure waves present are inspected visually and compared with the diastoles and systoles found by the detection algorithm. The results of this analysis are shown in Table 4.

Sensitivity of the algorithm on the total dataset is 98.9% if the diastoles and systoles linked to peaks identified during training of the R-peak detection algorithm are included and 99.9% if they are excluded. Precision is 99.8% and 99.9% respectively.

5.2.3 Further data processing and transfer function analysis

After analysing a 30 minute segment to find the series of R-R intervals and systolic blood pressures, it is necessary to process the data further to analyse the transfer function and to calculate the parameters used in the paper. This section will touch upon various aspects of the ensuing analysis, including the analysis of the transfer function and the preparatory steps needed to perform this, and the time-domain aspects of heart rate and blood pressure variability.

The description given here will be to the level necessary to understand the overview presented in the paper. For a more fundamental perspective on various subjects, we refer to Appendix I.

5.2.3.1 Equidistant sampling and filtering

R-R interval and SBP datasets contain data that is irregularly spaced in time. To perform spectral and cross-spectral analysis the datasets need to be resampled. The methods employed here are the same as used by Andriessen et al. (2003); Andriessen et al. (2005) and deviations from their method are explicitly stated. As there, the LF band for both the R-R interval variations and SBP variations are defined in the frequency range between 0.04 and 0.15 Hz.

Two otherwise empty sets of equal sample length to the original set, 1.8 million in this case because the original sets were sampled at 1000 Hz for 30 minutes, were created. In one set, the R-R interval values were allocated to the position of the R-peak, and in the other, the SBP values were placed at the

sample corresponding to the time of systole. Both sets were convoluted with a boxcar function of height 0.002 and a width of 500 samples and subsequently resampled to 4 Hz to obtain equidistant data points. A 60s example of both resampled datasets is shown in Figure 17A.

To remove baseline contributions, both datasets were filtered using a 4th order high-pass Butterworth filter with a cut-off frequency of 0.03 Hz. Note that this deviates from the method used by Andriessen et al. (2003) and de Boer et al. (1985), who removed contributions of the mean resampled R-R interval and resampled SBP from the respective datasets. The different approach is chosen because the contributions of the VLF-bands are noticeable in the 30 minute segments analysed and the purpose of removing baseline contributions is to remove these slow variations from influencing the further analysis.

Every 30 minute segment was then divided into non-overlapping 192 second subsegments for further analysis.

5.2.3.2 Spectral density and cross-spectral density

Welch's method is used for spectral analysis to reduce noise (Semmlow, 2004). Each 192 second subsegment is divided into 5 smaller half-overlapping subsegments of 64 seconds long. A Parzen window of equal length is applied to each subsegment to reduce spectral leakage.

An auto power spectral density function (autoPSD) is calculated using the MATLAB *cpsd* routine, which effectively applies a discrete Fourier transform to the autocorrelation function of each windowed 64 second subsegment and averages these over the 5 half-overlapping segments. The autoPSD is then corrected for the use of the window by dividing it by the total power of the Parzen window. The autoPSD was derived in this way for both the R-R interval, $S_{RR,RR}(f)$, and the SBP, $S_{SBP,SBP}(f)$, datasets.

The cross power spectral density function (crossPSD) $S_{SBP,RR}(f)$ of corresponding 192 second subsegments of the R-R interval and SBP datasets is likewise calculated using the MATLAB *cpsd* routine, yet instead of applying a discrete Fourier transform to the autocorrelation function of each windowed 64 second subsegment, it applies a discrete Fourier transform to the crosscorrelation function of the each corresponding windowed 64 second subsegment and averages. Similarly the window correction is applied to the crossPSD. For more information see 'Auto- and cross-correlation and DFT' on page 43.

The LF band power and total power is calculated for each 192 second subsegment in both the R-R interval and the SBP dataset by summing the autoPSD of each frequency bin over the frequency range 0.04 – 0.15 Hz and 0.04 – 2.00 Hz respectively. Examples of the R-R interval autoPSD, the SBP autoPSD and the crossPSD in a 192 second segment are shown in Figure 17B-D.

5.2.3.3 Transfer function analysis

The transfer function of a system describes the relation between input and output of a system. The baroreflex mediated heart rate response is modelled as a linear, stationary single-input/ single-output system, with SBP as input and R-R interval as output. The weighting function $h(t)$ describes the relationship between SBP and R-R interval in the time domain, as is shown in Figure 16. In the frequency domain the function $h(t)$ is transformed to the transfer function $H(f)$. The transfer gain $G(f)$, based on the autoPSD and crossPSD, is defined as

$$G(f) = \frac{|S_{SBP,RR}(f)|}{S_{SBP,SBP}(f)} \quad ,$$
(5)

and the transfer phase $\varphi(f)$ is defined as:

$$\varphi(f) = atan2\left(\frac{\Im(S_{SBP,RR}/S_{SBP,SBP})}{\Re(S_{SBP,RR}/S_{SBP,SBP})} \right) \quad ,$$
(6)

see 'Transfer function gain and phase' on page 45 for further details. Coherence is defined as:

$$C_{SBP,RR}(f) = \frac{|S_{SBP,RR}(f)|^2}{S_{SBP,SBP}(f) S_{RR,RR}(f)} \tag{7}$$

An example of the coherence in a 192 second segment is shown in Figure 17E.

Transfer gain, transfer phase and coherence are calculated for each 192 second segment. Note that phase, as determined here, is the instantaneous phase. This implies that the phase $\varphi(f)$ is found in the range $-\pi < \varphi(f) \leqslant \pi$, which might or might not be the correct phase shift. A real phase of $\varphi(f) + 2 n \pi$ will yield the same phase angle for any $n = \ldots -2, -1, 0, 1, 2, \ldots$, but with a different corresponding time shift $\tau(f) = \varphi(f)/(2 \pi f)$. The solution implemented in our study is described later.

$$SBP\,(t) \longrightarrow \boxed{h\,(t)} \longrightarrow RR\ interval\,(t)$$
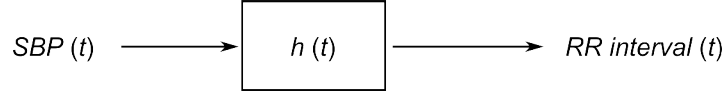
Figure 16: Linear system describing the transfer from the systolic blood pressure to the R-R interval by weighting function $h(t)$.

5.2.3.4 Time domain analysis of variability

As a measure of heart rate variability (HRV) the standard deviation of the N R-R intervals is calculated for each 192 seconds subsegment, based on the R-peaks located in the subsegment:

$$SDRR = \sqrt{\frac{1}{N} \sum_{i=1}^{N} \left(RR_i - \mu \right)^2} \quad , \tag{8}$$

where $\mu = \frac{1}{N} \sum_{i=1}^{N} RR_i$ is the mean R-R interval. This is one of the standard definitions by The Task force of the European Society of Cardiology and the North American Society of Pacing and Electrophysiology (Camm et al., 1996).

Likewise as a measure of blood pressure variability (BPV) the standard deviation of the N SBP values is calculated for each 192 seconds subsegment, based on the systoles located in the subsegment:

$$SDSBP = \sqrt{\frac{1}{N} \sum_{i=1}^{N} \left(SBP_i - \mu \right)^2} \quad , \tag{9}$$

where $\mu = \frac{1}{N} \sum_{i=1}^{N} SBP_i$ is the mean SBP.

5.2.3.5 Time shift between SBP and R-R interval changes

To determine the time shift between changes in SBP and subsequent changes in R-R interval length in the time domain, the cross-correlation between the SBP and R-R interval data is calculated for each 192 second subsegment, for a maximum time lag of 25 seconds. Values for the cross-correlation corresponding to negative time shifts, where changes in R-R interval length would precede changes in SBP, were removed. Local maxima and the global maximum were detected in the remaining data. The time shift corresponding to the local maximum with the smallest time shift for which the value was at least 70% of the global maximum was then used as the time-domain estimate for the time shift between changes in SBP and subsequent changes in R-R interval.

5.2.4 Final calculations and data processing

As in Andriessen et al. (2003) and Robbe et al. (1987) , the spontaneous baroreflex gain and phase is determined in the LF band, which is defined as the band with the frequencies 0.04 – 0.15 Hz. Originally after de Boer et al. (1985) the transfer gain and phase were assumed to be reliable for frequencies f satisfying $C_{SBP,RR}(f) \geqslant 0.5$. For every 192 second subsegment the frequency $f_{LF,max}$ within the frequency range defined by $0.04 \leqslant f_{LF,max} \leqslant 0.15$ Hz and where the coherence satisfies the condition $C_{SBP,RR}(f_{LF,max}) \geqslant 0.5$ and is maximal within the frequency range, is determined. If this $f_{LF,max}$ exists, , the transfer gain and transfer phase at this frequency is used as the spontaneous baroreflex gain and phase.

As mentioned above, the phase is an instantaneous phase, and to get a better estimate of the time delay τ_{freq} at the frequency $f_{LF,max}$ the time-domain time shift τ_{time} is used as a reference. More specifically, we minimize $\Delta\tau(n,f) = \left| \tau_{time}(f) - \dfrac{\varphi(f)+2n\pi}{2\pi f} \right|$ for $f = f_{LF,max}$ with regards to n and use this result to calculate the time delay $\tau_{freq}(n=n_{min}, f=f_{LF,max}) = \dfrac{\varphi(f)+2n\pi}{2\pi f}$.

Summarising, per 192s second subsegment, the following parameters were calculated: the mean R-R interval; the standard deviation of the R-R interval SDRR; the power in the LF-band of the R-R interval autoPSD SDSBP; the total power of the R-R interval autoPSD; the mean SBP; the standard deviation of the SBP; the power in the LF-band of the SBP autoPSD; the total power of the SBP autoPSD. Depending on coherence, the following parameters were also determined: the frequency in the LF-band with maximal coherence $f_{LF,max}$; the maximal coherence $C_{SBP,RR}(f_{LF,max})$; the transfer function gain $G(f_{LF,max})$; and the phase-offset corrected time delay $\tau_{freq}(n_{min}, f_{LF,max})$.
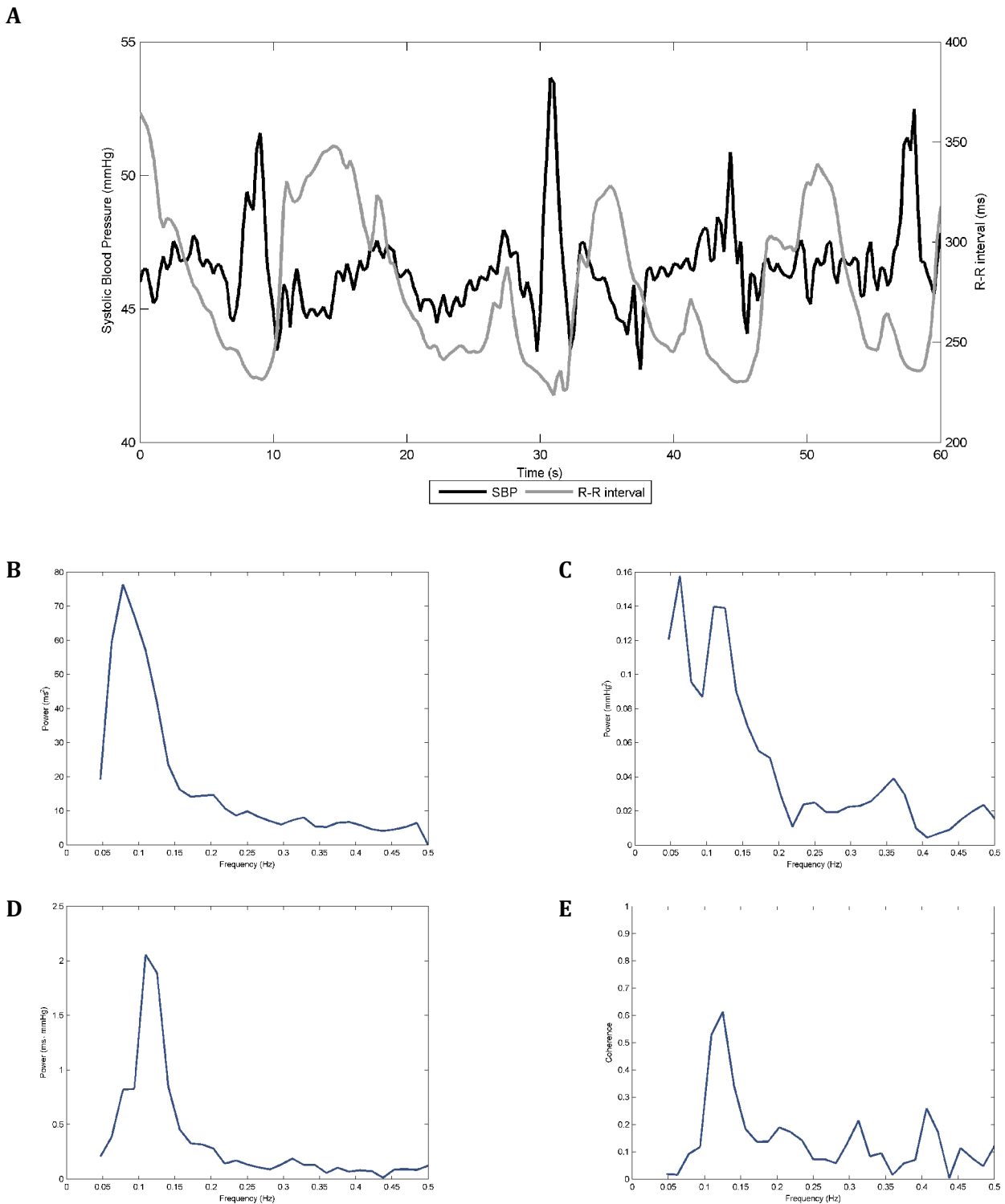
*Figure 17: Plots of raw R-R interval, SBP data and corresponding autoPSDs; crossPSD between the R-R interval and SBP and coherence. **A**: Plot of 60-s time series of the R-R interval and SBP, respectively. Note that a rise in blood pressure (black line) is followed by a increase in R-R interval (grey line) several seconds later. **B**: AutoPSD of the R-R interval time series in a 192-second segment. Most of the power is located in the low-frequency (LF: 0.04 – 0.15 Hz) band. **C**: AutoPSD of the SBP time series in a 192-second segment. Most of the spectral power is located in the LF-band, but the presence of higher frequency contents suggests respiratory associated fluctuations. **D**: CrossPSD of the R-R interval and SBP time series. **E**: Coherence. High coherence implies a significant transfer of power between the SBP and R-R interval series. The maximum coherence (approximately 0.6) in the LF-band is found at a frequency of 0.13 Hz.*

6 Recommendations

6.1 R-peak detection algorithm

Overall, the detection algorithm functioned quite well, especially since it is versatile. There are no assumptions about an initial value of the R-R interval, making it well suited to batch processing.

The R-peak detection algorithm currently only uses the information of one ECG leads, despite the fact that inclusion of information stored in different leads might aid detection. Using (at least) two leads it is possible to construct a vector cardiogram, an option we briefly explored, but did not pursue further due to time constraints. The section of the vector cardiogram corresponding to the R-peak would then be the large enveloping ellipsoid. This has two implications. One is that the signal attained by calculating the projection of the instantaneous heart vector – that is of the heart vector at a time t – along the major axis of this ellipsoid for all t, would maximise the contribution of the R-peak in the projecting. The second implication is that datapoints which do belong to the envelopping ellipsoid are rather irrelevant if the goal is to detect R-peaks and that these can be replaced or omitted. Successful implementation could potentially increase the robustness of the algorithm further.

The window function used can potentially be optimised, as it is somewhat arbitrary in its design, although it seems to perform quite well.

Furthermore we would recommend improving the training part in general. As demonstrated most peaks that were missed during detection in general were missed during training. It is be possible to analyse the training section of data using the values for R-R interval and magnitude w generated by training, for example by performing adaptive detection backwards from the first R-peak detected by adaptive detection. A simpler solution is to omit the R-peaks detected during training, at the cost of losing some datapoints.

6.2 Systole and diastole detection algorithm

The algorithm is, as it is, incapable of correcting for or detection of baseline artefacts and pulse pressure attenuation, and we had to exclude data during post-processing where pulse pressure was severely attenuated. Furthermore, it is not very elegant – it could well be that for the purpose of detecting systolic and diastolic pressures a much simpler analysis of finding the maximum and minimum values per heart period performs as well.

Because it is intimately linked to the R-peaks detected by the R-peak detection algorithm, the sensitivity and precision, or rate of false detections, is limited by that of the R-peak detection algorithm. However, as we have shown, this is not necessarily a bad thing as the R-peak detection algorithm is quite accurate and it potentially aids the blood pressure detection.

6.3 Use of transfer function to determine baroreceptor sensitivity

The transfer function method to determine the baroreceptor sensitivity has its merits and its drawbacks compared to other methods. Historically, one of the earliest methods, which is still very common to today's clinical experiments, to quantify the baroreceptor sensitivity uses vasoconstrictor drugs, which alter blood pressure and preferably do not influence the heart rate directly by affecting the sinoatrial node (Rovere et al., 2008). Measuring both the systolic blood pressure and the R-R intervals, the baroreceptor sensitivity is defined as the maximum slope of the curve, where SBP is plotted on the horizontal axis and the R-R interval on the vertical axis. Since this is a technique physicians are well-familiar with, it is important to realise that the transfer function method and the vasoconstrictor method do not measure the same quantity. The vasoconstrictor method studies the baroreceptor reflex response to challenges, whereas the semi-stationarity condition used in the transfer function method prevents the study of the short-term responses to challenges. What it is capable of telling us, and which any method that introduces challenges is incapable of, is the

functioning of the baroreflex under normally occurring conditions. Direct comparison of the results of both methods is therefore not straightforward, although the baroreceptor sensitivity should be in the same order of magnitude. A drawback of transfer function method is that, due to way physicians are currently educated, most physicians will lack the insights needed to understand the technical foundations on which it rests. An advantage of the transfer function method is that it is uncomplicated and able to perform continuous observations over long periods, especially since it does not require any other instrumentation than commonly available ones. Another major advantage is that this method virtually eliminates interobserver errors.

Another method to study the spontaneous baroreceptor reflex is the sequence method (Parati et al., 1995), where only those series of beats are studied where progressive increases or decreases in systolic blood pressure lead to respectively lengthening or shortening in R-R intervals. This method can separate the asymmetric sympathetic and parasympathetic effects on the spontaneous baroreflex, which the transfer function method can not perform. However, this preselection might introduce bias, potentially returning an effect of the baroreflex where this is unwarranted. The transfer function method has no such inherent bias, yet on the other hand, the coherence threshold is arbitrary, for it is only the human observer who judges that the heart rate response to blood pressure changes is reliable enough to be analysed.

Underlying the use of the transfer function method, however, is the assumption that the baroreceptor feedback from systolic blood pressure to heart rate is a linear, stationary process. However, it is at most so in approximation. The sympathetic and parasympathetic effects operate on different time scales (Rovere et al., 2008), and this observation in itself means that it is unlikely that the process is strictly linear, though in practice most effects are likely mitigated by the fact that the signal studied contains little challenges to the baroreflex. Preferably the transfer function method would be revised to separate the sympathetic and parasympathetic effects and study these separately, but without the inherent bias of the sequence method, but to our knowledge such a method has not yet been developed.

The use of a spectral method, such as the transfer function method, has the benefit over the time-domain methods in that it is easily possible to separate effects from different physical mechanisms that are connected to features in the frequency domain.

In all, until a better method is developed, the transfer function method is a very suitable method to study the spontaneous baroreflex effect of blood pressure variations on heart rate.

7 Conclusion

In this study we developed algorithms for the analysis of R-peaks in ECG and of blood pressure signal, required to analyse the baroreceptor sensitivity by the transfer function method. The algorithms were sensitive and precise, and allowed us to perform the analysis of the transfer function rapidly. Determination of baroreceptor sensitivity by the transfer function method is well-suited for longitudinal studies.

We were able to quantify the baroreflex mediated heart rate response in preterm fetal sheep by analysis of the transfer function and study the longitudinal effects on the baroreflex function due to asphyxia. We found that intra-uterine asphyxia limits the capacity of the baroreflex to buffer changes in blood pressure by heart rate control after 7 days following umbilical cord occlusion. This potentially contributes to damage to the immature vascular architecture and neonatal encephalopathy.

8 Appendix I

8.1 Parabolic fitting

A parabolic function is a second order polynomial, $p(x)=ax^2+bx+c$ with a, b and c constant values. The aim of parabolic fitting is to determine the values of the constants a, b and c based on a set of data points (x_n, y_n).

Here, a parabolic fitting is used to find the position of the critical point, based on three data points. The first question is thus: find a, b and c so that $p(x_1)=y_1$, $p(x_2)=y_2$ and $p(x_3)=y_3$.

We now have three equations:

$$y_1=ax_1^2+bx_1+c \tag{10}$$

$$y_2=ax_2^2+bx_2+c \tag{11}$$

$$y_3=ax_3^2+bx_3+c \tag{12}$$

By subtracting (10) from (11), we find

$$y_2-y_1=a(x_2^2-x_1^2)+b(x_2-x_1) \tag{13}$$

By rewriting (13) as an expression of a, we find

$$a=\frac{y_2-y_1-b(x_2-x_1)}{x_2^2-x_1^2} \tag{14}$$

By subtracting (10) from (12) and substituting a by (14), we find

$$y_3-y_1=\frac{y_2-y_1-b(x_2-x_1)}{x_2^2-x_1^2}(x_3^2-x_1^2)+b(x_3-x_1) \tag{15}$$

By rewriting (15) as an expression of b, we find

$$b=\frac{(y_2-y_1)\left(\dfrac{x_3^2-x_1^2}{x_2^2-x_1^2}\right)-(y_3-y_1)}{(x_2-x_1)\left(\dfrac{x_3^2-x_1^2}{x_2^2-x_1^2}\right)-(x_3-x_1)} \tag{16}$$

Since b in (16) is expressed solely in terms of input variables, likewise a is expressed solely by input variables, by substituting b in (14) with the expression in (16).

Reordering the terms in (10) yields:

$$c=ax_1^2+bx_1-y_1 \tag{17}$$

Hence c can be calculated by substituting the values of a and b into eqaution (17).

With constants a, b and c known, the coordinates of the critical point of $p(x)$ can be calculated. The first derivative of $p(x)$ is:

$$\frac{dp}{dx} = 2ax + b \tag{18}$$

Solving equation (18) for $\frac{dp}{dx} = 0$ yields:

$$x_{crit} = \frac{-b}{2a} \tag{19}$$

and

$$y_{crit} = c - \frac{b^2}{4a} \tag{20}$$

When the data points used are subsequent samples $n-1$, n and $n+1$, the expression for x_{crit} simplifies to

$$x_{crit} = x_n + \frac{y_{n-1} - y_{n+1}}{2\left(y_{n-1} + y_{n+1} - 2y_n\right)} \quad, \tag{21}$$

as used by Toonen (1998)

8.2   Auto- and cross-correlation and DFT

Let $x(n) = [x(0), x(1), x(2), ..., x(N-1)]$ be a sequence of N points, and let $y(n) = [y(0), y(1), y(2), ..., y(N-1)]$ be a sequence of N points as well.

The cross-correlation function for sequences $x(n)$ and $y(n)$ is defined as:

$$r_{xy}(n) = \sum_{k=0}^{M} y(k+n)x(k) \quad, \tag{22}$$

with $M = N-1-k$. The autocorrelation function for sequence $x(n)$ is defined as:

$$r_{xx}(n) = \sum_{k=0}^{M} x(k+n)x(k) \tag{23}$$

The autocorrelation function for sequence $y(n)$ is similar, substituting $x(n)$ for $y(n)$ in (23).

Discrete Fourier transform (DFT) transforms an input function of finite duration into its frequency representation. To apply a Fourier transform, the function must be periodic or infinite. In practice, input functions that represent data, such as sequence $x(n)$ and $y(n)$, are of finite duration and are generally not periodic. Hence the input function should be modified to make it semi-periodic. This is usually done by applying a window function to taper the ends of the input function, at the cost of spectral leakage into other frequencies. When it comes to window functions, there is no function that gives the least spectral leakage for every input function. For example, if the input function is the sequence $z(n) = \left[\frac{1}{\sqrt{2}}, 1, \frac{1}{\sqrt{2}}, 0, -\frac{1}{\sqrt{2}}, -1, -\frac{1}{\sqrt{2}}, 0\right]$ generated by sampling $f(t) = \sin(t\pi)$ at $t = \left[\frac{1}{4}, \frac{1}{2}, \frac{3}{4}, 1, \frac{5}{4}, \frac{3}{2}, \frac{7}{4}, 2\right]$, a rectangular window $w(n) = 1$ actually yields no spectral leakage at all, while in most circumstances this window is not the most suitable choice.

The discrete Fourier transform transforms input function $x(n)$ to Fourier coefficients $X(k)$, with $k = 0, \ldots, N-1$ as follows:

$$X(k) = \mathscr{F}(f(n)) = \sum_{n=0}^{N-1} x(n) e^{-i\frac{2\pi}{N}kn}$$

(24)

Inverse discrete Fourier transform transforms the Fourier coefficient $X(k)$ back to the original input function $x(n)$:

$$x(n) = \mathscr{F}^{-1}(X(k)) = \frac{1}{N} \sum_{n=0}^{N-1} X(k) e^{+i\frac{2\pi}{N}kn}$$

(25)

DFT is usually performed using a Fast Fourier Transform (FFT) algorithm. There are various kinds of FFT algorithms. MATLAB R2009a routines in the FFTW package (Frigo et al., 1998), which is based on the seminal work by Cooley et al. (1965).

According to the Wiener-Khinchin theorem, the power spectral density of a stochastic process with time-invariant first and second moments, or mean and variance, is the Fourier transform of the corresponding auto-correlation function (Kay et al., 1981).

The condition of time-invariance of the first and second moments is, in general, difficult to meet in experiments. To meet this condition sufficiently, a common practice is to divide measurement data in to smaller sections where this condition can be sufficiently met.

So, if sequence x_n is wide-sense stationary, as described above, then the power spectral density function is described as

$$S_{xx}(k) = \sum_{n=0}^{N-1} r_{xx}(n) e^{-i\frac{2\pi}{N}kn} \quad ,$$

(26)

with $r_{xx}(n)$ the auto-correlation function, as in (23).

An extension to the cross-correlation function $r_{xy}(n)$ is possible. The cross-power spectral density is then

$$S_{xy}(k) = \sum_{n=0}^{N-1} r_{xy}(n) e^{-i\frac{2\pi}{N}kn} \quad ,$$

(27)

as in (Riley et al., 2007)

8.3 Systole and diastole detection flowchart
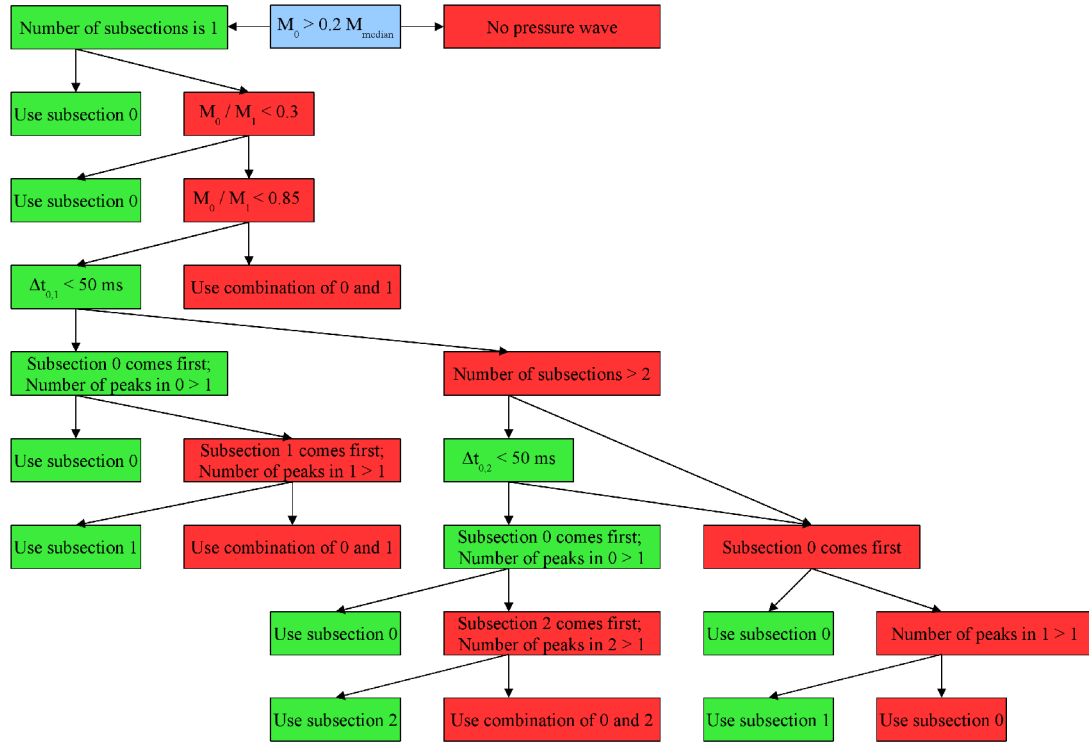
Figure 18: Flowchart for the sytsole and diastole detection algorithm. The subsection in the FDR which contains the global maximum M_0 is referred to as subsection 0. Subsections 1 and 2 are the subsections containing the second largest local maximum and the third largest local maximum respectively. M_{median} is the median magnitude M of the subsection in the FDR of the 10 previous pressure waves. $\Delta t_{0,1}$ and $\Delta t_{0,2}$ are the time differences between subsection 0 and 1 and subsection 0 and 2 respectively.

8.4 Transfer function gain and phase
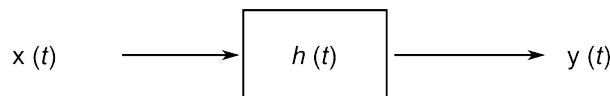
Figure 19: Linear system describing the transfer by weighting function $h(t)$ of the system from input function $x(t)$ to output function $y(t)$.

The derivation of transfer gain and phase, as described by Bartels (1997), follows the argument by Bendat et al. (1986), or more recently, by Bendat et al. (2010), for single-input/ single-output models.

Using the definition of $x(t)$ as input and $y(t)$ as output, with $h(t)$ as weighting function, the convolution $y(t)=h(t)*x(t)$ in the frequency domain is $Y(f)=H(f)\cdot X(f)$, with $X(f)=\mathscr{F}(x(t))$ the Fourier spectrum of $x(t)$, and transfer function $H(f)$ and $Y(f)$ defined likewise.

When no noise at either input or output exists and the system studied is time-invariant and linear, it is possible to derive the following two equations:

$$S_{yy}(f)=|H(f)|^2 S_{xx}(f) \tag{28}$$

$$S_{xy}(f)=H(f) S_{xx}(f) \tag{29}$$

with $S_{xx}(f)$ and $S_{yy}(f)$ the auto-spectral density functions of input $x(t)$ and output $y(t)$ respectively and $S_{xy}(f)$ the cross-spectral density function of $x(t)$ and $y(t)$.

Let

$$S_{xy}(f)=|S_{xy}(f)|e^{-i\theta_{xy}(f)} \tag{30}$$

$$H(f)=|H(f)|e^{-i\phi(f)} \tag{31}$$

$|H(f)|$ is known as the transfer gain and $\phi(f)$ as the transfer phase. It is now possible to express both gain and phase in terms of the auto- and cross-spectral density functions. Using equation (29)

$$|S_{xy}(f)|=|H(f)S_{xx}(f)| \tag{32}$$

Since by definition $\Im(S_{xx}(f))=0$ for any $f \in \mathbb{R}$:

$$|S_{xy}(f)|=|H(f)|S_{xx}(f) \tag{33}$$

The transfer gain is then:

$$|H(f)|=\frac{|S_{xy}(f)|}{S_{xx}(f)} \tag{34}$$

Inserting (33) into equation (30) yields:

$$S_{xy}(f)=|H(f)|S_{xx}(f)e^{-i\theta_{xy}(f)} \tag{35}$$

Replacing the left side of equation (35) by (29):

$$H(f)S_{xx}(f)=|H(f)|S_{xx}e^{-i\theta_{xy}(f)} \tag{36}$$

Inserting (31) into (36):

$$|H(f)|S_{xx}(f)e^{-i\phi(f)}=|H(f)|S_{xx}e^{-i\theta_{xy}(f)} \tag{37}$$

Therefore the transfer phase is defined as:

$$\phi(f)=\theta_{xy}(f+2m\pi) \quad , \tag{38}$$

with $m \in \mathbb{Z}$.

9   Appendix II

While the baroreflex mediated heart response is the main focus of this thesis, this report would be incomplete without at least a token description of the work done on the analysis of the EEGs in our collaboration with the the research group from the Department of Paedatrics at Maastricht University. We feel that the choice to incorporate this work into the main thesis would be unwarranted, given that aside from the fact that the data used came from the same experiment, there is little overlap between the baroreflex work and the EEG work, both in terms of physiology, analysis methodology and subject topic. This does not mean that it would not have been interesting to make a complete analysis – for example, we excluded the animals who had received treatment from this study while maybe the treatment effects a measurable change in baroreflex sensitivity and other parameters – rather that this work could not be completed within the time span provided.

9.1   Introduction to burst and interburst analysis of EEG

EEG has long been the staple method for assessing brain function. As the recording of electrical fields produced by the coherent activity of cortical neurons, EEG is employed in many fields of research and in clinical settings, where it can give physicians significant insights into potential pathologies. Here it is often studied by human interpretation of the data, commonly considered to be the gold standard in the analysis of EEGs.

EEG contains both background activity and specific features. During fetal maturation the dominant background activity and typical features change, and for a more complete overview we refer to André et al. (2010). A dominant aspect of fetal maturation is that background activity increases. The background activity develops from *tracé discontinue* at 24 weeks of gestational age, where the major part of the recorded signal is below a certain voltage threshold, to increasingly more continue tracings at term.

Most EEG interpretation methodology predates the digital era. Computer-assisted analysis can potentially offer different insights, as well as making analysis of long measurements more feasible (Niemarkt et al., 2008). The automated analysis of EEG is an important topic in research. In the recent years, several colleagues in the Medical Physics group have contributed to the automated analysis of burst and interburst segments in EEG (Hansen, 2005; Ruijs, 2007).

Burst and interburst segments signify segments of cortical activity and a lack of cortical activity respectively. These patterns are normally present in fetuses and premature children. However increases in interburst length and ratio are usually connected to developmental retardation and cerebral damage (Holmes et al., 1993; Watanabe et al., 1999; Hellström-Westas et al., 2005).

9.2   Prevention or reduction of brain damage due to fetal asphyxia

Severe fetal asphyxia expresses itself in brain damage. It is known that cerebral damage due to asphyxia is caused by a process that consists of multiple phases. The first phase is the acute stage of cerebral damage at the time of incident, which is followed by a reperfusion stage after the asphyxia subsides that lasts up to 6 hours after the incident. During this phase blood gas values normalise again. However, this is followed by a phase of latent cell damage which leads up to widespread secondary damage afterwards (Drury et al., 2010).

The prevention or the reduction of brain damage due to fetal asphyxia is a subject of interest in research. The research group at Maastricht University uses the ovine model to test potential treatments. I was involved in two of these projects. The first project studied the potential neuroprotective effects of propofol versus isoflurane, two anaesthetica, and the second project was designed to study the neuroprotective effects of G-CSF and stem cells. The publications describing our findings have been included in this appendix.

We analysed the EEG to provide possible further evidence for neuroprotective effects of the various treatments in addition to histological evidence. To do this we used the burst and interburst analysis script described by Loes Ruijs. Her original code was completely rewritten and optimised for a significant increase in computation speed. A spectral analysis of the EEG was also performed for both studies. For further information on the algorithm used, we refer to Ruijs (2007) and Jennekens et al. (2011b). For further details on the experiments themselves, we refer to the two following publications.

9.3 Early propofol administration to the maternal-fetal-unit improved fetal EEG and reduced cerebral apoptosis in late preterm lambs suffering from severe asphyxia.

Matthias Seehase, MD[1,2], Reint Jellema, MD[1], Ward Jennekens, MSc[3,4], Alex Zwanenburg, MSc[3,4], Peter Andriessen, MD, PhD[5], Jennifer J.P. Collins, MSc[1], Elke Kuypers, MSc[1], Johan S. H. Vles, MD, PhD[6], Antonio W.D. Gavilanes, MD, PhD[1], Boris W. Kramer, MD, PhD[1,2]

[1] Dept. of Paediatrics, Maastricht University Medical Center, Maastricht, The Netherlands

[2] School of Mental Health and Neuroscience; School of Oncology and Developmental Biology, Maastricht University, and European Graduate School of Neuroscience (EURON), Maastricht, The Netherlands

[3] Dept. of Clinical Physics, Máxima Medical Center, Veldhoven, The Netherlands

[4] Dept. of Applied Physics, Eindhoven University of Technology, Eindhoven, The Netherlands

[5] Dept. of Paediatrics, Máxima Medical Center, Veldhoven, The Netherlands

[6] Dept. of Neurology, Maastricht University Medical Center, Faculty of Health, Medicine and Life Sciences, School of Mental Health and Neuroscience, Maastricht University, and European Graduate School of Neuroscience (EURON), Maastricht, The Netherlands

First author: Matthias Seehase, MD, Dept. of Pediatrics, Maastricht University Medical Center, Postbus 5800, 6202 AZ Maastricht, The Netherlands, Ph: +31-43-388-2228, Fax +31-43-387-5246, email: m.seehase@maastrichtuniversity.nl

Corresponding author: Boris W. Kramer, MD PhD, Professor of Pediatrics/Experimental Perinatology, Dept. of Pediatrics, Maastricht University Medical Center, Postbus 5800, 6202 AZ Maastricht, The Netherlands, Ph: +31-43-387-7246, Fax +31-43-387-5246, email: b.kramer@mumc.nl

9.3.1 Abstract

Objectives: Preterm and term-born infants suffering from severe perinatal asphyxia resulting in cardiac arrest are at high risk to develop brain injury and life-long disability. Until now, there is no therapy available to reduce severe cerebral injury in preterm infants. We hypothesized that propofol administration to the maternal-fetal-unit can diminish injury in preterm fetuses in states of progressive severe asphyxia.

Design: Prospective, randomized, controlled animal study.

Setting: University.

Subjects: Late preterm lambs.

Interventions: 44 late preterm lambs underwent standardized total umbilical cord occlusion (UCO) or sham-treatment in utero. UCO resulted in global asphyxia and cardiac arrest. After emergency

Caesarean section under either maternal propofol or isoflurane anaesthesia the fetuses were resuscitated and anaesthetized the same way as their mothers.

Measurements and main results: EEG measurements were performed in utero, during UCO and postnatally during 8 hours of ventilation. Occurrence of apoptosis, reactive oxygen species (ROS) formation, and protein levels of NMDA receptors were determined in fetal cerebral frontal cortex. Lambs receiving isoflurane anaesthesia showed a profound increase of total and low-frequency spectral power in burst (indication for seizure activity) and marked increase of interburst interval length during UCO (more burst-suppression), whilst lambs receiving propofol anaesthesia showed less EEG changes. Propofol treatment reduced cerebral ROS formation and protein levels of activated caspase-3 and NMDA-R after severe asphyxia.

Conclusions: Perinatal neuroprotection in the ovine maternal-fetal-unit can be achieved by pre- and postconditioning with propofol. The underlying mechanism is probably an avoidance of lipid peroxidation by ROS scavenging and the reduction of glutamate induced cytotoxicity by downregulation of NMDA receptors.

9.3.2 Introduction

Perinatal asphyxia has been associated with severe neurological and psychiatric sequelae resulting from injury in the basal ganglia/thalamus and cerebral cortex[1]. Despite major improvements in perinatal care and the introduction of cooling in asphyctic term babies the incidence of neurological disabilities related to perinatal brain damage has not decreased significantly in Western countries over the last decades [2,3]. No specific treatments have yet been established for preterm babies. In the clinical setting, after resuscitation of an infant with severe birth asphyxia, the emphasis is on supportive therapy [4]. Brain injury after perinatal asphyxia often develops with delayed clinical onset, opening a therapeutic window [5].

Several promising neuroprotective compounds are in discussion to reduce perinatal hypoxic-ischemic brain injury. In the early postnatal and postasphyctic phase, suggested therapies concentrated on ion channel blockage (Xenon [6]), anti-oxidation (allopurinol [7,8]), anti-inflammation (erythropoietin [9], melatonin [10]), and anti-apoptosis (nuclear factor kappa B [11] and c-jun N-terminal kinase inhibitors [12]); in the later phase, therapies aim at neuronal regeneration by stimulation of neurotrophic properties of the neonatal brain such as stem cell transplantation[13]. Currently, the only clinically established approach is moderate hypothermia which only seems to be suitable for term born infants with minor brain injury due to mild or moderate asphyxia [14]. All these approaches (except for allopurinol) focus on the postnatal phase and seem to have no effect after severe asphyxia (including allopurinol). An additional hurdle consists of the fact that there are only limited to no experiences with these drugs in the neonatal intensive care setting and in preterm babies[15]. In adult patients undergoing surgical procedures and clinical situations where protecting the CNS is a priority (cardiopulmonary bypass, subarachnoid haemorrhage, stroke, and postcardiac arrest resuscitation), the choice of anaesthetic drug assumes a fundamental role[16]. Except for Xenon[6], anaesthetic agents have not been tested for their potential to protect the developing brain.

An advantage of anaesthetic drugs consists in the fact that it has been shown that some anaesthetic drugs have both pre- and postconditioning effects. This allows to administer it already before birth to the maternal-fetal-unit. The concrete example would be an emergency Caesarean section of a distressed fetus in a state of progressive asphyxia (so-called "non-reassuring intrapartum surveillance")[17]. This approach would allow an earlier intervention and by this possibly reduce not only the brain injury due to mild and moderate asphyxia but also the detrimental effects of severe perinatal asphyxia. One of the most promising anaesthetic agents in mediating neuroprotection after hypoxic insults in adults is propofol[18-21]. Apart from its multiple anaesthetic advantages, the short-acting intravenous anaesthetic agent exerts a number of nonanaesthetic effects. Propofol has immunomodulatory effects, scavenges reactive oxygen species (ROS) and proved to be able to reduce glutamate and NMDA receptors responses related cytotoxicity[21].

Based on these considerations, we developed the hypothesis that propofol will reduce neonatal brain injury resulting from severe asphyxia and fetal cardiac arrest in utero if propofol is administered to the maternal-fetal-unit already before birth and continued postnatally. To this purpose we established a perinatal global asphyxia and resuscitation model in late preterm sheep. Pregnant ewes were sedated either with propofol or with isoflurane, a volatile anaesthetic drug, which is in routine use for Caesarean section[22].

Based on the idea of the Ex utero Intrapartum Treatment (EXIT) procedure[23], fetal lambs were intubated endotracheally and catheterized while still being on placental support. Severe prenatal asphyxia was achieved by complete umbilical cord occlusion (UCO) resulting in cardiac arrest. Afterwards the lambs were surgically delivered. After successful resuscitation, the late preterm lambs were subjected to eight hours of standardized intensive care and sedated the same way as their mothers. The preconditioning effect was determined by fetal EEG measurements before and during UCO, the postconditioning effect by EEGs performed during the intensive care time. In addition to the functional EEG data, we determined the degree of fetal cerebral apoptosis by activated caspase-3 protein analysis. To elucidate with which injury pathway propofol would interfere, we determined the degree of lipid peroxidation as a marker of reactive oxygen species (ROS) formation and as a valid predictive marker for perinatal morbidity and mortality[24], and the protein levels of NMDA-receptors as indication for the involvement of excitatory amino acids[25].

9.3.3 Material and methods

9.3.3.1 Animals

The study was approved by the Animal Ethics Research Committee, Maastricht University, The Netherlands. Texel ewes were date-mated and the fetuses were randomized for umbilical cord

	GA control	Propofol control	Propofol asphyxia	Isoflurane control	Isoflurane asphyxia
Included fetal lambs	8	11	10	7	8
Female / male	4/4	3 / 8	6 / 4	4 / 3	2 / 6
Body weight [kg]	3.59±0.14	3.57±0.15	3.86±0.15	3.57±0.15	3.51±0.15
Exact time of MABP<30mmHg during UCO [min]	-	-	2.0±0.0	-	2.0±0.0
Mean time of UCO [min]	-	-	10.7±0.3	-	11.3±0.6
pH before birth (& UCO)	7.26±0.01	7.26±0.01	7.26±0.01	7.26±0.01	7.26±0.01
pH after birth	-	7.10±0.03	6.91±0.03	7.07±0.02	6.84±0.01
Statistical difference between pH after birth	-	p<0.01		p<0.01	
PH after 8 hours of intensive care	-	7.19±0.05	7.21±0.08	7.16±0.11	7.06±0.14
Statistical difference between pH after 8 hours	-	n.s.		n.s.	

Table 5: Numbers of lambs per group, gender, body weight, times of complete umbilical cord occlusion (UCO) and pH of cord blood. All data are given as absolute values or mean±SEM.

occlusion (UCO) and sedation. Observations were made in 44 late preterm fetal sheep of both genders at mean (range) gestational age of 133 or 134 days (term 150d). Eighteen sheep fetuses were subjected to total UCO in utero, and eighteen fetal sheep served as sham controls (Table 5). In each group half of the pregnant ewes and their offspring were sedated with propofol and the other ones with isoflurane. Eight lambs were euthanized directly after preterm delivery and served as gestational age controls.

9.3.3.2 Experimental protocol

The pregnant ewes of the isoflurane group were intubated after thiopental induction (15mg/kg), general anaesthesia was maintained with isoflurane (1-2%). The pregnant ewes of the propofol group received propofol both as induction bolus (6mg/kg) and for general anaesthesia (25mg/kg/h) during the caesarean section. Both anaesthesia types were supplemented by continuous remifentanyl infusion (3µg/kg/min). After a lower midline incision, the fetus was carefully extracted through a small incision of the uterus. An endotracheal tube was inserted and subsequently clamped to prevent fetal breathing. Catheters were placed in the femoral and umbilical artery and in the jugular vein and used for baseline blood sampling (Abbott i-STAT 1 Blood Gas Analyzer, Abbott Laboratories, Illinois, USA) and for continuous monitoring of fetal mean arterial blood pressure (MABP) and heart rate (HR). ECG and EEG electrodes were placed and stitched to the skin. The umbilical cord was gently extracted through the incision of the uterus and a vascular occluder (OC16HD, 16mm, IN VIVO METRIC, Healdsburg, California, USA) was placed around the umbilical cord.

The aim of the occlusion was a MABP below 30mmHg for two minutes (Figure 20). At the end of the occlusion the lambs always suffered from severe bradycardia (HR < 30/min) or even complete cardiac arrest. If there was no increase in HR after 20 seconds after the end of occlusion, resuscitation was started. The resuscitation protocol included immediate start of cardiac massage with a frequency of 120/min and adrenaline administration in augmenting dosage from 30µg over 60µg to 0.1mg. In addition, a volume bolus of ringerlactate of 10ml/kgBW was administered after the first shot of adrenaline and ventilation was given with a balloon (FiO$_2$=0,21, frequency=60/min). After its umbilical cord was cut, the fetus was brought to an open, heated incubator (IW930 Series CosyCot™ Infant Warmer, Fisher & Paykel Healthcare) maintaining a body temperature of 38.5°C and resuscitation was continued. The lambs were connected to pressure-regulated ventilation using a ventilator Servo 900C (Siemens-Elema, Solna, Sweden) with initial settings as follows: FiO$_2$=1, PEEP 5cmH$_2$0, PiP 30cmH$_2$0, frequency 60/min, I:E 1:2.
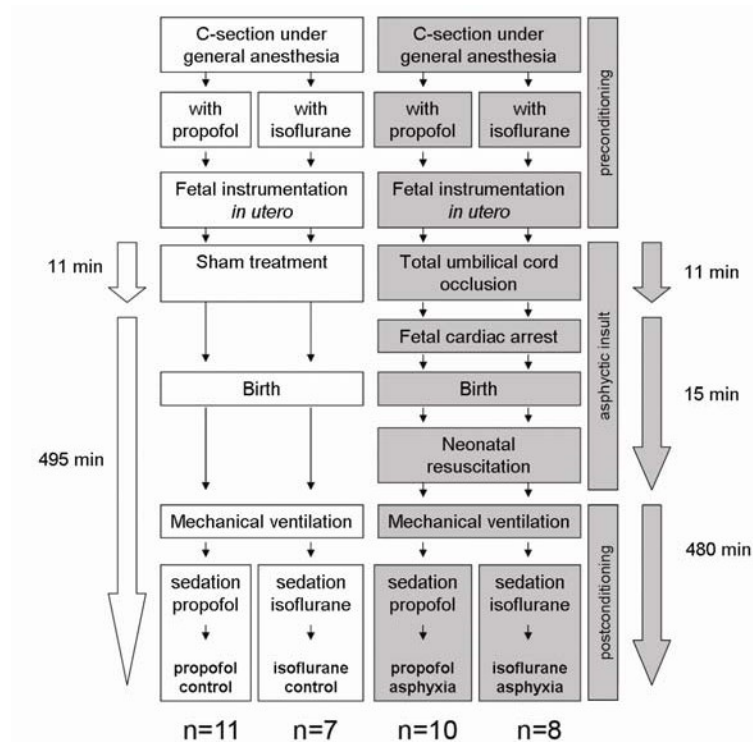
Figure 20: Study design and time course of experiments. Lambs were born at 89% of gestation. The ewes carrying the gestational age control group were euthanized and their offspring was delivered by caesarean section and subsequently euthanized. The ewes of the other groups underwent the caesarean section while being sedated with the same anaesthetic as their offspring later on intensive care unit. Two groups were exposed to total umbilical cord occlusion (UCO) leading to cardiac arrest.

Thereafter, inspiratory pressure was adjusted to achieve a targeted minute volume of 3.0 L/min and a P_aCO_2 of 35-45 mmHg. The ventilation and sedation was continued for 8 hours after delivery. The sedation was maintained either with isoflurane (0.5-1.0%) or propofol (1-3mg/kg/h) and supplemented with remifentanil (3µg/kg/min) in both groups. The remifentanil was dissolved in 20% glucose and ringerlactate solution in a concentration allowing for an infusion rate of 3mL/kg/h. All lambs (sham treated included) received surfactant (200 mg/kgBW Curosurf®, a generous gift of Chiesi, Italy) intra-tracheally and two times maternal blood transfusion of 10ml/kgBW during initial stabilization. All cord-occluded lambs developed a spontaneous HR (>150/min) and a sufficient MABP (>50mmHg) within 10 minutes after starting resuscitation with exception of two lambs, which were excluded from the study.

The eighteen sham treated fetuses were prepared *in utero*, with catheters inserted in the femoral and umbilical artery and jugular vein and endotracheal intubation as described above. Eleven minutes (mean time of occlusion in study group) after the end of the instrumentation, they were delivered, weighed, sedated, and connected to pressure-controlled ventilation (see above).

At eight hours after delivery the lambs were euthanized by an i.v. injection of T61® (Veterinaria AG, Zürich, Switzerland). The brain was immediately removed from the scull and separated in the midline. From one hemisphere tissue sections were taken and shock-frozen in liquid nitrogen. Tissue was subsequently stored at -80°C.

9.3.3.3 Electroencephalogram

Two bipolar pairs of electroencephalogram (EEG) silver ball electrodes (AS633-5SSF, Cooner wire Co., Chatsworth, CA, USA) were placed subcutaneously over the left and right parasagittal parietal cortex (5mm and 15mm anterior to bregma and 10mm lateral), with a reference electrode placed over the occiput.

The EEG signal was sampled at 250Hz and stored on hard-disk for off-line analysis. Data was filtered using a 0.5 Hz high-pass and 30Hz low-pass 4th order Butterworth filter. EEG signal with an amplitude >1000µV was considered an artifact and removed from analysis (1% of data). After filtering, background analysis of the EEG was performed using an amplitude- and timethreshold based algorithm[26-28]. Burst activity was defined as an epoch with an amplitude >15µV and a duration of >1s in both channels. Interburst intervals were defined as epochs with an amplitude <15µV and a duration >3s in both channels[29,30]. Segments not meeting above criteria were classified as undefined.

Subsequently, spectral analysis was performed using Matlab® (The MathWorks, Massachusetts, USA). Data was divided into half-overlapping 4-s segments around the center of each burst. Each segment was multiplied by a Hamming window before Fourier transform. The frequency spectrum was determined for each segment, and was divided in δ_1 (0.5-1 Hz), δ_2 (1-4 Hz), θ (4-8 Hz), α (8-13 Hz) and β (13-30 Hz) band. Likewise, spectral analysis was performed for the interburst intervals.

Three aspects of the transformed signal were calculated: (a) absolute power (defined as the integral of all powers within the frequency band 0.5-30 Hz, expressed in $\mu V2$), (b) relative power (defined as the ratio of absolute band power to total power of all bands, expressed in percentage); (c) spectral edge frequency (SEF) (defined as the frequency that delimits 90 % of the power between 0.5-30 Hz). Finally, the obtained parameters were averaged over the left and right channel to obtain median burst frequency parameters per measurement.

In addition, the raw EEG signal was converted in an amplitude-integrated EEG (aEEG) using the software of the NicoletOneTM device (Viasys Healthcare, Conshohocken, PA, USA). The aEEG is a technique in which the EEG signal is expressed in a simplified and time-compressed manner[31]. The aEEG has shown to be very useful tool for long-term bed-side monitoring of neonatal seizures and background patterns[32].

9.3.3.4 Western Blotting

Frozen brain tissue of the frontal cortex was homogenized in ice-cold RIPA buffer (R0278-50ML, Sigma-Aldrich Corp., St. Louis, MO, USA) containing Halt Protease and Phosphatase Inhibitor Cocktail, EDTA-free (100X) (#78445, Thermo Fisher Scientific Inc., Rockford, IL 61105 USA). The samples were then centrifuged at 500 x g for 20min at 4°C to remove cellular debris. Protein content in the supernatant was determined using the Micro BCA Protein Assay Kit (#23235, Thermo Fisher Scientific Inc., Rockford, IL 61105 USA), with BSA as the standard. Western blots were performed as described previously[33]. The following dilutions for antibodies were used: 1:1000 for monoclonal anti-β-actin clone AC-1 (Sigma-Aldrich Catalog Number A5441), anti-cleaved-caspase-3 (Asp175) (#9664, Cell Signaling Technology, Inc., Danvers, MA, USA)[34], and anti-NMDA receptor (#4212, Cell Signaling Technology, Inc., Danvers, MA, USA). As secondary antibody IRDye® 680 conjugated goat (polyclonal) antirabbit IgG, IRDye® 800 conjugated goat (polyclonal) anti-rabbit IgG, and IRDye® 800 conjugated goat (polyclonal) anti-mouse IgG, (LI-COR, Lincoln, Nebraska, USA) were used in a dilution of 1:6000. The blots were analyzed using the LICOR Odyssey Infrared Imaging System, and images were acquired using Adobe Photoshop CS4 software.

9.3.3.5 Immunohistochemistry

The left cerebral hemisphere was immersion-fixated in 4% paraformaldehyde and imbedded in gelatin. Serial sections of the prefrontal cortex of 50µm thick were cut on a vibrotome and stained for

cleaved caspase-3 by free-floating. Briefly, endogenous peroxidase activity was blocked with 0,3% H_2O_2 after rinsing with 0.01M Tris-buffered Saline (TBS) and 0.01M Trisbuffered Saline with 0,2%Triton X-100 (TBS-T). The sections were incubated overnight at 4°C with the diluted primary antibody (cleaved caspase-3 (Asp175) 1:100, #9661, Cell Signaling Technology, Boston, USA). After rinsing with TBS and TBS-T, the sections were incubated with a secondary donkey-anti-rabbit biotinylated antibody (1:800, Jackson, West Grove, PA, USA) for 2 hours at room temperature. The immunostaining was enhanced with Vectastain ABC peroxidase Elite Kit (PK-6200, Vector Laboratories, Burlingame, USA) followed by a 3,3`-Diaminobenzidine (DAB) staining. Subsequently, the sections were rinsed with TBS, mounted on glass slides and dried overnight. After dehydration, the slides were coverslipped using DePeX (Serva, Heidelberg, Germany). Evaluation was performed by light microscopy (Axioskop 40, Zeiss, Germany) with LeicaQWin Pro v.3.4.0 software (Leica Microsystems, Germany).

9.3.3.6 *Lipid peroxidation assay*

Lipid peroxides include reactive aldehydes, of which the most abundant is malondialdehyde (MDA). Therefore, measurement of MDA is widely used as an indicator of lipid peroxidation[35]. For brain tissue analysis we used the ALdetect (MDA-Specific) Lipid Peroxidation Assay Kit (ALdetect (MDA-Specific) Lipid Peroxidation Assay Kit BML-AK-171, Enzo Life Sciences International, Inc., Plymouth Meeting, PA 19462-1202, USA) according to the manufacturer's manual.

9.3.3.7 *Data Analysis*

Data with a normal distribution are expressed as a mean±SEM, otherwise data are expressed as a median and inter quartile range (IQR). Physiologic variables were analyzed using 2-way ANOVA. All other data were analyzed by the Mann-Whitney-Wilcoxon test. A p-value<0.05 was considered significant. All statistical analyses were performed using the statistical software GraphPad Prism 5.0.

9.3.4 Results

The lambs had similar gestational ages of 133.7±0.16 days and similar birth weights of 3.6±0.07kg. All animals developed a bradycardia with a frequency of <30/min and a cardiac arrest upon reperfusion. Gender distribution and physiologic data are given in Table 5 and Figure 23.
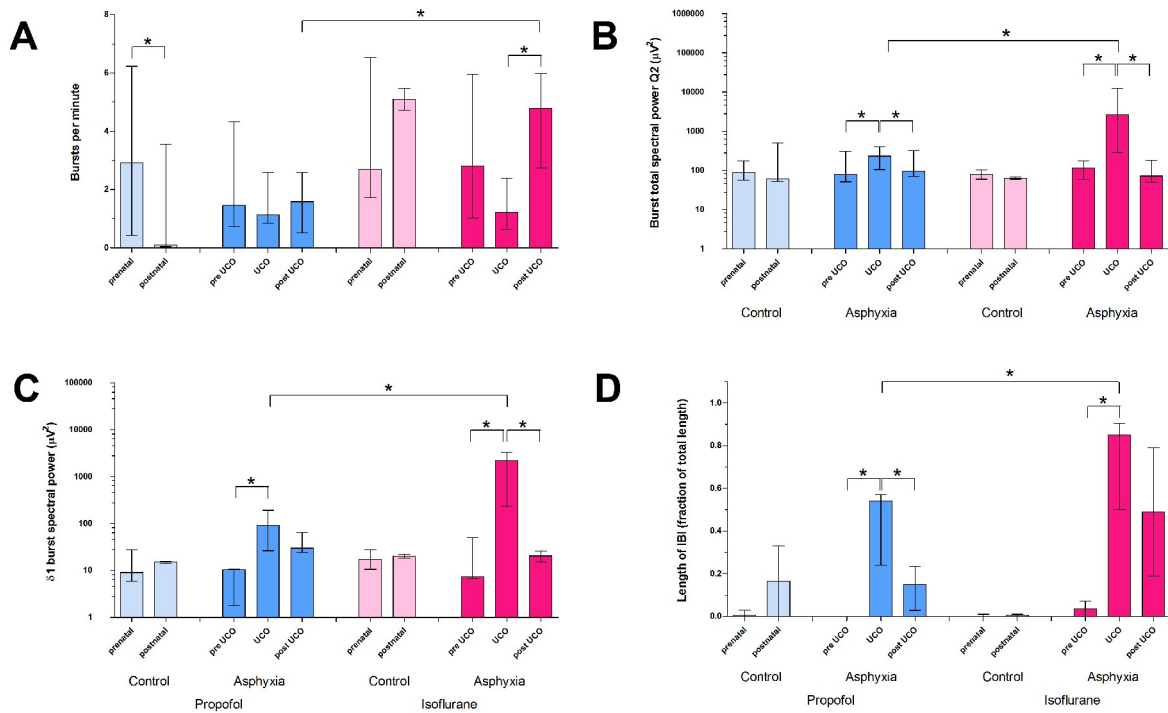
Figure 21: Pre- and postnatal EEG of control groups and EEG before, during and after UCO in asphyxia groups. Depicted are (A) the median burst per minute, (B) the median total spectral power, (C) the relative spectral power for δ1, and (D) the interburst interval length as median and interquartile range. Significant differences (p<0.05) are marked by *.
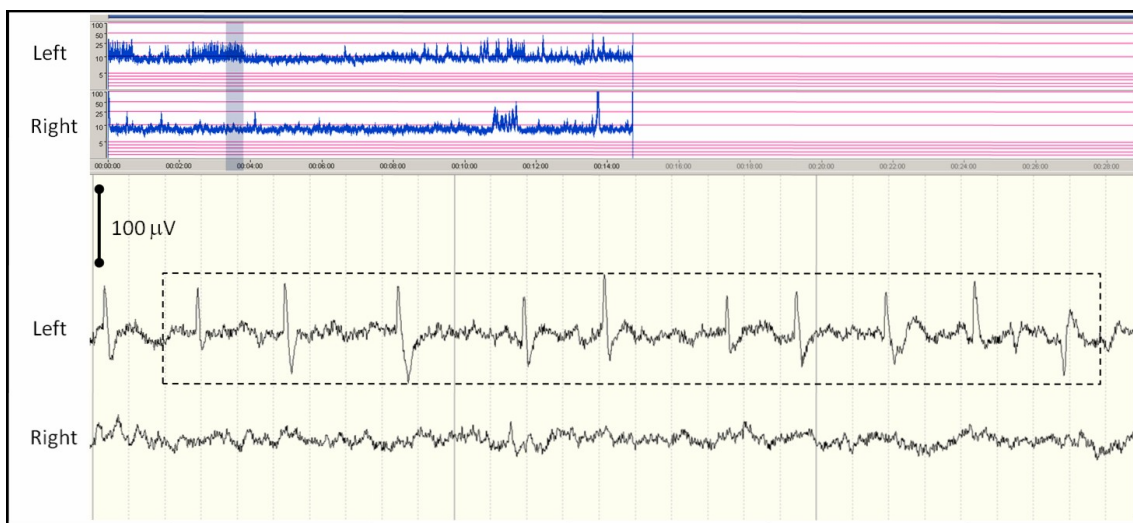
Figure 22: A 15-min epoch of amplitude-integrated EEG during the post occlusion phase (top, x-axis shows time in min, y-axis shows the amplitude of the signal and is displayed semilogarithmic:linear 0-10 μV and logarithmic 10-100 μV) shows a slight increase of the lower margin amplitude and increase of bandwidth, indicated by the shaded blue vertical band.

Illustration of the accessory bilateral EEG during the shaded vertical band of the aEEG (bottom, time resolution 1 s/dotted vertical line, sensitivity indicated by vertical stick) showing repetitive sharp waves every 2-3 s, suggestive of seizure activity in the left hemisphere. The rectangular box indicates the period over which spectral analysis is performed and shows a relative delta power of 84%.
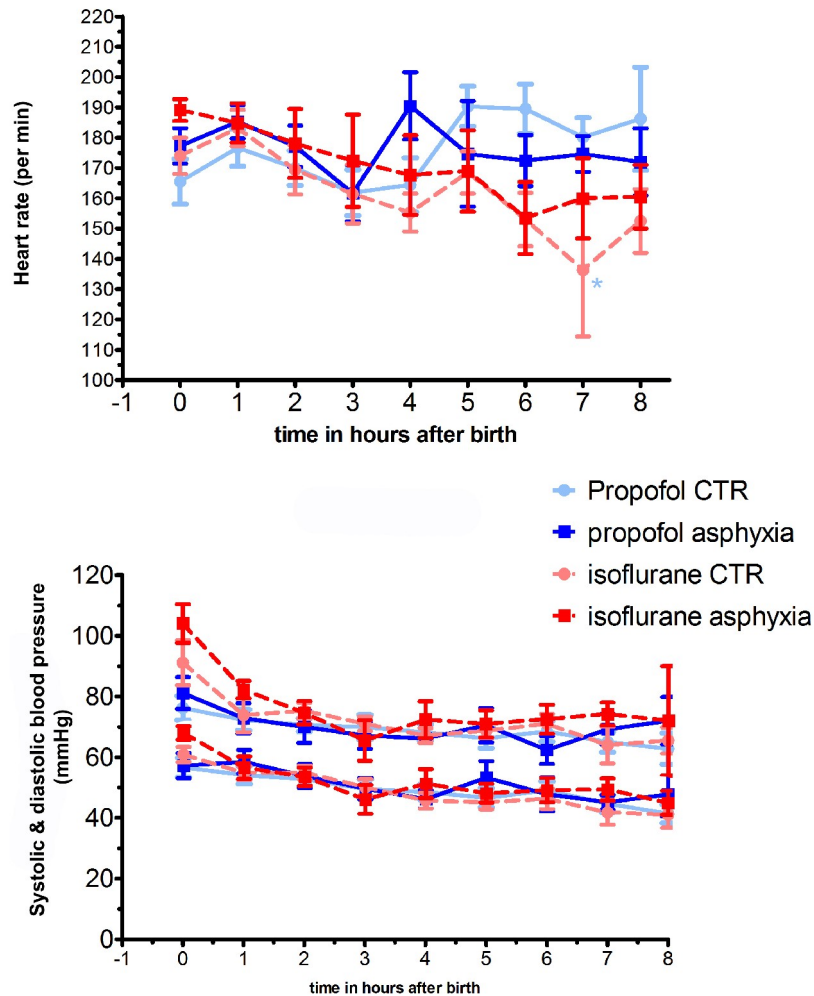
*Figure 23: Heart rate and blood pressure of all lambs after birth. Depicted are mean and SEM. Significant differences (p<0.05) compared to other groups are marked by * in colour of respective group.*

9.3.4.1 EEG

Baseline measures before UCO

The algorithm detected burst, interburst interval and undefined segments in 47%, 28% and 25% of cases, respectively. The median burst per minute before UCO was 2.4 (IQR, 1.1-4.5) per minute and was not different between the four experimental groups. The median total spectral power before UCO was 138 (IQR, 55-195) μV^2 and was not different between the groups. The relative spectral power for δ_1, δ_2, θ, α and β did not differ between group before UCO and median values were 25 (IQR, 18-32), 43 (IQR, 38-50), 10 (IQR, 8-15), 4 (IQR, 3-7) and 3 (IQR, 2-6) percent, respectively. Median SEF before UCO was 10 (IQR, 9-12) Hz and was not different between the groups.

Figure 24: Illustration of the bilateral amplitude-integrated EEG before, during and after occlusion of the umbilical cord. The x-axis shows time in min. The y-axis shows the amplitude of the signal and is displayed semi-logarithmic: linear 0-10 µV and logarithmic 10-100 µV. The vertical arrow (left) represent the onset of occlusion. Before occlusion the lower margin amplitude is 20-25 µV. Within 1 min the lower margin amplitud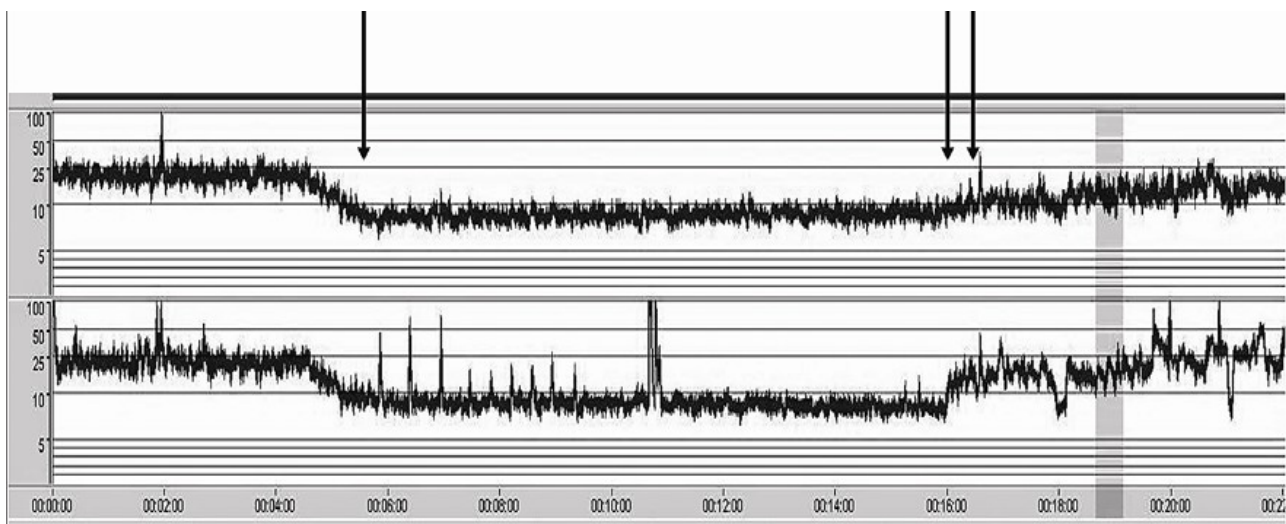e decreased to values < 10 µV. After occlusion (double arrow) the lower margin amplitude increases to pre-occluding values.

Changes of burst activity

The aEEG rapidly suppressed, within 60s, after the onset of UCO in both occlusion groups (Figure 24). In isoflurane treated lambs we observed a 60% decrease in burst per minute during UCO, with significant more burst activity than the propofol treated lambs in the post UCO phase (median burst/minute 4.8 vs. 1.6, p<0.05). In propofol treated lambs no significant changes in burst activity was observed during or after UCO (Figure 21A). In isoflurane treated lambs burst total spectral power during UCO increased more than propofol treated lambs (Figure 21B). Of the relative spectral power measures, δ_1 and δ_2 were particularly responsible for the increase of burst spectral power in isoflurane treated lambs (Figure 21C). In isoflurane treated lambs, δ_1 and δ_2 spectral power measures increased from 45 to 75% in the burst. In propofol treated lambs δ_1 and δ_2 spectral power decreased only 5%. The increase of burst spectral power and relative delta activity was associated with characteristic repetitive patterns of sharp waves of the raw EEG, indicating seizure activity (Figure 22).

We observed no significant change in SEF during UCO or postnatally between isoflurane and propofol treated lambs.

Changes of interburst interval

We observed a significant increase in interburst interval length during UCO, which was significantly greater in isoflurane than propofol treated lambs (Figure 21D). In the post UCO phase this difference became smaller.

9.3.4.2 Western blot analysis

Cleaved Caspase-3

In propofol control group protein level of cleaved caspase-3 decreased to 34.2±9.0% (p<0.04) in the frontal brain cortex compared to gestational age (GA) control group (Figure 25A). Cleaved caspase-3 increased by 375.3% in the propofol asphyxia group compared to propofol control (p<0.04) but remained unchanged compared to GA control group. In isoflurane control group cleaved caspase-3 remained unchanged compared to GA control group. After prenatal asphyxia cleaved caspase-3 increased in isoflurane treated lambs by 266.7% compared to isoflurane controls (p=0.01), by 261.2±69.9% (p<0.05) compared to GA control group, and up to 203.2% ±54.44% (p<0.03) compared to propofol asphyxia group.
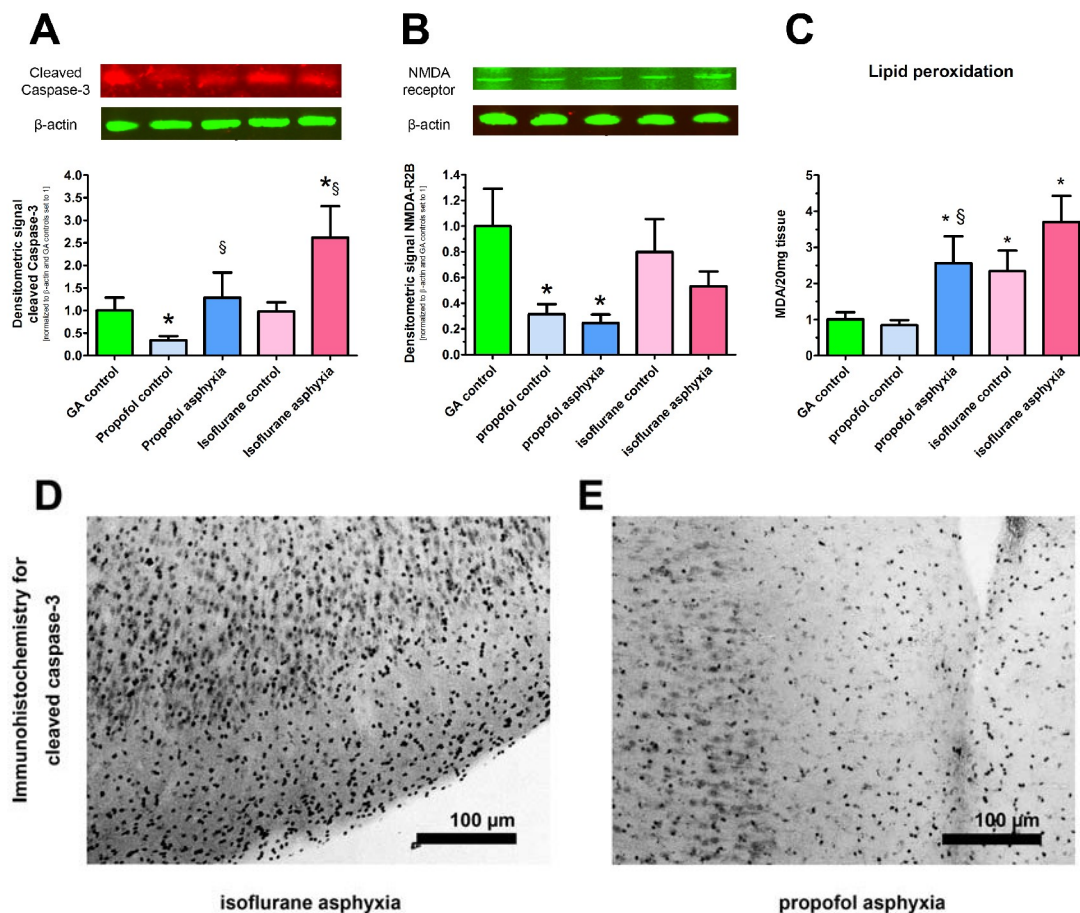
*Figure 25: (**A**) Western blot for cleaved caspase-3 (indication for apoptosis) and (**B**) NMDA receptors in frontal cortex of fetal brain normalized to β-actin. (**C**) Malondialdehyde (MDA) level in cerebral fetal cortex as indication of lipid peroxidation due to reactive oxygen species (ROS) formation. Levels of gestational age control group was set to 1 in panel A, B and C. Depicted are mean and SEM. Significant differences (p<0.05) compared to gestational age control groups are marked by *. Significant differences (p<0.05) between asphyxiated and corresponding not asphyxiated drug control group are marked by § and significant differences between asphyxiated propofol and asphyxiated isoflurane treated lambs are marked by $. Representative immunohistochemical staining for cleaved caspase-3 for (**D**) isoflurane asphyxia and (**E**) propofol asphyxia group.*

N-methyl-d-aspartate-receptor (NMDA-R)

In propofol control group the level of NMDA-R decreased to 31.5%±7.8% (p<0.02) compared to GA control group (Figure 25B). After prenatal asphyxia NMDA-R level decreased in propofol treated lambs to 24.6%±6.6% (p=0.04) compared to GA controls and to 46.2%±21.7% (p<0.05) when compared to isoflurane asphyxia group. In isoflurane groups the level of NMDA-R was unchanged compared to GA controls.

9.3.4.3 *Lipid peroxidation assay*

Malondialdehyde (MDA)

In propofol control group malondialdehyde (MDA) level in frontal brain cortex remained unchanged compared to gestational age (GA) control group (Figure 25C). MDA increased by 302.9% in the propofol asphyxia group compared to propofol control (p<0.01) and by 256.1±74.4% (p=0.04) compared to GA control group. In isoflurane control group MDA increased by 234.0±57.0% (p=0.02) compared to GA control group. After prenatal asphyxia MDA increased by 158.3% compared to isoflurane control (p=0.29) and up to 370.4±71.9% (p<0.01) compared to GA control group.

9.3.5 Discussion

In this paper we demonstrate structural and functional changes of the cerebrum of late preterm lambs in an unique experimental sequence of severe asphyxia due to complete umbilical cord occlusion in utero, fetal cardiac arrest, emergency Caesarean section, postnatal resuscitation of the fetus and intensive care for the first eight hours after birth. The structural and functional changes indicate that medication has the potential to mediate neuroprotection for the fetus when administered already before birth to the maternal-fetal unit during caesarean section and postnatally to the baby on the NICU.

Neonatal hypoxic–ischemic (HI) encephalopathy due to birth asphyxia is a major predictor of neurodevelopmental disability in term infants and occurs in 1 to 6 of every 1000 live term births[36]. Neonatal HI encephalopathy is a serious condition: 15 to 20% of affected infants die during the newborn period, and an additional 25% have permanent neurologic deficits[5]. Currently, the only clinically established approach is moderate hypothermia in term born infants with minor brain injury due to mild or moderate asphyxia[14]. No specific treatments have yet been established for preterm babies suffering from severe asphyxia[37]. Therefore, the emphasis is on supportive therapy after neonatal resuscitation[4]. Importantly, the cascade of events leading to neuronal death occurs over hours after termination of the hypoxic-ischemic insult. The implication of this study is that interruption of this deleterious cascade even after termination of the insult could prevent or ameliorate the consequences of brain injury in hypoxic-ischemic disease[38].

Until now, except for Xenon[6], anaesthetic agents have not been tested in regards to their possible neuroprotective properties in the developing brain. We observed that isoflurane administration to the maternal-fetal unit before and during the umbilical cord occlusion (UCO) resulted in EEG changes with increased burst spectral power when compared to the propofol treated and occluded group. The observations of increased spectral power in the burst and increased amount of δ_1 and δ_2 spectral power suggested that isoflurane is associated with high voltage low-frequency waves which may indicate seizure activity (Figure 22). Despite sedation, activity of clinical convulsion was observed in all animals that underwent UCO. In order to quantify this extremely biased clinical judgment, we used this standardized analysis. To quantify the effects is extremely important in this new approach since seizures in the neonatal period can be extremely refractory to therapy. The immature brain may be more susceptible to the epileptogenic effects of provoking stimuli, such as hypoxia. Seizures may alter brain development to result in later epilepsy and neurologic impairment, even in the absence of obvious infarction or other structural injury[39]. In this context, the smaller increase of (lowfrequency) spectral power during bursts during UCO in our propofol treated lambs may be considered beneficial.

This is also supported by the fact that the length of the interburst interval as a predictive EEG marker of later neonatal brain injury[40] was less increased during UCO when propofol group was compared to isoflurane treated animals. Hence, during propofol sedation less burst-suppression of the EEG was recorded.

A potential concern in using anaesthetic drugs in preterm and term newborn infant has come from animal studies[41,42]. Anaesthetics induced massive induction of apoptosis in the developing brain of newborn rodents[43]. The short gestation in rats (22.5 d) and mice (19.5d) compared to the situation during the relatively long human gestation (280d) raised the question to which extent the effect of a pharmacological intervention aiming at crucial development mediating elements as NMDA-receptors differed in rodents with their consequently faster brain development. In addition, it has to be taken into account that important steps such as white matter myelination occurs in rodents after birth in contrast to humans[44]. Therefore, sheep appear to be an appropriate model since the ovine gestation period is 150d with a prenatal white matter myelination which is much closer to the human development. In addition, sheep have been already extensively used to study the effects of fetal and perinatal asphyxia[45,46]. We therefore assessed apoptosis by determination of cysteinyl aspartate-specific protease-3 (caspase-3). Caspase-3 is the most effective apoptotic regulator because it plays a decisive role in the occurrence of apoptosis by acting as the effector caspase which determines the incidence of apoptosis[47]. In our study, activated caspase-3 expression was unchanged in isoflurane sedated control lambs compared to gestational age controls suggesting no neurotoxic effect due to isoflurane administration over eight hours. Surprisingly, caspase-3 activation even decreased in propofol treated control lambs compared to gestational age controls and isoflurane treated ones. After UCO, cardiac arrest, successful resuscitation and eight hours of sedation with isoflurane caspase-3 activation increased nearly 3-fold compared to normal situation at this time point in gestation. But after severe asphyxia, caspase-3 activation showed no increase if lambs were treated with propofol, suggesting neuroprotection.

The principal mechanisms leading to cell death operate after termination of the hypoxicischemic insult and upon reperfusion, are initiated by energy depletion, and are followed by activation of glutamate receptors as NMDA receptor. Neurotoxicity associated with overstimulation of NMDA receptors is thought to be mediated by an excessive Ca^{2+}-influx and plays a major role in the series of potentially neurotoxic events[38]. One of these events is the stimulation of phospholipase A2 or Ca^{2+} overload of mitochondria, leading to the generation of reactive oxygen species (ROS). Therefore, inhibition of NMDA receptor, or preventing accumulation of ROS, would attenuate brain damage. A recent study by Sandoval et al.[48] provided data that even a down-regulation of NMDA receptors mediates neuroprotection in cortical cultures. They proposed that the down-regulation is part of a complex "survival program". Synaptic NMDA receptors have anti-apoptotic activity, whereas stimulation of extrasynaptic NMDA receptors caused loss of mitochondrial membrane potential (an early marker for glutamate-induced neuronal damage) and cell death[49]. Specific blockade of extrasynaptic NMDA receptors may effectively prevent neuron loss neuropathological conditions associated with ischemia and glutamate toxicity[49]. Hardingham showed that the NMDA receptor NR2A subunits are localized primarily at synapses and promote cell survival whereas NR2B subunits are contained predominantly in extra-synaptic NMDA-Rs and promote cell death[49]. Consistent with the concept that NR2B is involved in cell death, Sandoval et al. found that the selective pharmacological blockade of NR2B prevented cell death in cortical cultures. In line with this, all propofol sedated lambs in our study showed not only better EEG features and less cerebral apoptosis compared with isoflurane treated animals, but also a downregulation of the NMDA receptor subunit NR2B.

ROS mediated lipid peroxidation and DNA damage appears to be the final common pathway for neuronal cell death[38]. The preterm brain seems particularly vulnerable to ROS formation and the resulting oxidative injury after asphyxia because of immature scavenging mechanisms and a relative abundance of iron that acts as a catalyst for the formation of free radicals[50]. One pathway by which propofol exerts in adults its cell protective properties is the reduction of the occurrence of ROS after ischemia[21]. The reduced lipid peroxidation in our propofol treated lambs suggests, that in fact the scavenging properties of propofol may play an important role in mediating protection in the premature

brain, too. Consistent with this notion, it has been demonstrated in human newborns that the degree of lipid peroxidation represents a valid predictive marker for birth asphyxia related morbidity and mortality[24].

One limitation of our study is that we only studied one time point in gestation, namely late preterm sheep with a gestational age of 133d. The brain maturation especially during the last third of gestation is a very fast changing system. Observations made at one time point cannot be easily extrapolated to earlier or later time points of gestation[51]. Comparing our findings to the ones made in infant rodent models show that there are also significant differences between species. In spite of the fact that the ovine brain development is much closer to the human situation one has to be careful in extrapolating our data to the clinical situation in the NICU[45,46,52]. An additional limitation is that we sedated the lambs only for eight hours whereas preterm and late preterm infants with complications as birth asphyxia have to be sedated for days or sometimes even for weeks. And we only examined immediate occurring changes and injury in brain tissue not knowing in what extent molecular repair systems would be capable to cope with the produced injury. We used EEG recordings to speculate how the lambs coped and would cope with the produced brain injury. However, the two-channel EEG represents a basic surveillance tool for brain activity which is also used in the clinical scenario but which is not fully comparable with results gained from a full EEG.

Finally, an often mentioned concern associated with the use of propofol in neonates is the occurrence of the propofol infusion syndrome (PRIS)[53]. This is characterized by haemodynamic abnormalities, lactic acidosis and rhabdomyolysis, and carries a mortality of approximately 85 per cent[54]. As shown in Table 5 and Figure 23, the propofol treated lambs in our study developed no acidosis and no severe haemodynamic disturbances within eight hours. But we cannot rule out that a longer use of propofol or a higher number of treated individuals would be accompanied with the occurrence of PRIS due to a relatively high inter-individual variability in propofol pharmacokinetics in preterm and term neonates[55].

9.3.6 Conclusion

Perinatal neuroprotection is a major health care priority, given the enormous burden of human suffering and financial cost caused by perinatal brain damage. Anaesthetic drugs may alter the normal development of the brain, which proceeds at a fast pace during the perinatal period. We showed that early propofol administration to the maternal-fetal unit during severe fetal asphyxia was associated with less cerebral dysfunction and apoptosis in late preterm lambs. The observed propofol related neuroprotection seemed to be mediated by its ROS scavenging properties and its depressing influence on the NMDA pathway. The feasibility of designing a strategy that blocks brain damage without disrupting normal development in humans will have to be further evaluated.

9.3.7 Acknowledgement:

9.3.8 References

1. Jouvet P., Cowan F.M., Cox P., et al. (1999) *Reproducibility and accuracy of MR imaging of the brain after severe birth asphyxia*. AJNR Am J Neuroradiol. **20**, 1343-1348

2. Himmelmann K., Hagberg G. and Uvebrant P. (1999) *The changing panorama of cerebral palsy in Sweden. X. Prevalence and origin in the birth-year period 1999-2002*. Acta Paediatr. **99**, 1337-1343

3. Vincer M.J., Allen A.C., Joseph K.S., Stinson D.A., Scott H. and Wood E. (2006) *Increasing prevalence of cerebral palsy among very preterm infants: a population-based study*. Pediatrics **118**, e1621-1626

4. Herrera-Marschitz M., Morales P., Leyton L., et al. (2010) *Perinatal asphyxia: current status and*

approaches towards neuroprotective strategies, with focus on sentinel proteins. Neurotox Res. **19**, 603-627

5. Ferriero D.M. (2004) *Neonatal brain injury.* N Engl J Med. **351**, 1985-1995

6. Hobbs C., Thoresen M., Tucker A., Aquilina K., Chakkarapani E. and Dingley J. (2008) *Xenon and hypothermia combine additively, offering long-term functional and histopathologic neuroprotection after neonatal hypoxia/ischemia*. Stroke **39**,1307-1313

7. Benders M.J., Bos A.F., Rademaker C.M., et al. (2006) *Early postnatal allopurinol does not improve short term outcome after severe birth asphyxia*. Arch Dis Child Fetal Neonatal **91**, F163-165

8. Torrance H.L., Benders M.J., Derks J.B., et al. (2009) *Maternal allopurinol during fetal hypoxia lowers cord blood levels of the brain injury marker S-100B*. Pediatrics **124**, 350-357

9. Zhu C., Kang W., Xu F., et al. (2009) *Erythropoietin improved neurologic outcomes in newborns with hypoxic-ischemic encephalopathy*. Pediatrics **124**, e218-226

10. Welin A.K., Svedin P., Lapatto R., et al. (2007) *Melatonin reduces inflammation and cell death in white matter in the mid-gestation fetal sheep following umbilical cord occlusion.* Pediatr Res. **61**, 153-158

11. van der Kooij M.A., Nijboer C.H., Ohl F., et al. (2010) *NF-kappaB inhibition after neonatal cerebral hypoxia-ischemia improves long-term motor and cognitive outcome in rats*. Neurobiol Dis. **38**, 266-272

12. Nijboer C.H., van der Kooij M.A., van Bel F., Ohl F., Heijnen C.J. and Kavelaars A. (2010) *Inhibition of the JNK/AP-1 pathway reduces neuronal death and improves behavioral outcome after neonatal hypoxic-ischemic brain injury*. Brain Behav Immun. **24**, 812-821

13. van Velthoven C.T., Kavelaars A., van Bel F. and Heijnen C.J. (2010) *Mesenchymal stem cell treatment after neonatal hypoxic-ischemic brain injury improves behavioral outcome and induces neuronal and oligodendrocyte regeneration*. Brain Behav Immun. **24**, 387-393

14. Gluckman P.D., Wyatt J.S., Azzopardi D., et al. (2005) *Selective head cooling with mild systemic hypothermia after neonatal encephalopathy: multicentre randomised trial*. Lancet **365**, 663-670

15. Pickler R.H., McGrath J.M., Reyna B.A., et al. (2010) *A model of neurodevelopmental risk and protection for preterm infants*. J Perinat Neonatal Nurs. **24**, 356-365

16. Schifilliti D., Grasso G., Conti A. and Fodale V. (2010) *Anaesthetic-related neuroprotection: intravenous or inhalational agents?* CNS Drugs **24**, 893-907

17. Littleford J. (2004) *Effects on the fetus and newborn of maternal analgesia and anesthesia: a review*. Can J Anaesth. **51**, 586-609

18. Chen L,. Xue Z. and Jiang H. (2008) *Effect of propofol on pathologic time-course and apoptosis after cerebral ischemia-reperfusion injury*. Acta Anaesthesiol Scand. **52**, 413-419

19. Acquaviva R., Campisi A., Raciti G., et al. (2005) *Propofol inhibits caspase-3 in astroglial cells: role of heme oxygenase-1*. Curr Neurovasc Res. **2**, 141-148

20. Hans P. and Bonhomme V. (2006) *Why we still use intravenous drugs as the basic regimen for neurosurgical anaesthesia*. Curr Opin Anaesthesiol. **19**, 498-503

21. Vasileiou I., Xanthos T., Koudouna E., et al. (2009) *Propofol: A review of its non- anaesthetic effects*. Eur J Pharmacol. **605**, 1-8

22. Abboud T.K., Gangolly J., Mosaad P. and Crowell D. (1989) *Isoflurane in obstetrics*. Anesth Analg. **68**, 388-391

23. Abraham R.J., Sau A. and Maxwell D. (2010) *A review of the EXIT (Ex utero Intrapartum Treatment) procedure*. J Obstet Gynaecol. **30**, 1-5

24. Mondal N., Bhat B.V., Banupriya C. and Koner B.C. (2010) *Oxidative stress in perinatal asphyxia in relation to outcome*. Indian J Pediatr. **77**, 515-517

25. Wang C., Zhang X., Liu F., Paule M.G. and Slikker W., Jr. (2010) *Anesthetic-induced oxidative stress and potential protection*. ScientificWorldJournal **10**,1473-1482

26. Gavilanes A.W., Gantert M., Strackx E., et al. (2010) *Increased EEG delta frequency corresponds to chorioamnionitis-related brain injury*. Front Biosci (Schol Ed). **2**, 432-438

27. Niemarkt H.J., Andriessen P., Peters C.H., Pasman J.W., Zimmermann L.J. and Bambang Oetomo S. (2010) *Quantitative analysis of maturational changes in EEG background activity in very preterm infants with a normal neurodevelopment at 1 year of age*. Early Hum Dev. **86**, 219-224

28. Niemarkt H.J., Andriessen P., Peters C.H., et al. (2010) *Quantitative analysis of amplitudeintegrated electroencephalogram patterns in stable preterm infants, with normal neurological development at one year*. Neonatology **97**,175-182

29. Williams C.E., Gunn A.J., Mallard C. and Gluckman P.D. (1992) *Outcome after ischemia in the developing sheep brain: an electroencephalographic and histological study*. Ann Neurol. **31**, 14-21

30. Fraser M., Bennet L., Gunning M., et al. (2005) *Cortical electroencephalogram suppression is associated with post-ischemic cortical injury in 0.65 gestation fetal sheep*. Brain Res Dev Brain Res. **154**, 45-55

31. Rosen I. (2006) *The physiological basis for continuous electroencephalogram monitoring in the neonate*. Clin Perinatol. **33**, 593-611

32. Toet M.C., van der Meij W., de Vries L.S., Uiterwaal C.S. and van Huffelen K.C. (2002) *Comparison between simultaneously recorded amplitude integrated electroencephalogram (cerebral function monitor) and standard electroencephalogram in neonates*. Pediatrics **109**, 772-779

33. Seehase M., Gantert M., Ladenburger A., et al. (2011) *Myocardial Response in Preterm Fetal Sheep Exposed to Systemic Endotoxinaemia*. Pediatr Res. **70**, 242-246

34. Kunzmann S., Glogger K., Been J.V., et al. (2010) *Thymic changes after chorioamnionitis induced by intraamniotic lipopolysaccharide in fetal sheep*. Am J Obstet Gynecol. **202**, e471-479

35. Esterbauer H., Schaur R.J. and Zollner H. (1991) *Chemistry and biochemistry of 4-hydroxynonenal, malonaldehyde and related aldehydes*. Free Radic Biol Med. **11**, 81-128

36. Perlman M. and Shah P.S. (2011) *Hypoxic-ischemic encephalopathy: challenges in outcome and prediction*. J Pediatr. **158**, Suppl 2, e51-54

37. Fan X. and van Bel F. (2010) *Pharmacological neuroprotection after perinatal asphyxia*. J Matern Fetal Neonatal Med. **23**, Suppl 3, 17-19

38. Volpe J.J. (2001) *Perinatal brain injury: from pathogenesis to neuroprotection*. Ment Retard Dev Disabil Res Rev. **7**, 56-64

39. Jensen F.E. (2002) *The role of glutamate receptor maturation in perinatal seizures and brain injury*. Int J Dev Neurosci. **20**, 339-347

40. Hellström-Westas L. and Rosen I. (2005) *Electroencephalography and brain damage in preterm infants*. Early Hum Dev. **81**, 255-261

41. Wang S., Peretich K., Zhao Y., Liang G., Meng Q. and Wei H. (2009) *Anesthesia-induced neurodegeneration in fetal rat brains*. Pediatr Res. **66**, 435-440

42. Cattano D., Young C., Straiko M.M. and Olney J.W. (2008) *Subanesthetic doses of propofol induce neuroapoptosis in the infant mouse brain*. Anesth Analg. **106**,1712-1714

43. Mellon R.D., Simone A.F. and Rappaport B.A. (2007) *Use of anesthetic agents in neonates and young children*. Anesth Analg. **104**, 509-520

44. Watson R.E., Desesso J.M., Hurtt M.E. and Cappon G.D. (2006) *Postnatal growth and morphological development of the brain: a species comparison*. Birth Defects Res B Dev Reprod Toxicol. **77**, 471-484

45. Gunn A.J. and Bennet L. (2009) *Fetal hypoxia insults and patterns of brain injury: insights from*

animal models. Clin Perinatol. **36**, 579-593

46. Back S.A., Riddle A. and Hohimer A.R. (2006) *Role of instrumented fetal sheep preparations in defining the pathogenesis of human periventricular white-matter injury*. J Child Neurol. 21, 582-589

47. Reed J.C. (2000) *Mechanisms of apoptosis*. Am J Pathol. **157**, 1415-1430

48. Sandoval R., Gonzalez A., Caviedes A., et al. (2011) *Homeostatic NMDA receptor downregulation via brain derived neurotrophic factor and nitric oxide-dependent signalling in cortical but not in hippocampal neurons*. J Neurochem. **118**, 760-772

49. Hardingham G.E., Fukunaga Y. and Bading H. (2002) *Extrasynaptic NMDARs oppose synaptic NMDARs by triggering CREB shut-off and cell death pathways*. Nat Neurosci. **5**, 405-414

50. Blomgren K. and Hagberg H. (2006) *Free radicals, mitochondria, and hypoxia-ischemia in the developing brain*. Free Radic Biol Med. **40**, 388-397

51. Kramer B.W. (2008) *Antenatal inflammation and lung injury: prenatal origin of neonatal disease*. J Perinatol. **28**, Suppl 1, S21-27.

52. Clancy B., Finlay B.L., Darlington R.B. and Anand K.J. (2007) *Extrapolating brain development from experimental species to humans*. Neurotoxicology **28**, 931-937

53. Bray R.J. (1998) *Propofol infusion syndrome in children*. Paediatr Anaesth. **8**, 491-499

54. Wappler F. and Horn J. (2007) *Propofol infusion syndrome: is there any more information?* Anesthesiology. **107**, 175-176

55. Allegaert K., Peeters M.Y., Verbesselt R., et al. (2007) *Inter-individual variability in propofol pharmacokinetics in preterm and term neonates*. Br J Anaesth. 99, 864-870

9.4 Publication Reint

[This is a placeholder – paper is currently being written]

10 References

Akselrod S., Gordon D., Madwed J. B., Snidman N. C., Shannon D. C. and Cohen R. J. (1985) *Hemodynamic regulation: investigation by spectral analysis.* Am J Physiol **249**, H867-H875

Andriessen P., Koolen A. M. P., Berendsen R. C. M., Wijn P. F. F., ten Broeke E. D. M., Oei S. G. and Blanco C. E. (2003) *Cardiovascular fluctuations and transfer function analysis in stable preterm infants.* Pediatr Res **53**, 89-97

Andriessen P., Oetomo S. B., Peters C., Vermeulen B., Wijn P. F. F. and Blanco C. E. (2005) *Baroreceptor reflex sensitivity in human neonates: the effect of postmenstrual age.* J Physiol **568**, 333-341

André M., Lamblin M.-D., d'Allest A. M., Curzi-Dascalova L., Moussalli-Salefranque F., S Nguyen The T., Vecchierini-Blineau M.-F., Wallois F., Walls-Esquivel E. and Plouin P. (2010) *Electroencephalography in premature and full-term infants. Developmental features and glossary.* Neurophysiol Clin **40**, 59-124

Ashworth M. T. (2007). *The Cardiovascular System*. In: Keeling J. W. and Khong T. Y. (Ed.), *Fetal and Neonatal Pathology*, Springer-Verlag London Limited

Barnett V. A. (2005). *Cardiac Myocytes*. In: Iaizzo P. A. (Ed.), *Handbook of cardiac anatomy, physiology, and devices*, Humana Press

Bartelds B., van Bel F., Teitel D. F. and Rudolph A. M. (1993) *Carotid, not aortic, chemoreceptors mediate the fetal cardiovascular response to acute hypoxemia in lambs.* Pediatr Res **34**, 51-55

Bartels L. W. (1997). *A cross spectral analysis method between heart rate and blood pressure variability*, Eindhoven University of Technology

Batchinsky A. I., Cooke W. H., Kuusela T. A., Jordan B. S., Wang J. J. and Cancio L. C. (2007) *Sympathetic nerve activity and heart rate variability during severe hemorrhagic shock in sheep.* Auton Neurosci **136**, 43-51

Bendat J. S. and Piersol A. G., (1986) *Random Data: Analysis and Measurement Procedures*. John Wiley and Sons, Inc.

Bendat J. S. and Piersol A. G., (2010) *Random Data: Analysis and Measurement Procedures*. John Wiley and Sons, Inc.

Bennet L. and Gunn A. J. (2009) *The fetal heart rate response to hypoxia: insights from animal models.* Clin Perinatol **36**, 655-672

Bennet L., Rossenrode S., Gunning M. I., Gluckman P. D. and Gunn A. J. (1999) *The cardiovascular and cerebrovascular responses of the immature fetal sheep to acute umbilical cord occlusion.* J Physiol **517 (Pt 1)**, 247-257

Blanco C. E., Dawes G. S., Hanson M. A. and McCooke H. B. (1988) *Carotid baroreceptors in fetal and newborn sheep.* Pediatr Res **24**, 342-346

de Boer R. W., Karemaker J. M. and Strackee J. (1985) *Relationships between short-term blood-pressure fluctuations and heart-rate variability in resting subjects. I: A spectral analysis approach.* Med Biol Eng Comput **23**, 352-358

Bojanov G. (2005). *Blood Pressure, Heart Tones, and Diagnoses*. In: Iaizzo P. A. (Ed.), *Handbook of cardiac anatomy, physiology, and devices*, Humana Press

Booth L. C., Malpas S. C., Barrett C. J., Guild S.-J., Gunn A. J. and Bennet L. (2009) *Is baroreflex control of sympathetic activity and heart rate active in the preterm fetal sheep?* Am J Physiol Regul Integr Comp Physiol **296**, R603-R609

Camm A. J., Malik M., Bigger J. T., Breithardt G., Cerutti S., Cohen R. J., Coumel P., Fallen E. L., Kennedy H. L., Kleiger R. E., Lombardi F., Malliani A., Moss A. J., Rottman J. N., Schmidt G., Schwartz P. J. and Singer D. H. (1996) *Heart rate variability: standards of measurement, physiological interpretation and clinical use.*

Task Force of the European Society of Cardiology and the North American Society of Pacing and Electrophysiology. Circulation **93**, 1043-1065

Chobanian A. V., Bakris G. L., Black H. R., Cushman W. C., Green L. A., Jr. J. L. I., Jones D. W., Materson B. J., Oparil S., Jr. J. T. W., Roccella E. J. and the National High Blood Pressure Education Program Coordinating Committee (2003) *Seventh report of the Joint National Committee on Prevention, Detection, Evaluation, and Treatment of High Blood Pressure.* Hypertension **42**, 1206-1252

Cooley J. W. and Tukey J. W. (1965) *An algorithm for the machine calculation of complex fourier series* Mathematics of Computation **19**, 297-301

Dat M. (2010). *Modeling autonomic cardiovascular regulation of the preterm infant*, Eindhoven University of Technology

Drury P. P., Bennet L. and Gunn A. J. (2010) *Mechanisms of hypothermic neuroprotection.* Semin Fetal Neonatal Med **15**, 287-292

DuBrow I. W., Fisher E. A., Denes P. and Hastreiter A. R. (1976) *The influence of age on cardiac refractory periods in man.* Pediatr Res **10**, 135-139

Dupre A., Vincent S. and Iaizzo P. A. (2005). *Basic ECG Theory, Recordings and Interpretation*. In: Iaizzo P. A. (Ed.), *Handbook of cardiac anatomy, physiology, and devices*, Humana Press

Einthoven W. (1912) *The different forms of the human electrocardiogram and their signification.* The Lancet **179**, 853-861

Fitzgerald K., Wilson R. F. and Iaizzo P. A. (2005). *Autonomic Nervous System*. In: Iaizzo P. A. (Ed.), *Handbook of cardiac anatomy, physiology, and devices*, Humana Press

Frasch M. G., Müller T., Wicher C., Weiss C., Löhle M., Schwab K., Schubert H., Nathanielsz P. W., Witte O. W. and Schwab M. (2007) *Fetal body weight and the development of the control of the cardiovascular system in fetal sheep.* J Physiol **579**, 893-907

Frigo M. and Johnson S. G. (1998) FFTW: an adaptive software architecture for the FFT **3**, 1381-1384

Gaillot T., Beuchée A., Jaillard S., Storme L., Nuyt A. M., Carré F. and Pladys P. (2005) *Influence of sympathetic tone on heart rate during vagal stimulation and nitroprusside induced hypotension in ovine fetus.* Auton Neurosci **123**, 19-25

George S., Gunn A. J., Westgate J. A., Brabyn C., Guan J. and Bennet L. (2004) *Fetal heart rate variability and brain stem injury after asphyxia in preterm fetal sheep.* Am J Physiol Regul Integr Comp Physiol **287**, R925-R933

Giussani D. A., Spencer J. A., Moore P. J., Bennet L. and Hanson M. A. (1993) *Afferent and efferent components of the cardiovascular reflex responses to acute hypoxia in term fetal sheep.* J Physiol **461**, 431-449

Gournay V., Drouin E. and Rozé J.-C. (2002) *Development of baroreflex control of heart rate in preterm and full term infants.* Arch Dis Child Fetal Neonatal Ed **86**, F151-F154

Green L. R., McGarrigle H. H., Bennet L. and Hanson M. A. (1998) *Angiotensin II and cardiovascular chemoreflex responses to acute hypoxia in late gestation fetal sheep.* J Physiol **507 (Pt 3)**, 857-867

Gunn A. J. and Bennet L. (2009) *Fetal hypoxia insults and patterns of brain injury: insights from animal models.* Clin Perinatol **36**, 579-593

Hansen H. (2005). *Quantification of the EEG of full-term newborns*, Eindhoven University of Technology

Head G. A., Lukoshkova E. V., Burke S. L., Malpas S. C., Lambert E. A. and Janssen B. J. (2001) *Comparing spectral and invasive estimates of baroreflex gain.* IEEE Eng Med Biol Mag **20**, 43-52

Hellström-Westas L. and Rosén I. (2005) *Electroencephalography and brain damage in preterm infants.* Early Hum Dev **81**, 255-261

Hill A. J. and Iaizzo P. A. (2005). *Anatomy of the Human Heart*. In: Iaizzo P. A. (Ed.), *Handbook of cardiac*

anatomy, physiology, and devices, Humana Press

Holmes G. L. and Lombroso C. T. (1993) *Prognostic value of background patterns in the neonatal EEG.* J Clin Neurophysiol **10**, 323-352

Honzíková N., Fiser B. and Honzík J. (1992) *Noninvasive determination of baroreflex sensitivity in man by means of spectral analysis.* Physiol Res **41**, 31-37

Hossmann K. A. (1997) *Reperfusion of the brain after global ischemia: hemodynamic disturbances.* Shock **8**, 95-101; discussion 102-3

Iaizzo P. A. (2005). *General Features of the Cardiovascular System*. In: Iaizzo P. A. (Ed.), *Handbook of cardiac anatomy, physiology, and devices*, Humana Press

Ikeda T., Murata Y., Quilligan E. J., Parer J. T., Theunissen I. M., Cifuentes P., Doi S. and Park S. D. (1998) *Fetal heart rate patterns in postasphyxiated fetal lambs with brain damage.* Am J Obstet Gynecol **179**, 1329-1337

Janse M. K., Anderson R. H., van Capelle F. J. and Durrer D. (1976) *A combined electrophysiological and anatomical study of the human fetal heart.* Am Heart J **91**, 556-562

Japundzic-Zigon N. (1998) *Physiological mechanisms in regulation of blood pressure fast frequency variations.* Clin Exp Hypertens **20**, 359-388

Jardine D. L., Charles C. J., Melton I. C., May C. N., Forrester M. D., Frampton C. M., Bennett S. I. and Ikram H. (2002) *Continual recordings of cardiac sympathetic nerve activity in conscious sheep.* Am J Physiol Heart Circ Physiol **282**, H93-H99

Jennekens W., Dat M., Bovendeerd P. H., Wijn P. and Andriessen P. (2011) *Validation of a preterm infant cardiovascular system model under baroreflex control with heart rate and blood pressure data.* Proc. IEEE Eng Med Biol Soc 2011

Jennekens W., Ruijs L. S., Lommen C. M. L., Niemarkt H. J., Pasman J. W., van Kranen-Mastenbroek V. H. J. M., Wijn P. F. F., van Pul C. and Andriessen P. (2011b) *Automatic burst detection for the EEG of the preterm infant.* Physiol Meas **32**, 1623-1637

Jensen A. and Hanson M. A. (1995) *Circulatory responses to acute asphyxia in intact and chemodenervated fetal sheep near term.* Reprod Fertil Dev **7**, 1351-1359

Kay S. and Marple S. (1981) Spectrum analysis - A modern perspective **69**, 1380 - 1419

Laske T. G. and Iaizzo P. A. (2005). *The Cardiac Conduction System*. In: Iaizzo P. A. (Ed.), *Handbook of cardiac anatomy, physiology, and devices*, Humana Press

Laude D., Elghozi J.-L., Girard A., Bellard E., Bouhaddi M., Castiglioni P, Cerutti C., Cividjian A., Rienzo M. D., Fortrat J.-O., Janssen B., Karemaker J. M., Lefthériotis G., Parati G., Persson P. B., Porta A., Quintin L., Regnard J., Rüdiger H. and Stauss H. M. (2004) *Comparison of various techniques used to estimate spontaneous baroreflex sensitivity (the EuroBaVar study).* Am J Physiol Regul Integr Comp Physiol **286**, R226-R231

Li X., Tang D., Zhou S., Zhou G., Wang C., Zhuang Y., Wu G. and Shen L. (2004) *Redistribution of power spectrum of heart rate variability during acute umbilical artery embolism and hypoxemia in late-gestation fetal sheep.* Eur J Obstet Gynecol Reprod Biol **114**, 137-143

Liem K. D. and Greisen G. (2010) *Monitoring of cerebral haemodynamics in newborn infants.* Early Hum Dev **86**, 155-158

Lumbers E. R. and Yu Z. Y. (1999) *A method for determining baroreflex-mediated sympathetic and parasympathetic control of the heart in pregnant and non-pregnant sheep.* J Physiol **515 (Pt 2)**, 555-566

Maestri R., Pinna G. D., Mortara A., Rovere M. T. L. and Tavazzi L. (1998) *Assessing baroreflex sensitivity in post-myocardial infarction patients: comparison of spectral and phenylephrine techniques.* J Am Coll Cardiol **31**, 344-351

Mallard E. C., Williams C. E., Johnston B. M. and Gluckman P. D. (1994) *Increased vulnerability to neuronal damage after umbilical cord occlusion in fetal sheep with advancing gestation.* Am J Obstet Gynecol **170**, 206-214

Maloney J. E., Cannata J., Dowling M. H., Else W. and Ritchie B. (1977) *Baroreflex activity in conscious fetal and newborn lambs.* Biol Neonate **31**, 340-350

Martinsen B. J. and Lohr J. L. (2005). *Cardiac Development.* In: Iaizzo P. A. (Ed.), *Handbook of cardiac anatomy, physiology, and devices*, Humana Press

Matsuda Y., Maeda T. and Kouno S. (2003) *The critical period of non-reassuring fetal heart rate patterns in preterm gestation.* Eur J Obstet Gynecol Reprod Biol **106**, 36-39

McIntosh G. H., Baghurst K. I., Potter B. J. and Hetzel B. S. (1979) *Foetal brain development in the sheep.* Neuropathol Appl Neurobiol **5**, 103-114

Mehta A. V., Wolff G. S., Tamer D., Pickoff A. S., Casta A., Garcia O. L. and Gelband H. (1981) *Determinants of ventricular refractory periods in children with congenital heart disease: effects of cycle length and age.* Am Heart J **102**, 75-79

Mortara A., Rovere M. T. L., Pinna G. D., Prpa A., Maestri R., Febo O., Pozzoli M., Opasich C. and Tavazzi L. (1997) *Arterial baroreflex modulation of heart rate in chronic heart failure: clinical and hemodynamic correlates and prognostic implications.* Circulation **96**, 3450-3458

Nelson K. B., Dambrosia J. M., Ting T. Y. and Grether J. K. (1996) *Uncertain value of electronic fetal monitoring in predicting cerebral palsy.* N Engl J Med **334**, 613-619

Nelson K. B. and Leviton A. (1991) *How much of neonatal encephalopathy is due to birth asphyxia?* Am J Dis Child **145**, 1325-1331

Niemarkt H., Andriessen P., Pasman J., Vles J., Zimmermann L. and Oetomo S. B. (2008) *Analyzing EEG maturation in preterm infants: The value of a quantitative approach.* Journal of Neonatal-Perinatal Medicine **1**, 131-144

Parati G., Saul J., Rienzo M. D. and Mancia G. (1995) *Spectral analysis of blood pressure and heart rate variability in evaluating cardiovascular regulation. A critical appraisal.* Hypertension **25**, 1276-1286

Peeters L. L., Sheldon R. E., Jones M. D., Makowski E. L. and Meschia G. (1979) *Blood flow to fetal organs as a function of arterial oxygen content.* Am J Obstet Gynecol **135**, 637-646

Penáz J., Honzíková N. and Fiser B. (1978) *Spectral analysis of resting variability of some circulatory parameters in man.* Physiol Bohemoslov **27**, 349-357

Perlman J. M. (2009) *The relationship between systemic hemodynamic perturbations and periventricular-intraventricular hemorrhage - a historical perspective.* Semin Pediatr Neurol **16**, 191-199

Persson P. B., DiRienzo M., Castiglioni P., Cerutti C., Pagani M., Honzikova N., Akselrod S. and Parati G. (2001) *Time versus frequency domain techniques for assessing baroreflex sensitivity.* J Hypertens **19**, 1699-1705

Pinna G. D., Maestri R., Capomolla S., Febo O., Robbi E., Cobelli F. and Rovere M. T. L. (2005) *Applicability and clinical relevance of the transfer function method in the assessment of baroreflex sensitivity in heart failure patients.* J Am Coll Cardiol **46**, 1314-1321

Pourcyrous M., Parfenova H., Bada H. S., Korones S. B. and Leffler C. W. (1997) *Changes in cerebral cyclic nucleotides and cerebral blood flow during prolonged asphyxia and recovery in newborn pigs.* Pediatr Res **41**, 617-623

Pryds O. and Edwards A. D. (1996) *Cerebral blood flow in the newborn infant.* Arch Dis Child Fetal Neonatal Ed **74**, F63-F69

Riley K. F., Hobson M. P. and Bence S., (2007) *Mathematical Methods for Physics and Engineering*. Cambridge University Press

Robbe H. W., Mulder L. J., Rüddel H., Langewitz W. A., Veldman J. B. and Mulder G. (1987) *Assessment of baroreceptor reflex sensitivity by means of spectral analysis.* Hypertension **10**, 538-543

Rosenberg A. A. (1988) *Regulation of cerebral blood flow after asphyxia in neonatal lambs.* Stroke **19**, 239-244

Rovere M. T. L., Bigger J. T., Marcus F. I., Mortara A. and Schwartz P. J. (1998) *Baroreflex sensitivity and heart-rate variability in prediction of total cardiac mortality after myocardial infarction. ATRAMI (Autonomic Tone and Reflexes After Myocardial Infarction) Investigators.* Lancet **351**, 478-484

Rovere M. T. L., Pinna G. D. and Raczak G. (2008) *Baroreflex sensitivity: measurement and clinical implications.* Ann Noninvasive Electrocardiol **13**, 191-207

Ruijs L. (2007). *Automatic detection of burst, IBI and continuous patterns of EEG of premature infants: Towards a quantitative description of the change of continuity of EEG of premature infants*, Eindhoven University of Technology

Sörnmo L. and Laguna P., (2005) *Bioelectrical signal processing in cardiac and neurological applications*. Elsevier Academic Press

Saul J. P., Berger R. D., Albrecht P., Stein S. P., Chen M. H. and Cohen R. J. (1991) *Transfer function analysis of the circulation: unique insights into cardiovascular regulation.* Am J Physiol **261**, H1231-H1245

Segar J. L. (1997) *Ontogeny of the arterial and cardiopulmonary baroreflex during fetal and postnatal life.* Am J Physiol **273**, R457-R471

Segar J. L., Hajduczok G., Smith B. A., Merrill D. C. and Robillard J. E. (1992) *Ontogeny of baroreflex control of renal sympathetic nerve activity and heart rate.* Am J Physiol **263**, H1819-H1826

Semmlow J. L. (2004). *Spectral Analysis: Classical Methods*. In: (Ed.), *Biosignal and Biomedical Image Processing*, Marcel Dekker, Inc.

Shinebourne E. A., Vapaavuori E. K., Williams R. L., Heymann M. A. and Rudolph A. M. (1972) *Development of baroreflex activity in unanesthetized fetal and neonatal lambs.* Circ Res **31**, 710-718

Sykora M., Diedler J., Rupp A., Turcani P., Rocco A. and Steiner T. (2008) *Impaired baroreflex sensitivity predicts outcome of acute intracerebral hemorrhage.* Crit Care Med **36**, 3074-3079

Taylor J., Carr D., Myers C. and Eckberg D. (1998) *Mechanisms underlying very-low-frequency RR-interval oscillations in humans* Circulation **98**, 547-555

Timmers H. J. L. M., Wieling W., Karemaker J. M. and Lenders J. W. M. (2003) *Denervation of carotid baro- and chemoreceptors in humans.* J Physiol **553**, 3-11

Toonen F. A. J. (1998). *The possibilities for automated p- and r-peak detection in neonatal electrocardiograms*, Eindhoven University of Technology

Ursino M. and Magosso E. (2003) *Role of short-term cardiovascular regulation in heart period variability: a modeling study.* Am J Physiol Heart Circ Physiol **284**, H1479-H1493

Volpe J. J. (1997) *Brain injury in the premature infant. Neuropathology, clinical aspects, pathogenesis, and prevention.* Clin Perinatol **24**, 567-587

ten Voorde B. J. (1992). *Modeling the Baroreflex: a systems analysis approach*, VU University Amsterdam

Wassink G., Bennet L., Booth L. C., Jensen E. C., Wibbens B., Dean J. M. and Gunn A. J. (2007) *The ontogeny of hemodynamic responses to prolonged umbilical cord occlusion in fetal sheep.* J Appl Physiol **103**, 1311-1317

Watanabe K., Hayakawa F. and Okumura A. (1999) *Neonatal EEG: a powerful tool in the assessment of brain damage in preterm infants.* Brain Dev **21**, 361-372

Watkins L. L., Grossman P. and Sherwood A. (1996) *Noninvasive assessment of baroreflex control in borderline hypertension. Comparison with the phenylephrine method.* Hypertension **28**, 238-243

Weinhaus A. J. and Roberts K. P. (2005). *Anatomy of the Human Heart*. In: Iaizzo P. A. (Ed.), *Handbook of cardiac anatomy, physiology, and devices*, Humana Press

Williams K. P. and Galerneau F. (2003) *Intrapartum fetal heart rate patterns in the prediction of neonatal acidemia.* Am J Obstet Gynecol **188**, 820-823

11 Acknowledgements

I started work on this thesis in November 2010. At that time the idea was to focus on the effect of hypothermia treatment in the prevention or reduction of cerebral damage due to asphyxia during birth and link observations from EEG data to the subsequent outcomes of the patients. The following months, however, it appeared data was not really forthcoming, and there is little to analyse if one has no data.

Due to contacts with the research group from the department of paediatrics at Maastricht University, I gradually got involved with these researchers while I worked on EEG analysis. Findings, not just from the analysis of the EEGs, but also on how to improve their measurements in a practical way led to the involvement in a second project, which had by then just started. It was this project which provided the data that was to be the eventual main part of the thesis, though truth be told, the work included in the appendix probably does constitute a large amount of work time wise and to do it justice properly, I probably should have written a second thesis on that work.

During this year I worked closely with my two supervisors, Ward Jennekens, medical physicist in training and PhD student, and Peter Andriessen, neonatologist, whom I like to thank for their continuing interest in my work and for their advice, although I did not always heed it. I'd like to thank the people I collaborated with at Maastricht University, Matthias Seehase and Reint Jellema in particular. Furthermore I'd like to thank my professor, Pieter Wijn, for taking care of the things necessary for me and other students to function properly, and for his advice and thoughtful suggestions in various matters. Importantly, I'd like to thank my fellow-students for putting up with my antics and tea-guzzling behaviour during the course of a year and for their help and ideas. I also very much like to thank my parents, whom I have grown to love and respect ever more during the later years of my studies, for their support and just for being there.

Last, but first of all, I'm deeply grateful to our Sustainer, Who has endowed me with a glimpse of the richness and the potentialities that lie hidden in every human being. Not only has He expanded my vision to be world-embracing, it is becoming more and more clear to me that those Teachings actually can provide the healing balm for a much-suffering human race. As a last word I would like to share with the dear reader a quotation that is as a pearl from a very rich Ocean. It deals with science and its importance in man's life: "*The third Tajalli* [effulgence] *is concerning arts, crafts and sciences. Knowledge is as wings to man's life, and a ladder for his ascent. Its acquisition is incumbent upon everyone. The knowledge of such sciences, however, should be acquired as can profit the peoples of the earth, and not those which begin with words and end with words. Great indeed is the claim of scientists and craftsmen on the peoples of the world. Unto this beareth witness the Mother Book on the day of His return. Happy are those possessed of a hearing ear. In truth, knowledge is a veritable treasure for man, and a source of glory, of bounty, of joy, of exaltation, of cheer and gladness unto him. Thus hath the Tongue of Grandeur spoken in this Most Great Prison.*"